STRUCTURAL INVESTIGATIONS OF THE ACTIVE SITES OF AZURIN, HEMERYTHRIN, AND HEMOCYANIN, AND VIBRATIONAL ANALYSES OF THE COPPER (II) AND COPPER (III) COMPLEXES OF BIURET AND OXAMIDE

Thomas Joseph Thamann
B.S., Indiana University
M.S., Purdue University

A dissertation submitted to the faculty
of the Oregon Graduate Center
in partial fulfillment of the
requirement for the degree
Doctor of Philosophy
in
Chemistry

October, 1979

This dissertation has been examined and approved by the following Examination Committee:

Thomas M. Loehr, Thesis Advisor
Professor

Michael H. Gold
Associate Professor

James J. Huntzicker
Associate Professor

Thomas G. Dunne, Outside Examiner
Associate Professor, Reed College

DEDICATION

To Mom and Dad

They have given me everything

ACKNOWLEDGMENTS

I wish to express my deepest thanks to my research advisor Professor Thomas M. Loehr, for his many helpful comments and suggestions, especially in the preparation of this thesis. I also wish to thank Dr. William Keyes and Larry Willis for many informative discussions, Dr. Phil Pincus, Dale Larson, and George Hickok for help with the computer and the computer programs, and Nancy Golobish for typing this manuscript. Finally, I wish to recognize the students, staff, and faculty of the Oregon Graduate Center for making my stay here truly a memorable one.

TABLE OF CONTENTS

Page

Page

ABSTRACT

Structural Investigations of the Action Sites of Azurin Hemerythrin, and Hemocyanin, and Vibrational Analyses of the Copper (II) and Copper (III) Complexes of Biuret and Oxamide

Thomas Joseph Thamann, Ph.D.
Oregon Graduate Center, 1979

Supervising Professor: Thomas M. Loehr

The infrared and Raman spectra of the N-coordinated bis(biuretato)- and bis(oxamidato)-cuprate(II, III) complexes have been recorded, and normal coordinate analyses have been carried out using a Urey-Bradley force field for the copper complexes. The Cu(II)-biuret system undergoes little change upon oxidation to Cu(III), but is characterized by ring tightening and a general increase in mode frequencies. On copper oxidation, the oxamide system undergoes more drastic structural changes, most notably a strengthening of the C-C bond in the oxamide rings, as shown by a 19% increase in K(C-C), and an increase in electron density in the O-C-C-O framework.

The Wilson GF matrix method of vibrational frequency calculation was used to investigate various possible active site geometries for the "blue" copper protein azurin. Models representing trigonal bipyramidal, square planar, regular tetrahedral, and distorted tetrahedral active sites were examined, and it was found that a distorted tetrahedral, CuN_2S_2 model most accurately described the observed resonance Raman spectrum.

Various active site geometries for the oxygen-carrying proteins hemerythrin and hemocyanin were also examined by the Wilson GF matrix method. The models examined for hemerythrin were μ-monooxygen and μ-oxo bridged active site structures. It was determined that the structure which best described the resonance Raman spectrum of oxyhemerythrin, including the available data on the unsymmetrically labeled dioxygen adduct, was one that had a single oxygen of the O_2 molecule bound to both iron atoms. This model exhibited a Fe-O-O angle of 70°, whereas the angle made between the O_2 bond and the Fe-O-Fe plane was found to be 110°.

A similar experiment utilizing mixed isotope dioxygen was performed on oxyhemocyanin. The resonance Raman data were interpreted in terms of an active site geometry in which the oxygen atoms occupied spectroscopically equivalent position, such as a μ-peroxo bridged structure. Wilson GF matrix calculations confirmed the μ-peroxo model as being favorable, but in addition, the calculations describe other favorable models for the active site of oxyhemocyanin. One such model was a μ-monooxygen bridge structure which had a Cu-O-O angle of 80° and an O_2 bond angle of 110° with respect to the Cu-O-Cu plane. Such a structure is very similar to the one determined to be favorable for oxyhemerythrin. Normal coordinate analysis, therefore, does not provide unique structures but drastically restricts those possible from the available experimental data.

INTRODUCTION

Transition metals play an important role in many biological systems. Metals are found in many proteins and are generally located near the active site, which indicates that they are directly involved in the reaction mechanism. The respiratory proteins hemoglobin and myoglobin contain iron at the active sites, and it is known that the O_2 molecule, as superoxide (O_2^-), bonds directly to the metals. Two other respiratory proteins which bind O_2, as peroxide (O_2^{2-}), are hemerythrin and hemocyanin. These proteins are found in small marine animals (crabs, worms, etc.) and contain iron (hemerythrin) and copper (hemocyanin) at their active sites. Knowledge of the structure of the active site, particularly the mode of metal-O_2 binding, is very useful in determining the mechanism of action of these proteins.

Spectroscopic techniques are generally used to determine the structure of a metal-ligand system. Resonance Raman spectroscopy is particularly useful for studying biological systems containing transition metals, because the intensities of the metal-ligand vibrations may be enhanced, enabling these modes to be distinguished from non-metal protein vibrations, thus allowing one to "zero-in" on the metal center. The largest problem usually encountered when using Raman spectroscopy, as well as any other spectroscopic techniques, is to determine which observable peak corresponds to which metal-ligand vibrational mode.

Model systems generally are used to help solve this problem. However for hemerythrin and hemocyanin, no model systems have been developed which accurately explain all the observed experimental data.

In this thesis, group theoretical calculations are used in an attempt to shed some light on the mode of O_2 binding in hemerythrin and hemocyanin. Basically, this method involves the calculation of the frequency of a vibrational mode, given a certain geometry and a force field. It can be seen that these calculations can be made for numerous variations of an active site, and when the calculated frequencies match those experimentally observed, a favorable geometry has been determined. Details of the methods of calculation are the topic of Chapter 1, while the calculations involving hemerythrin and hemocyanin are the subjects of Chapters 4 and 5 respectively. Chapter 3 contains calculations and Raman band assignments for the "blue" copper protein azurin. Several geometries and various ligand sets are examined as possibilities for azurin's active site.

It has recently been proposed that trivalent copper participates in the enzymatic reaction mechanism of galactose oxidase. In light of this possibility it is useful to inspect the electronic and structural changes that a Cu-ligand system undergo as the oxidation state of copper changes. Copper (II,III) bis(biuretato) and Copper (II,III) bis(oxamidato) complexes have been examined, and the structural changes they undergo upon oxidation ($Cu^{2+} \rightarrow Cu^{3+}$) are described in Chapter 2.

CHAPTER 1

THEORY

Normal coordinate analysis uses molecular symmetry to predict either the frequencies of vibration, or the force constants between atoms in a molecule. Wilson's G and F matrix method is most widely used.[1-5] Wilson's equation relates force constants to vibrational frequencies as follows:

$$[FG - E\lambda] = 0$$

The left side of the equation is a determinant. F is a matrix containing force constants, G is a matrix containing reciprocal atomic masses and terms which relate the atoms in space according to their bonding geometry. E is a unit matrix and λ is related to the vibrational frequencies as follows:

$$\lambda = 4\pi^2\nu^2c^2$$

For a nonlinear system containing N atoms, the F and G matrix method involves the solution of a 3N-6 order determinantal equation. For equations of this size, computer solutions are often the only practical way to approach the problem. The Schachtschneider program provides such a computer solution.[6] The entire procedure is subdivided into five smaller programs, each one being independent and providing a solution for a part of the problem. The five programs are:

1) CART: puts the molecule in a cartesian coordinate system and defines the coordinates of each atom.

2) GMAT: calculates the G matrix (inverse kinetic energy matrix).

3) UBZM: calculates the transformation from Urey Bradley space to internal coordinate space, or calculates the F matrix.

4) ZSYM: symmetrizes the F matrix.

5) GVIB: solves the secular equation in internal coordinates.

The following example illustrates how the Wilson GF matrix method calculates the vibrational frequencies for the water molecule. Water will have 3N - 6 = 3 vibrations. Group theory predicts these vibrations to be: a symmetric (A_1) O-H stretch, an H-O-H angle bend (A_1), and an asymmetric (B_1) O-H stretch. These three vibrations described in terms of internal coordinates are Δr_1, Δr_2, and $\Delta\alpha$,

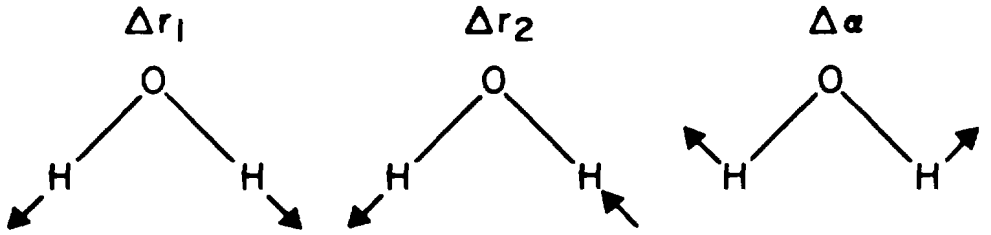

each having an associated force constant, f_{11}, $f_{22}(=f_{11})$, and f_{33} respectively. The F matrix can be set up as follows:

F =

	Δr_1	Δr_2	$\Delta\alpha$
Δr_1	f_{11}	f_{rr}	$f_{r\alpha}$
Δr_2	f_{rr}	f_{11}	$f_{r\alpha}$
$\Delta\alpha$	$f_{r\alpha}$	$f_{r\alpha}$	f_{33}

f_{rr} and $f_{r\alpha}$ are stretch-stretch interactions and angle-stretch interactions, respectively. The G matrix is similarly calculated:

		Δr_1	Δr_2	$\Delta\alpha$
	Δr_1	g_{11}	g_{12}	g_{13}
G =	Δr_2	g_{21}	g_{22}	g_{23}
	$\Delta\alpha$	g_{31}	g_{32}	g_{33}

g's are calculated from reciprocal masses and internal coordinates:

R = Bx where R is a set of internal coordinates, B is the transformation from cartesian displacement coordinates, x, to internal coordinates.

$g = BM^{-1}B'$ where M^{-1} is the reciprocal mass.

The remaining calculations can be simplified by describing the three vibrations in terms of symmetry coordinates, S_1, S_2, and S_3, which transform as A_1, A_1, and B_1 respectively. These three coordinates can be described in matrix form.

		Δr_1	Δr_2	$\Delta\alpha$	Symmetry Type
	S_1	$1/\sqrt{2}$	$1/\sqrt{2}$	0	A_1
U =	S_2	0	0	1	A_1
	S_3	$1/\sqrt{2}$	$-1/\sqrt{2}$	0	B_1

The F and G matrices can now be block-factored.

U			G			U^{-1}		
$1/\sqrt{2}$	$1/\sqrt{2}$	0	g_{11}	g_{12}	g_{13}	$1/\sqrt{2}$	0	$1/\sqrt{2}$
0	0	1	g_{21}	g_{22}	g_{23}	$1/\sqrt{2}$	0	$-1/\sqrt{2}$
$1/\sqrt{2}$	$-1/\sqrt{2}$	0	g_{31}	g_{32}	g_{33}	0	1	0

$$= \begin{vmatrix} (g_{11}+ g_{12}) & \sqrt{2}g_{13} & 0 \\ \sqrt{2}g_{13} & g_{33} & 0 \\ 0 & 0 & (g_{11}- g_{12}) \end{vmatrix} \rightarrow \begin{vmatrix} (g_{11}+ g_{12}) & \sqrt{2}g_{13} \\ \sqrt{2}g_{13} & g_{33} \end{vmatrix} , \ (g_{11}-g_{12})$$

Similarly, a block-factored F matrix can be set up. Now the secular equation, $(FG - E\lambda) = 0$, can be solved. In this case, λ will be obtained and converted to ν, for the three normal vibrations. Alternately, the observed ν can be put into the equation and F calculated, thus giving the molecular force constants.

The calculations in the subsequent chapters were performed using a set of three computer programs, which are modifications of the Schachtschneider programs.[7] The three programs are:

1. CART: this program is identical to the Schachtschneider cartesian coordinate program.
2. GMAT: calculates the G matrix and has the option of symmetrizing the G matrix when a U matrix is included.
3. FPERT: this program combines the Schachtschneider UBZM, ZSYM, and GVIB programs. FPERT also has the option of refining a calculated force field.

The refinement option of FPERT is crucial in calculations involving larger molecules when a large number of force constants are required. The refinement proceeds as follows:

1. FPERT calculates a group of vibrational frequencies from a set of trial force constants.

2. The calculated frequencies are compared to the actual experimentally observed frequencies to test for a predetermined convergence.
3. If the convergence test is passed, the force constants are not refined. If the test fails, the force constants are varied by a predetermined weighting factor, and the frequencies are recalculated.
4. The calculated and observed frequencies are compared and the convergence test is applied. If the test fails, the refinement continues until the test is passed.

As mentioned above, a set of force constants must be used in the programs GVIB and FPERT. These force constants constitute a model force field, which describes the interatomic forces within a molecule. Many model force fields have been used, and no single force field model works well in every situation. The most complete and accurate model is described by the general quadratic potential function,[8] $2V = \sum_{tt'}^{3N-6} F_{tt'} S_t S_{t'}$, where S_t, $S_{t'}$ are internal coordinates, N is the number of atoms in the molecule, and $F_{tt'}$ are the force constants. It can be seen that for 3N - 6 internal coordinates there will be $(3N - 6)^2$ force constants. This large number of force constants becomes quite cumbersome and impractical for larger molecules. For this reason, several models which approximate the general quadratic potential function have been devised.

The general valence force field[8] considers only those forces which resist the extension or compression of valence bonds, together

with those which oppose the bending or torsion of bonds; forces between nonbonded atoms are not considered. An improvement on the general valence model is provided by the Urey-Bradley force field.[9] This model considers the same forces as the general valence model, plus the forces between nonbonded atoms, typically referred to as repulsive forces. These repulsive forces are described by creating an imaginary bond between two nonbonded atoms and assigning a force constant to it. Figure 1-1 describes the force constants for the water molecule when using the general valence and Urey-Bradley force fields.

The Urey-Bradley force field generally works well and has been used often by Nakamoto and others on transition metal complexes, thus providing many force constants.[10-12] For these reasons, the Urey-Bradley force field has been used exclusively in the calculations in the following chapter, which examines copper complexes.

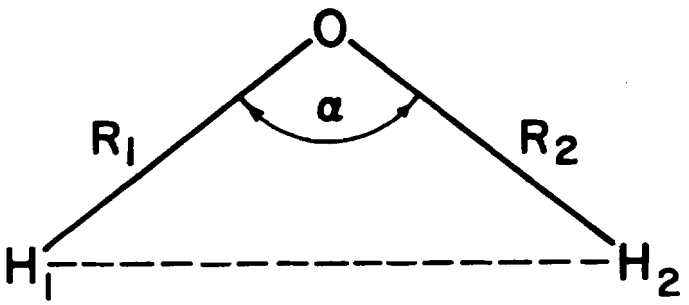

$f_{R_1} = f_{R_2}$ = OH stretching force constants
f_α = HOH bending force constant
q_{12} = repulsive force constant

] General Valence] Urey-Bradley

Figure 1-1. Definitions of the force constants for the water molecule, when using the general valence, or Urey-Bradley force fields.

CHAPTER 2

COPPER (II,III) COMPLEXES OF BISBIURET AND BISOXAMIDE

Introduction

Biuret and oxamide are known to coordinate to divalent copper, forming oxygen-coordinated complexes in an acidic medium and nitrogen-coordinated complexes in a basic medium. X-ray crystallography has been used to determine that the nitrogen-coordinated biuret complex is

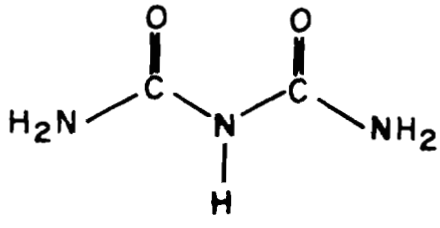

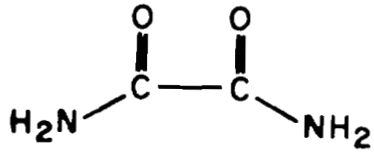

approximately square planar about the copper atom, and the corresponding oxamide complex was found to be structurally similar due to the close similarity of its infrared spectrum to that of the biuret complex.[13-15]

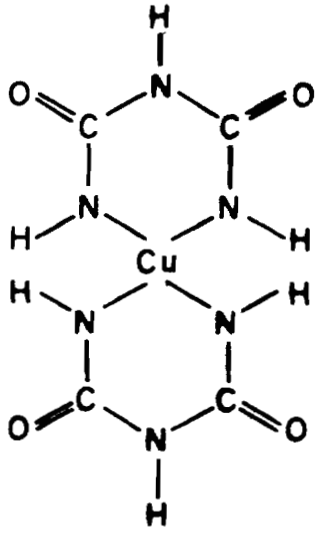

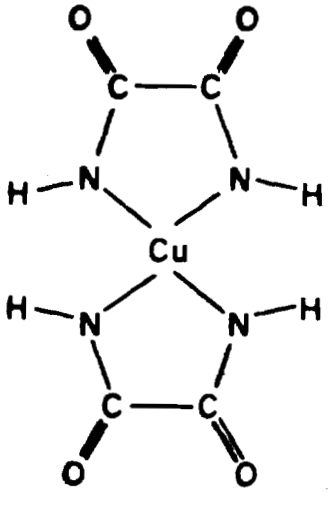

The N-coordinated Cu(II) complexes of biuret and oxamide have been oxidized, and the copper ions in these product complexes have been determined to be trivalent on the basis of their lack of EPR signals and an electronic absorption near 350 nm, characteristic of copper(III). Vibrational analyses, using isotopic substitution and normal coordinate analysis have been carried out on the Cu(II) complexes.[14,15] The normal coordinate calculations yielded a refined Urey-Bradley force field, which was used to assign the in-plane vibrational transitions observed in the infrared spectra of these complexes.

In light of the recent suggestions that Cu(III) may participate in some enzymatic reaction mechanisms[16], vibrational analyses of the Cu(III) complexes of biuret and oxamide are highly desirable. Such studies are useful in elucidating the Cu(III)-N stretching frequencies, and for obtaining a force field for Cu(III)-N complexes, which can be used in metal-protein model calculations. In the present study we have assigned the Raman vibrational transitions of the N-coordinated Cu(II) complexes and we have obtained the infrared and Raman spectra of the N-coordinated Cu(III) complexes of biuret and oxamide. Based on a normal coordinate analysis, we have found that on oxidation the Cu(II) bis(biuretato) complex undergoes minimal structural changes, while oxidation of the Cu(II) bis(oxamidato) complex yields a Cu(III) bis(oxamidato) complex which is significantly different than its Cu(II) counterpart, the major differences being a much stronger C-C bond in the oxamide rings and thus a significant shifting of electron density within the ring system.

Results and Discussion

Figures 2-1 and 2-2 show the Raman spectra of the complexes, and Tables 2-3 and 2-4 list observed Raman transitions. Only general similarities exist between the spectra of the copper complexes of the two different ligands. Furthermore, there is no obvious correlation among peaks, when comparing the Cu(II) and Cu(III) Raman spectra, although a close resemblance was noted in the infrared spectra by Bour, et al.[17] In order to facilitate these comparisons, and to make individual band assignments, a normal coordinate analysis has been carried out on all the copper complexes.

The Wilson GF matrix method was employed using computer programs obtained from the National Research Council of Canada, which were slightly modified for our purposes. All complexes were assumed planar, and only one of the chelated ligands was considered in the calculations. This method is valid due to the fact that the vibrational modes in one chelate ring do not couple appreciably with those modes in the second chelate ring, as shown by Nakamoto.[18,19] Figures 2-3 and 2-4 show the molecular models. The structural parameters were those reported in previous studies.[14,15] A simple Urey-Bradley force field was used in the solution of the secular equation. The final set of force constants is the result of a least-squares refinement of an initial trial set obtained by Nakamoto, et al., for their normal coordinate calculations of the Cu(II) bis(biuretato) and bis(oxamidato) complexes which, however, did not include Raman data.[14,15] These trial force constants gave calculated vibrational frequencies which did not

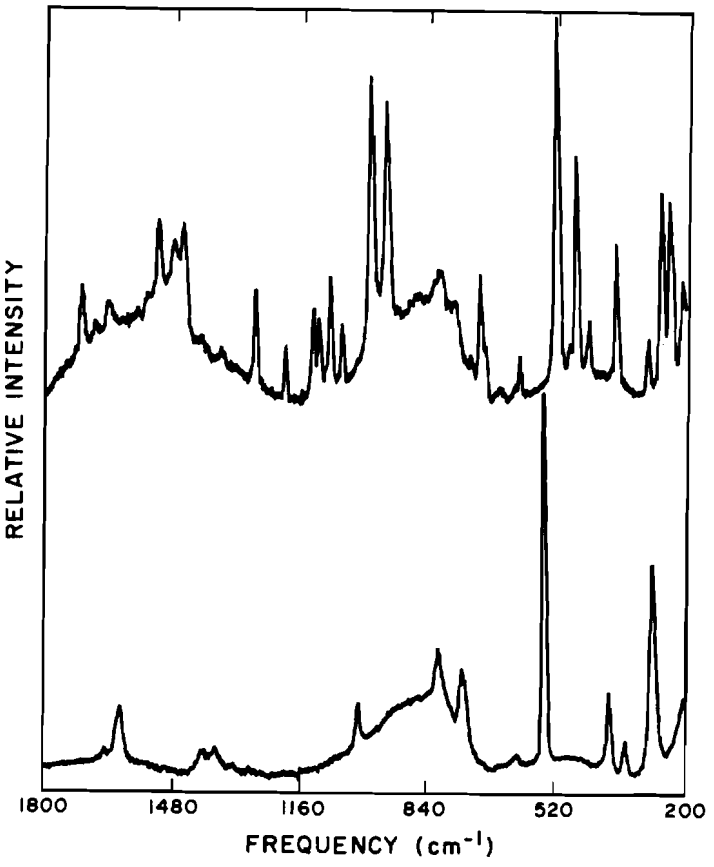

Figure 2-1. Raman Spectra of $K_2[Cu(biu)_2]\cdot 2H_2O$ (top) and $K[Cu(biu)_2]$ (bottom). Spectra were run at -150°C in glass capillary tubes. Scan rate = 4 $cm^{-1}sec^{-1}$, spectral slit width = 10 cm^{-1}, excitation λ = 6471A, and laser output power = 150 mw. The top spectrum is the sum of 34 scans and the bottom spectrum is the sum of 71 scans.

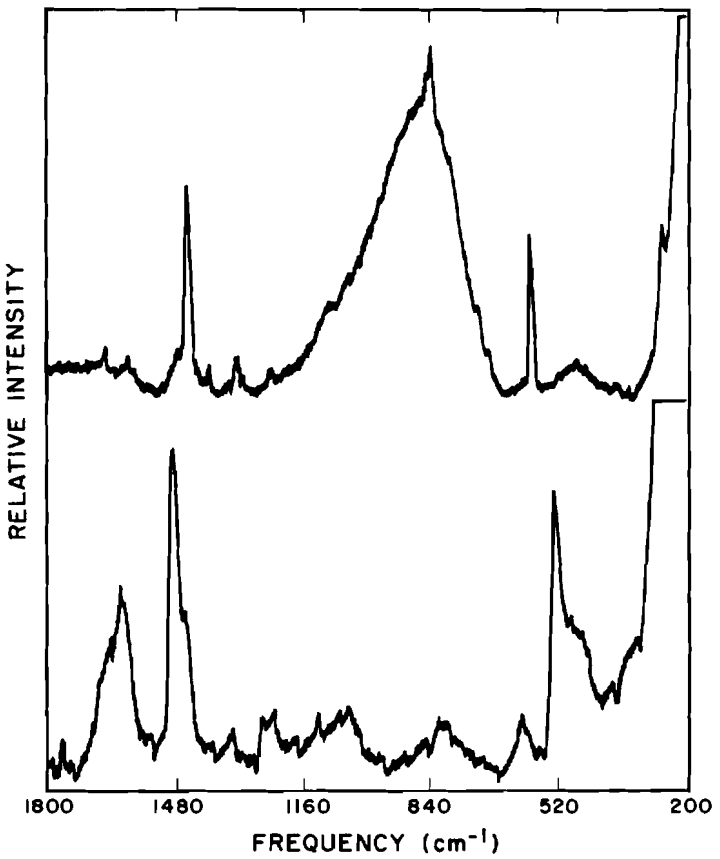

Figure 2-2. Raman Spectra of $K_2[Cu(ox)_2]$ (top) and $K[Cu(ox)_2]$ (bottom). Spectra were run at -150°C in glass capillary tubes. Scan rate = $4cm^{-1}sec^{-1}$, spectral slit width = 10 cm^{-1}, excitation λ = 6471Å [$K(Cu(ox)_2]$ and 5145Å ($K[Cu(ox)_2]$), and laser output power = 150 mw. The top spectrum is the sum of 106 scans and the bottom spectrum 285 scans.

agree satisfactorily with those observed in the Raman spectra. The final sets of force constants obtained for the Cu(II) complexes were similar to the initial trial sets, except for some slightly higher values for bending and repulsion force constants. Tables 2-1 and 2-2 list the initial and final sets of force constants used on all the complexes, and the change (Δ) in force constants encountered upon oxidation of the Cu(II) complexes. The initial set of force constants used for the Cu(III) complexes were the final set obtained for the corresponding Cu(II) complexes, except for K(Cu-N), which was calculated from the formula

$$K(Cu^{3+}\text{-}N) = \left[\frac{R(Cu^{2+}\text{-}N)}{R(Cu^{3+}\text{-}N)}\right]^6 \cdot K(Cu^{2+}\text{-}N)$$

where $K(Cu^{3+}\text{-}N)$ and $K(Cu^{2+}\text{-}N)$ are the stretching force constants (mdyne Å^{-1}), for the Cu^{3+} and Cu^{2+} complexes and $R(Cu^{3+}\text{-}N)$ and $R(Cu^{2+}\text{-}N)$ are the Cu-N distances (Å) in the copper complexes. This approximate relationship derives from the general assumption that the attractive potential between two atoms is inversely proportional to the sixth power of the equilibrium distance between the atoms.[20,21] This initial force field for the Cu(III) complexes was generally satisfactory, yielding average frequency errors of about two percent. Slight refining brought the average error to less than one percent. Tables 2-3 and 2-4 list the observed infrared and Raman frequencies as well as the band assignments for all the complexes.

The calculations reveal that the observed vibrational frequencies are generally complex mixtures of different vibrational modes, as shown in the different band assignments. The assignments

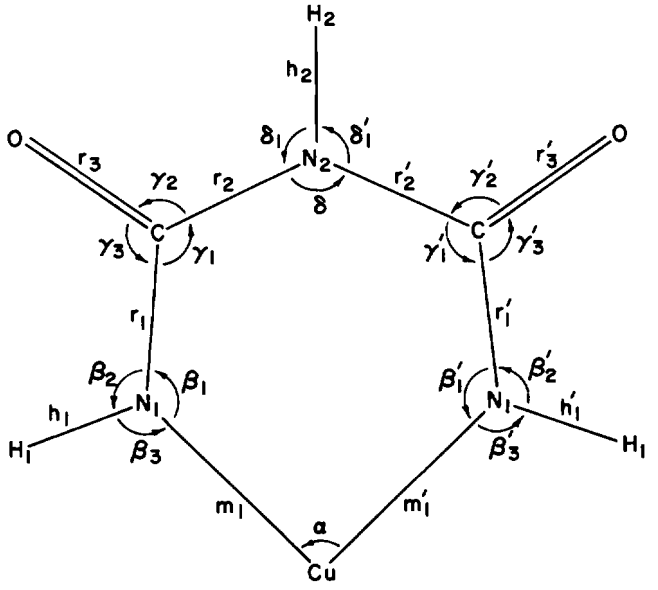

Figure 2-3. Molecular model of 1:1 copper-biuret complex.
$r_1=r_1'=1.34\text{Å}$, $r_2=r_2'=1.39\text{Å}$, $r_3=r_3'=1.26\text{Å}$, $m_1=m_1'=1.93\text{Å}$,
$h_1=h_1'=1.02\text{Å}$, $h_2=1.04\text{Å}$, $\alpha=90^\circ$, $\beta_1=\beta_1'=130^\circ$,
$\beta_2=\beta_2'=\beta_3=\beta_3'=115^\circ$. $\gamma_1=\gamma_1'=\gamma_2=\gamma_2'=\gamma_3=\gamma_3'=120^\circ$,
$\delta=130^\circ$, $\delta_1=\delta'_1=115^\circ$ for Cu(III), $m_1=m_1'=1.84\text{Å}$.

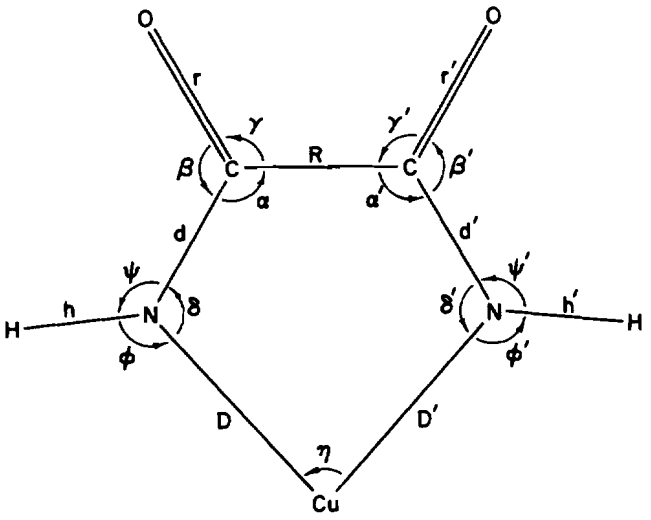

Figure 2-4. Molecular model of 1:1 copper-oxamide complex. $D=D'=2.03\text{Å}$, $d=d'=1.32\text{Å}$, $R=1.40\text{Å}$, $r=r'=1.28\text{Å}$ $h=h'=1.02\text{Å}$, $\alpha=\alpha'=\beta=\beta'=\gamma=\gamma'=120^{\circ}$, $\delta=\delta'=108^{\circ}$, $\psi=\psi'=\phi=\phi'=126^{\circ}$, $\eta=84^{\circ}$, for Cu(III), $D=D'=1.84\text{Å}$

Table 2-1. Force Constants for the Copper-Biuret Complexes (mdyne $Å^{-1}$)

MODE	COPPER(II)BISBIURET		COPPER(III)BISBIURET		
Stretching	Original Set	Final Set	Final Set	Δ	± % Δ
K(Cu-N_1)	0.908	1.042	1.456	0.414	39.7
K(C-N_1)	4.400	4.476	4.510	0.034	0.8
K(C-N_2)	3.400	3.410	3.380	-0.030	- 0.9
K(N_1-H)	5.500	5.540	5.502	-0.038	- 0.7
K(C=O)	7.700	7.741	7.838	0.097	1.3
K(N_2-H)	5.150	4.970	5.067	0.097	2.0
Bending					
H(N-Cu-N)	0.015	0.096	0.147	0.051	53.1
H(Cu-N-C)	0.106	0.214	0.221	0.007	3.3
H(C-N_1-H)	0.100	0.132	0.138	0.006	4.5
H(Cu-N-H)	0.170	0.151	0.278	0.127	84.1
H(N-C-N)	0.200	0.206	0.312	0.106	51.5
H(O-C-N_2)	0.736	1.015	1.047	0.032	3.2
H(N_1-C-O)	0.350	0.382	0.333	-0.049	-12.8
H(C-N-C)	0.780	1.081	1.165	0.084	7.8
H(C-N_2-H)	0.220	0.293	0.311	0.018	6.1
Repulsive					
F(Cu...C)	0.020	0.134	0.296	0.162	120.9
F(N_1...N_1)	0.020	0.218	0.225	0.007	3.2
F(C...C)	0.680	0.825	0.881	0.056	6.8
F(N_1...N_2)	0.660	0.959	1.039	0.080	8.3
F(Cu...H)	0.080	0.236	0.263	0.027	11.4
F(C...H_1)	0.925	1.067	0.942	-0.125	-11.7
F(N_1...O)	1.400	1.525	1.542	0.017	1.1
F(O...N_2)	1.100	1.154	1.158	0.004	0.3
F(C...N_2	0.558	0.481	0.478	-0.003	- 0.6

Table 2-2. Force Constants for the Copper-Oxamide Complexes (mdyne $Å^{-1}$)

MODE	COPPER(II)BISOXAMIDE		COPPER(III)BISOXAMIDE		
Stretching	Original Set	Final Set	Final Set	Δ	± % Δ
K(Cu-N)	0.908	0.958	1.349	0.391	40.8
K(C-N)	4.500	4.510	4.228	-0.282	- 6.3
K(C-C)	2.500	2.618	3.114	0.496	18.9
K(N-H)	5.830	5.782	5.686	-0.096	- 1.7
K(C=O)	8.800	8.862	8.866	0.004	0.0
Bending					
H(N-Cu-N)	0.020	0.070	0.161	0.091	130.0
H(Cu-N-C)	0.050	0.341	0.337	-0.004	- 1.2
H(C-C-N)	0.300	0.423	0.238	-0.185	-43.7
H(H-N-Cu)	0.230	0.356	0.423	0.067	18.8
H(H-N-C)	0.100	0.125	0.157	0.032	25.6
H(O=C-N)	0.500	0.504	0.480	-0.024	- 4.8
H(O=C-C)	0.550	0.643	0.502	-0.141	-21.9
Repulsive					
F(N...N)	0.020	0.210	0.402	0.192	91.4
F(Cu...C)	0.020	0.134	0.133	-0.001	- 0.7
F(C...N)	0.050	0.396	0.438	0.042	10.6
F(H...Cu)	0.080	0.036	0.064	0.028	77.8
F(H...C)	0.530	0.428	0.112	-0.316	-73.8
F(O...N)	1.500	1.533	1.820	0.287	18.7
F(O...C)	0.550	0.748	1.097	0.349	46.7

TABLE 2-3 OBSERVED INFRARED AND RAMAN FREQUENCIES AND CALCULATED VIBRATIONAL FREQUENCIES (cm^{-1}) AND THEIR BAND ASSIGNMENTS FOR THE COPPER BISBIURET COMPLEXES[a]

$K_2[Cu(biu)_2]$				$K[Cu(biu)_2]$			
IR OBSVD	RAMAN OBSVD	CALC	ASSIGNMENT	IR OBSVD	RAMAN OBSVD	CALC	ASSIGNMENT
3371	3373	3353	$\nu(N_1-H)$	3330	3330	3329	$\nu(N_1-H)$
3355	3353	3353	$\nu(N_1-H)$	3330	3330	3128	$\nu(N_1-H)$
3185	3150	3149	$\nu(N_2-H)$	3180	3180	3176	$\nu(N_2-H)$
1640	1643	1614	$(62)\nu(C=O) + (15)\nu(C-N_1)$	1690	1651	1643	$(60)\nu(C=O) + (15)\nu(C-N_1)$
1570	1571	1575	$(59)\nu(C=O) + (12)\nu(C-N_1)$	1600	1613	1598	$(57)\nu(C=O) + (12)\nu(C-N_1)$
1450	1459	1452	$(17)\nu(C-N_1) + (19)\nu(C-N_2) + (11)\delta(C=O)$	1505	1505	1451	$(16)\nu(C-N_1) + (18)\nu(C-N_2) + (11)\delta(C=O)$
1410	1414	1423	$(19)\nu(C-N_1) + (22)\nu(C-N_2)$	1440	1408	1420	$(14)\nu(C-N_1) + (17)\nu(C-N_2) + (10)\delta(N_1-H)$
1365	1365	1351	$(16)\nu(C=O) + (39)\delta(N_2-H) + (10)\nu(C-N_2)$	1370	1376	1369	$(11)\nu(C-N_2) + (16)\nu(C=O) + (37)\delta(N_2-H)$
1255	1277	1240	$(13)\nu(C-N_1) + (27)\delta(N_1-H)$	1327	1331	1309	$(13)\nu(C-N_1) + (34)\delta(N_1-H)$
1235	1202	1232	$(17)\nu(C-N_1) + (26)\delta(N_1-H)$	1270	1290	1299	$(21)\nu(C-N_1) + (12)\nu(C-N_2) + (30)\delta(N_1-H)$
1080	1059	1063	$(15)\nu(C-N_1) + (24)\nu(C-N_2)$	1117	1073	1073	$(14)\nu(C-N_1) + (23)\nu(C-N_2)$
965	986	982	$(23)\nu(C-N_1) + (11)\nu(C-N_2)$	990	1013	998	$(23)\nu(C-N_1) + (10)\nu(C-N_2) + (11)$Ring def
715	770	764	$(10)\delta(C=O) + (19)$Ring def	805	810	800	(19)Ring def
670	736	728	$(31)\delta(C=O) + (10)\nu(Cu-N)$	745	750	752	$(26)\delta(C=O) + (16)\nu(Cu-N)$
518	518	512	(11)Ring def $+ (14)\delta(C=O) + (12)\nu(Cu-N) + (11)\nu(C-N_2)$	580	542	547	(23)Ring def $+ (21)\delta(C=O)$
500	518	510	(25)Ring def $+ (17)\delta(C=O)$	560	542	539	(11)Ring def $+ (21)\nu(Cu-N) + (14)\nu(C-N_2)$
350	370	371	$(13)\nu(Cu-N) + (24)$Ring def $+ (20)\delta(C=O)$	410	381	388	$(11)\nu(Cu-N) + (23)$Ring def $+ (23)\delta(C=O)$
295	291	293	$(56)\nu(Cu-N)$	341	344	337	$(52)\nu(Cu-N)$
	237	232	$(35)\nu(Cu-N) + (21)$Ring def		274	273	$(25)\nu(Cu-N) + (21)$Ring def
860	864		$\pi(N_1-H) + \pi(N_2-H)$	815			$\pi(N_1-H) + \pi(N_2-H)$
815	811		$\pi(N_1-H)$	780			$\pi(N_1-H)$
770			$\pi(N_1-H) + \pi(N_2-H)$	670			$\pi(N_1-H) + \pi(N_2-H)$
385			$\pi(C=O)$	415			$\pi(C=O)$
365			$\pi(C=O)$	395			$\pi(C=O)$

[a] Numbers in parentheses are the %-age contribution of the force constant representing the internal coordinate assigned. Repulsive force constants are not included, although in some instances, their contribution is significant. Only %-ages >10% are listed. Observed frequencies listed on the same line are not necessarily corresponding modes between ir and Raman spectra. Weak features in the spectra listed in the Table may not be readily visible in the representative spectra shown in the Figures. For $K_2[Cu(biu)_2]$, Raman spectral features at 1710, 1520, 1133, 1114, 946, 709, 613, 469, and 437 cm^{-1} correlate well with lines observed in free biuret and are presumed to be due to free ligand.

TABLE 2-4 OBSERVED INFRARED AND RAMAN FREQUENCIES, CALCULATED VIBRATIONAL FREQUENCIES (cm^{-1}) AND THEIR BAND ASSIGNMENTS FOR THE COPPER BISOXAMIDE COMPLEXES[a]

$K_2[Cu(Ox)_2]$				$K[Cu(Ox)_2]$			
IR OBSVD	RAMAN OBSVD	CALC	ASSIGNMENT	IR OBSVD	RAMAN OBSVD	CALC	ASSIGNMENT
3385	3320	3315	ν(N-H)	3260	3238	3239	ν(N-H)
3270	3310	3314	ν(N-H)	3260	3238	3237	ν(N-H)
1635	1661	1675	ν(C=O)	1650	1645	1644	ν(C=O)
1600	1602	1609	ν(C=O)	1590	1613	1615	ν(C=O)
	1478				1485		
	1450				1456		
1380	1331	1323	(52)ν(C-N) + (24)ν(C-C)	1335	1339	1334	(48)ν(C-N) + (27)ν(C-C)
1212	1246	1257	(51)ν(C-N) + (11)ν(C=O) + (10)δ(C=O)	1255	1267	1264	(47)ν(C-N) + (15)δ(N-H)
1105	1154	1135	δ(N-H)		1242		
1035	1101	1114	δ(N-H)		1155	1151	δ(N-H)
840	830	830	(14)ν(C-N) + (15)ν(C-C) + (12)δ(N-H)	1070	1078	1088	δ(N-H)
720	718	718	δ(C=O)		1053		
583	584	574	(21)Ring def + (24)δ(C=O)	860	860	851	(20)ν(C-N) + (22)δ(N-H)
525	527	530	(27)ν(Cu-N) + (13)Ring def + (12)ν(C-C)	750	747	750	(13)ν(Cu-N) + (18)δ(C=O) + (10)δ(N-H)
350	347	354	(36)δ(C=O) + (11)Ring def	620	622		
320	308	310	(72)ν(Cu-N)		607	613	(31)ν(Cu-N)
	258	258	(40)ν(Cu-N) + (16)Ring def		568	561	(17)Ring def + (17)δ(C=O)
780			π(N-H)		530		
765			π(N-H)	385	384	374	δ(C=O)
380			π(C=O)		358		
365			π(C=O)	320	336	349	(70)ν(Cu-N)
					274	275	(37)ν(Cu-N) + (21)Ring def

[a] Numbers in parentheses are the %-age contribution of the force constant representing the internal coordinate assigned. Repulsive force constants are not included, although in some instances, their contribution is significant. Only %-ages >10% are listed. Observed frequencies listed on the same line are not necessarily corresponding modes between ir and Raman spectra. Weak features in the spectra listed in the Table may not be readily apparent in the representative spectra shown in the Figures. Table entries without corresponding assignments are significant Raman spectral features for which no values were calculated; these peaks could be due to site symmetry splittings or possible impurities.

generally agree with those given by Nakamoto and coworkers for the Cu(II) complexes. One which does differ is the out-of-plane carbonyl bend. Nakamoto, et al., assign two bands around 525 cm^{-1} to the out-of-plane carbonyl bend. However, our calculations for the Cu(II) bis(biuretato) systems show that the out-of-plane bends of (N_1-H), (N_2-H), and (C=O) are coupled, and would yield carbonyl bending modes around 380 cm^{-1}. Indeed, two bands were observed at 385 and 365 cm^{-1} in the infrared. Studies by Cossie and Schachtschneider on acetone, acetaldehyde, and formaldehyde have shown the out-of-plane (C=O) bend to be at about 350-390 cm^{-1}, using several different force field models in the calculations.[22]

Symmetry was left out of the calculations because no definite point group could be assigned to the complexes. All the complexes exhibit "general" mutual exclusion, however, there are a few modes in each complex which are both infrared and Raman active.

Table 2-5 lists the possible point groups and the expected number of IR and Raman active modes for the bis(oxamidato) complexes. All point groups that allow partial coincidence permit the noncoincident modes to be only Raman active. Inspection of the spectra for all the complexes reveal more IR active than Raman active modes. This can probably be accounted for by a poor scattering ability of the complexes. Indeed, some of the compounds, especially the Cu(III) complexes, give generally weak Raman spectra with very few observable bands, compared to their infrared spectra. For the bis(oxamidato) complexes the ν(N-H) modes are active in both the infrared and Raman, which rule out a totally centrosymmetric structure, and favor C_s, C_2, and C_{2v} as possible

TABLE 2-5: SYMMETRIES OF THE 45 VIBRATIONAL MODES OF THE BIS(OXAMIDATO)CUPRATE (II,III) COMPLEXES

Point Group	Mode Symmetries	# Only Raman Active	# Only IR Active	# IR & R Active	# Inactive
C_s	$27A' + 18A''$	0	0	45	0
C_2	$23A + 22B$	0	0	45	0
C_{2v}	$16A_1 + 7A_2 + 15B_1 + 7B_2$	7	0	38	0
C_{2h}	$15A_g + 6B_g + 8A_u + 16B_u$	21	24	0	0
D_2	$12A + 11B_1 + 11B_2 + 11B_3$	12	0	33	0
D_{2d}	$8A_1 + 3A_2 + 4B_1 + 8B_2 + 11E$	12	0	19[a]	3
D_{2h}	$8A_g + 7B_{1g} + 3B_{2g} + 3B_{3g} + 4A_u + 4B_{1u} + 8B_{2u} + 8B_{3u}$	21	20	0	4

[a] 11 degenerate modes

point groups. Similarly, the $\nu(N_1\text{-}H)$, modes in the bis(biuretato) complexes are active in both the Raman and infrared, but the $\nu(N_2\text{-}H)$ modes in Cu(II) bis(biuret) are mutually exclusive, which would indicate a structure with at least a "limited" inversion center. In general, the Cu(III) complexes show more coincidence than their Cu(II) counterparts, indicating less centrosymmetric structures. Inspection of atomic coordinates obtained from crystallographic studies of Cu(II) bis(biuretato) reveals that no true center of symmetry exists for the complex.[13]

Both the biuret and oxamide complexes undergo changes when the copper is oxidized. Oxidation of bis(biuretato)cuprate(II) is accompanied by a slight increase in the energy of most of the vibrational transitions. This is to be expected, since there is a general ring tightening, due to the decreased Cu-N distance. One mode that decreases in energy is ν(N-H). This decrease is accompanied by a corresponding decrease in the frequency of the out-of-plane bending mode, π(N-H). Since the Cu(II) bis(biuretato) and Cu(III) bis(biuretato) spectra are similar, one would expect similar structures for these compounds. Likewise, one would expect the spectrum of Ni(II) bis(biuretato) to be very similar to the Cu(III) bis(biuretato) spectrum, since both metals have spin-paired d^8 electronic configurations, and both generally form square planar complexes. The nickel complex has been shown to be square planar about the metal atom.[14] Indeed, the spectra of these two complexes are very similar, as shown in Figures 2-1 and 2-5. Normal coordinate calculations of the Ni(II) complex, using the Cu(III) bis(biuretato) force field, except for K(Ni-N), gave satisfactory results with an average error of 1.8%. X-ray crystallography of o-phenylenebis(biuretato)

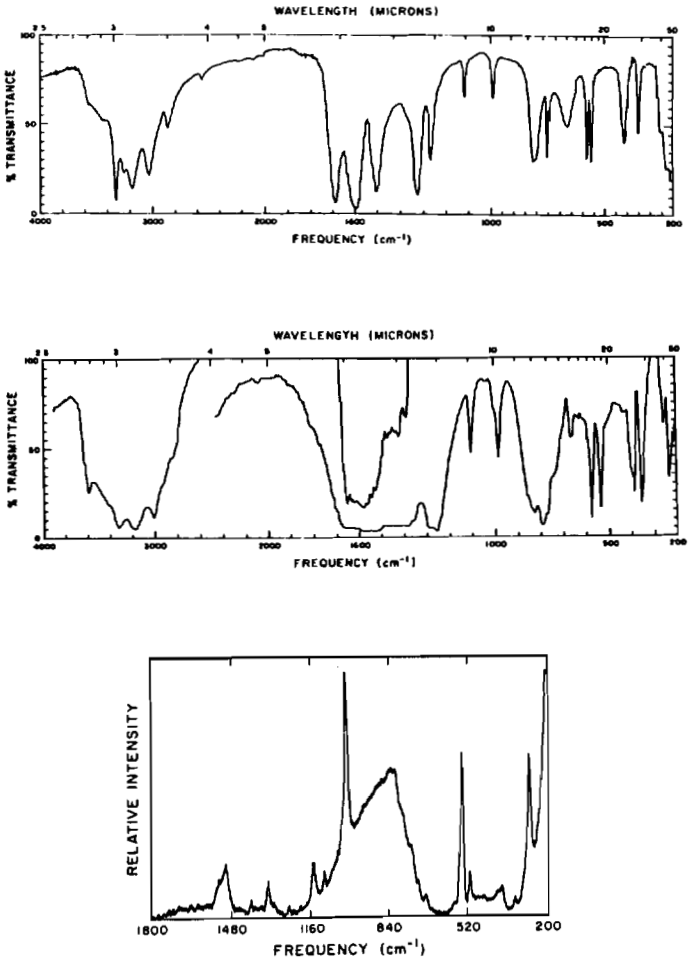

Figure 2-5. Infrared spectrum of $K[Cu(biu)_2]$ (top), $K_2[Ni(biu)_2]$ (middle), and Raman spectrum of $K_2[Ni(biu)_2]$ (bottom). Raman parameters are the same as those listed in Figure 2-1. The Raman spectrum is the sum of 67 scans.

cuprate(III) has shown this complex to be square planar about copper.[23] Thus, it is likely that the Cu(III) bis(biuretato) structure is very similar to that of the corresponding Cu(II) complex.

The copper bis(oxamidato) complex seems to undergo different changes on oxidation. These structural changes generally are more drastic than with the biuret complexes, as would be expected, because of the smaller ring size. A change in the Cu-N distance comparable to that found in the biuret complex would cause greater strain in the five-membered oxamide ring system. The oxamide ring tends to relieve this strain by decreasing the distance between the two carbon atoms, as illustrated by a 19% increase in the value of K(C-C). A 47% increase in F(C...O) strongly suggests increased electron density in the O-C-C-O framework. Increased electron density in the carbon oxygen framework would have to be accompanied by significant π back bonding from copper to nitrogen as shown in Figure 2-6B. Such systems, generally involving highly conjugated, nitrogen coordinating macrocylic ligands, are common with metals utilizing spin-paired d^8 electronic configurations.[24-27] An increase in π bonding between copper and nitrogen would weaken the C-N bond by placing electrons into the π^* C-N molecular orbital. This effect is reflected in a 6.3% decrease in K(C-N). Since K(N-H) decreases in both biuret and oxamide systems upon oxidation, one can conclude that a strengthening in the Cu-N bond is accompanied by a weakening of the N-H bond. The proposed model for the Cu(III) bis(oxamidato) complex claims a greater relative strengthening of the Cu-N bond on oxidation than expected in the biuret model, and would be accompanied by a larger relative decrease in K(N-H). Tables 2-1 and 2-2

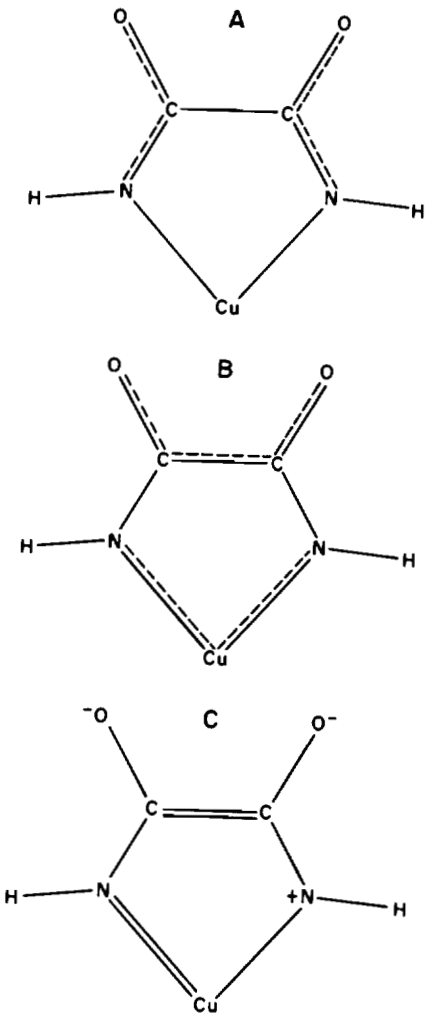

Figure 2-6. Approximate electron density in (A) copper (II) bisoxamide, (B) copper (III) bisoxamide, and (C) a major contributing resonant form of copper (III) bisoxamide.

list a K(N-H) decrease of 0.7% and 1.7% for the biuret and oxamide complexes, respectively. Consequently, the ν(N-H) decrease in the oxamide system is about 100 cm^{-1} greater than in the biuret complexes. The Raman bands at 1456 and 1485 cm^{-1} are at rather low frequencies for carbonyl groups,[28,29] and could be due to a major contribution of the resonant form shown in Figure 2-6C.

Conclusion

The normal coordinate calculations have revealed that upon oxidation the bis(biuretato) complex undergoes little structural and electronic change, while oxidation of the bis(oxamidato) complex induces a significant shortening of the C-C bond in the oxamide rings. This bond shortening is accompanied by a shift in electron distribution, which places higher electron density in the N-Cu-N, and O-C-C-O frameworks.

The calculations of the vibrational transitions have yielded Urey-Bradley force fields for the Cu(III) bis(biuretato) and Cu(III) bis(oxamidato) complexes. The force constants from these force fields may be helpful in making band assignments in some of the more stable Cu(III)-peptide complexes recently synthesized.[30] In view of the recent proposal that galactose oxidase contains trivalent copper, knowledge of the frequencies of Cu(III)-ligand modes could prove useful in searching for similar possible Cu(III) modes in the vibrational spectra of proteins.[16]

CHAPTER 3

AZURIN

Introduction

Azurin is a "blue" copper protein which can be isolated from bacteria such as Pseudomonas fluorescens and Pseudomonas aeruginosa. This protein has a molecular weight in the range 14,600-17,000 Daltons, contains one cupric atom, and is thought to be an electron transport component functioning between cytochrome oxidase and cytochrome c in the bacterium. Azurin is classified as a "blue" copper protein because of its intense absorption around 625 nm ($\varepsilon \sim 5.7 \times 10^3$ $M^{-1}cm^{-1}$).[30a]

The active site structure in azurin is not completely known at present, but a clearer picture is beginning to emerge. A 3 Å resolution electron density map for P. aeruginosa azurin reveals that cysteine, two histidines and methionine are ligated to copper in an approximately tetrahedral geometry.[32] Likewise, X-ray absorption spectroscopic (EXAFS) data has been used to identify the copper ligands as a thiolate sulfur with an unusually short Cu-S distance, two nitrogens, and a more distant sulfur.[33] Analysis of Raman intensitites have led Miskowski, et al., to propose a trigonal bipyramidal model, in which copper is bound to a sulfur and two nitrogens in the equatorial plane, and less strongly bound to nitrogen or oxygen ligands at the axial positions.[34] However, electronic absorption, circular dichroism, and magnetic circular dichroism studies of P. aeruginosa azurin[35] and its Co(II)-substituted derivatives[36,37] have been interpreted in terms of a ligand field model for a tetragonally

distorted tetrahedral geometry. Further support for a tetrahedral arrangement of two histidines, one cysteine and one methionine about Cu(II) comes from the X-ray crystallographic structural determination[38] of plastocyanin, a "blue" copper protein isolated from poplar leaves having properties similar to those of azurin.[31]

The resonance Raman spectrum of azurin shows three intense bands at 424, 404, and 369 cm^{-1}, plus a weak but distinct peak at 261 cm^{-1}, all of which should be due to Cu-ligand vibrations. The present study attempts to calculate the Cu-ligand vibrational frequencies using regular and distorted tetrahedral, trigonal bipyramidal, and square planar models in order to test which structural model best describes the resonance Raman spectrum of azurin.

Methods

The vibrational frequencies were calculated by the Wilson GF matrix method, utilizing Fortran IV computer programs modified slightly from those developed by Schachtschneider.[1,6,39] Figures 3-1, 3-2, and 3-3 show the molecular models considered in this study; the indicated bond distances are those obtained from EXAFS.[33] A general valence force field was used for all the models, and the initial values of the force constants were those typically found for Cu(II)-N, and Cu(II)-S complexes.[15,40-42]

Results and Discussion

I. Trigonal bipyramid model.

Table 3-1 lists the observed frequencies calculated frequencies and band assignments for a trigonal bipyramid (tbp) model of azurin.

The set of refined force constants are given in Table 3-2. The resonance Raman spectrum of azurin (Fig. 3-4) clearly shows more peaks than the nine expected for a five atom system, therefore, only the four most intense bands at 424, 404, 369, and 261 cm^{-1} were used in the refinement of the force constants, since these should be primarily Cu-ligand vibrations. Some of the calculated frequencies agree very well, especially with the four strongest Raman bands, however, they do not match well in the lower frequency region. For example, this tbp model predicts four bands in the 240-260 cm^{-1} region. Although the actual Raman spectrum shows a broad band near 260 cm^{-1}, it is doubtful that up to four components are contained within it.

The refined force field obtained for the trigonal bipyramid model is also not satisfactory, for instance, H(N-Cu-S) is nearly three times greater than $K(Cu\text{-}N_{eq})$, the value for $H(N_{eq}\text{-}Cu\text{-}N_{ax})$ is about two times greater than $K(Cu\text{-}N_{eq})$, and the value for $H(N_{eq}\text{-}Cu\text{-}N_{ax})$ is very high. Conversely, K(Cu-N eq) at 0.5 mdyne$\mathring{A}^{-1}$ is very low, a normal value being $\sim$ 1.0 mdyne $\mathring{A}^{-1}$, close to that obtained for $K(Cu\text{-}N_{ax})$. In addition, one would expect $K(Cu\text{-}N_{eq})$ to be approximately equal to $K(Cu\text{-}N_{ax})$, since the Cu-N distances were shown to be similar by EXAFS.[33]

II. Square Planar Model, CuN_3S

Table 3-3 lists the calculated frequencies and band assignments for the CuN_3S square planar model. The calculated peaks at 406 and 274 cm^{-1} correspond with the observed Raman bands at 404 and 275 cm^{-1}. However, all attempts to obtain calculated frequencies at <u>both</u> 424 and 369 cm^{-1} failed. A calculated peak at 424 cm^{-1} could be obtained, but

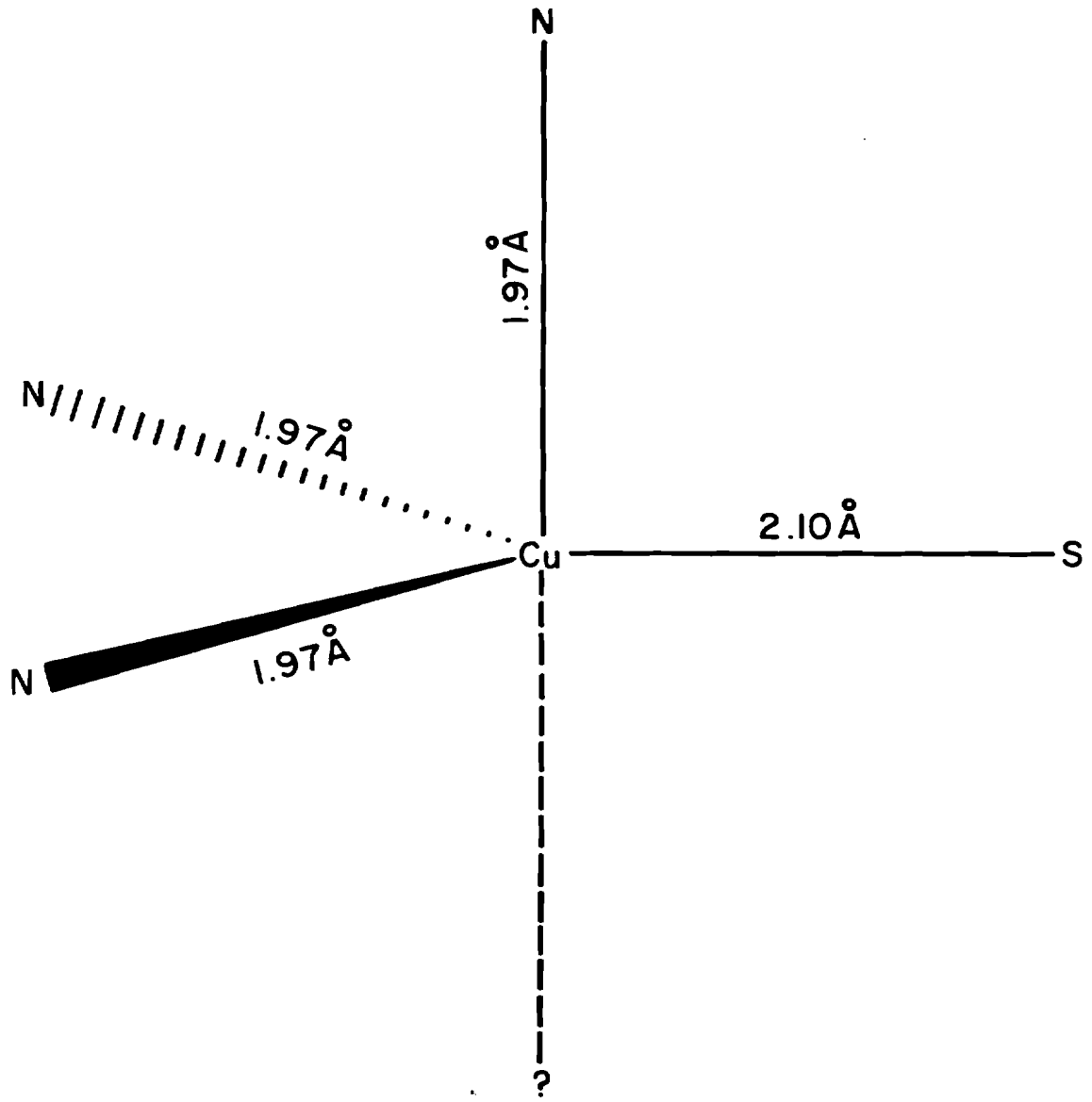

Figure 3-1. Geometric parameters for the trigonal bipyramidal model. Equatorial angles are 120°, and axial-equatorial angles are 90°. No atom is used at the fifth position.

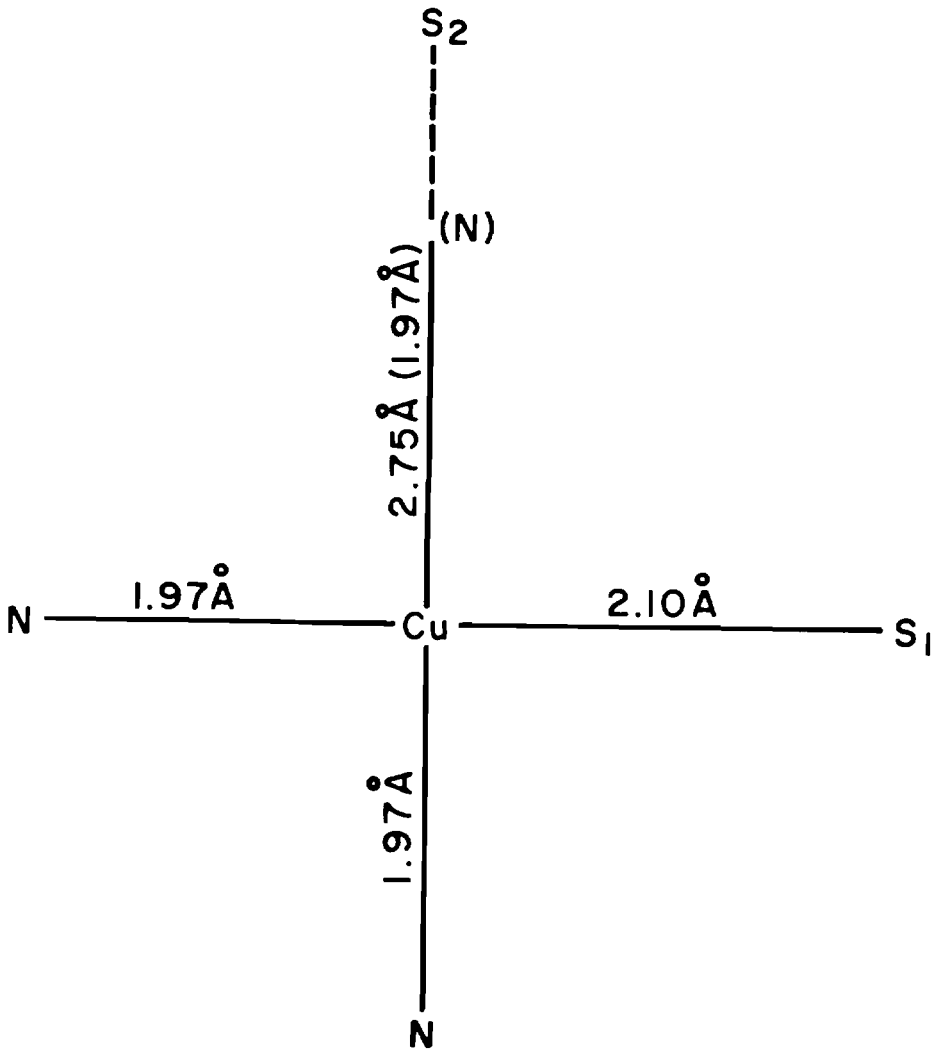

Figure 3-2. Geometric parameters for the square planar CuN_2S_2 and CuN_3S models.

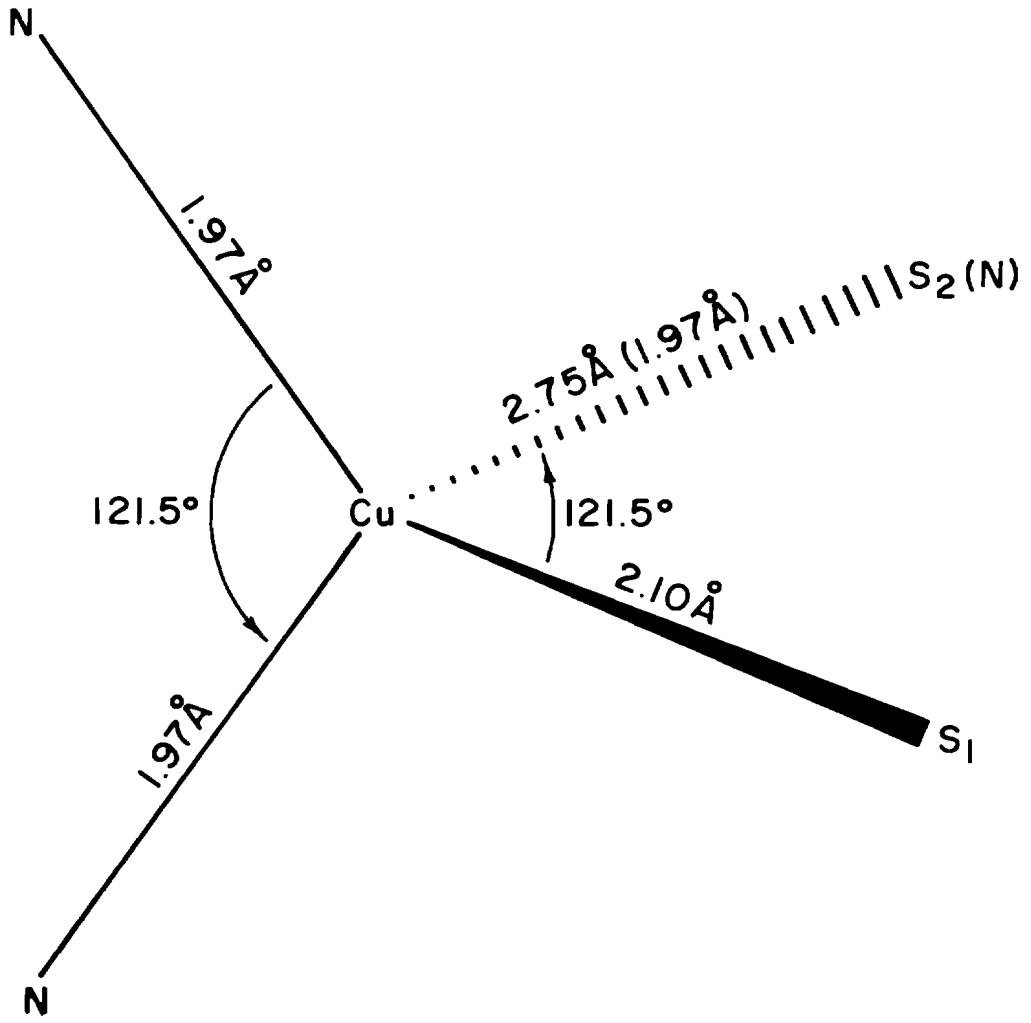

Figure 3-3. Geometric parameters for the tetragonally distorted tetrahedral CuN_2S_2 and CuN_3S models.

The regular tetrahedral models are identical, except the bond angles are 109° 28'.

Table 3-1. Observed Frequencies, Calculated Frequencies, and Band Assignments for the Trigonal Bipyramidal Model[a]

Observed Frequencies (cm^{-1})[b]	Calculated Frequencies (cm^{-1})	Band Assignments
491 w		
473 w		
452 w		
424 s	424	83% $\nu(Cu-S)$
404 vs	404	96% $\nu(Cu-N_{ax})$
369 s	368	24% $\nu(Cu-N_{eq})$ + 12% $\delta(N_{eq}-Cu-N_{ax})$ + 65% $\delta(N_{eq}-Cu-S)$
302 w		
275 (sh) w	262	40% $\nu(Cu-N_{eq})$ + 15% $\nu(Cu-S)$ + 10% $\delta(N_{eq}-Cu-N_{eq})$ + 30% $\delta(N_{eq}-Cu-S)$
261 m	261	69% $\delta(N_{ax}-Cu-N_{eq})$ + 26% $\delta(N_{eq}-Cu-S)$
218 w	251	71% $\nu(Cu-N_{eq})$ + 19% $\delta(N_{eq}-Cu-N_{ax})$ + 11% $\delta(N_{eq}-Cu-S)$
208 (sh), vw	242	56% $\nu(Cu-N_{eq})$ + 10% $\delta(N_{eq}-Cu-N_{eq})$ + 31% $\delta(N_{eq}-Cu-S)$
194 (sh), w	227	83% $\delta(N_{eq}-Cu-N_{ax})$
183 w		
158 vw		
146 vw		
137 vw		
115 m	128	92% $\delta(S-Cu-N_{ax})$

[a] v = very, s = strong, m = medium, w = weak, sh = shoulder
Contributions to band assignments which are less than 10% are not listed.

[b] The observed spectrum is shown in Figure 3-4; features marked vw may likely be within the noise level of the spectrum.

Table 3-2. Refined Force Constants for the Molecular Models (mdyne $Å^{-1}$)

Mode	CuN_3S Trigonal bipyramid*	CuN_3S Sq. Plane	CuN_2S_2 Sq. Plane	CuN_3S dist. tetrahedron	CuN_2S_2 Dist. tetrahedron
stretching					
K(Cu-N)	0.5	1.1	1.0	1.1	1.1
$K(Cu-S_1)$	2.0	1.1	1.9	2.0	1.6
$K(Cu-S_2)$			0.8		0.8
$K(Cu-N_{ax})$	1.1				
bending					
H(N-Cu-N)	0.2	0.1	0.0	0.4	0.1
$H(N-Cu-S_1)$	1.3	0.1	0.4	0.0	0.7
$H(S-Cu-S_2)$			0.2		0.3
$H(N-Cu-S_2)$			0.5		0.6
$H(S-Cu-N_{ax})$	0.4				
$H(N-Cu-N_{ax})$	0.9				

* Nitrogens not listed as N_{ax} are the equatorial nitrogens, which are designated as N_{eq} in the text.

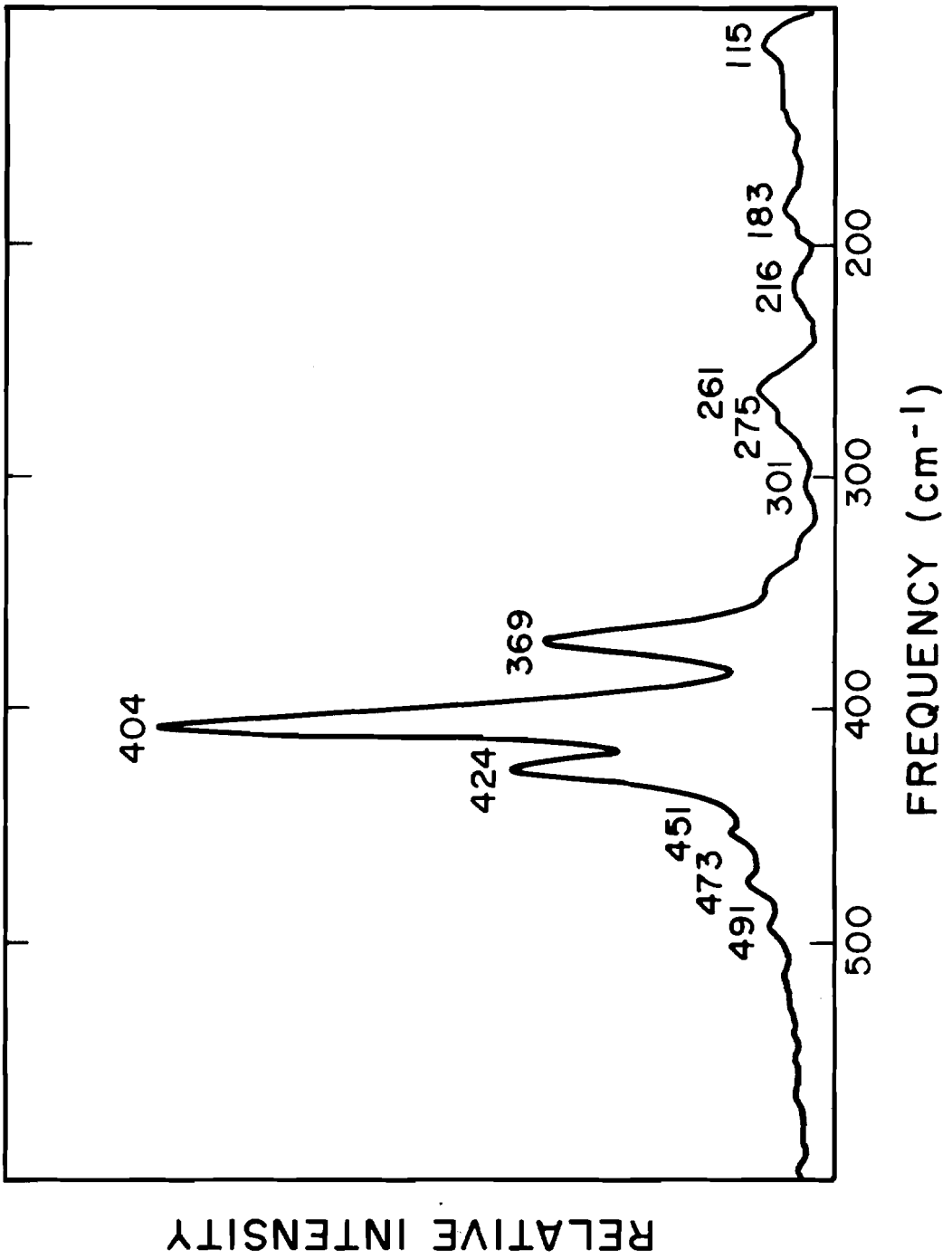

Figure 3-4. Resonance Raman spectrum of azurin. The spectrum is a composite of 136 scans with 6471 Å excitation. Spectral slit width is 4.5 cm^{-1}, scan rate is 2.0 $cm^{-1}sec^{-1}$, and the spectrum has been smoothed. Azurin was kept at ice temperature throughout the experiment.

Table 3-3. Observed Frequencies, Calculated Frequencies, and Band Assignments for the CuN_3S Square Planar Model[a]

Observed Frequencies (cm^{-1})[b]	Calculated Frequencies (cm^{-1})	Band Assignments
491 w		
473 w		
452 w		
424 s	431	100% ν(Cu-N)
404 vs	406	88% ν(Cu-N) + 11% ν(Cu-S)
369 s	358	100% ν(Cu-N)
302 w		
275 (sh), w	274	88% ν(Cu-S) + 11% ν(Cu-N)
261 m		
218 w		
208 (sh), vw		
194 (sh), w		
183 w		
158 vw		
146 vw		
137 vw		
115 m		

[a] v = very, s = strong, m = medium, w = weak, sh = shoulder
Contributions to band assignments which are less than 10% are not listed. Calculated frequencies less than 100 cm^{-1} are not listed.

[b] The observed spectrum is shown in Fig. 3-4; features marked vw may likely be within the noise level of the spectrum.

the lower frequency band calculated from this force field was at 328 cm^{-1}. When the 328 cm^{-1} band was adjusted to correspond to the observed 369 cm^{-1} peak, the 424 cm^{-1} increased substantially to 450 cm^{-1}. The lower frequency bands which were calculated for this model were all less than 100 cm^{-1}, as a result of very low bending force constants (Table 3-2).

III. Square Planar Model, CuN_2S_2

The observed and calculated frequencies for the square planar CuN_2S_2 model are listed in Table 3-4. The characteristic problems of this model are generally the same as those encountered for the square planar CuN_3S model. The calculations show a band at 404 cm^{-1}, thus matching the experimental result. However, as with the previous model, no refinements could fit both the 424 and 369 cm^{-1} Raman bands. The potential energy matrix shows that these two peaks are both ≈ 50% ν(Cu-N) + 50% ν(Cu-S), therefore their frequency difference is fixed, thus making it impossible to fit both frequencies simultaneously.

The model yields a calculated frequency at 244 cm^{-1}, which is close to the 261 cm^{-1} peak experimentally observed. There are lower frequency bands calculated at 152 and 133 cm^{-1}, which are also close to experimentally observed Raman peaks, albeit very weak in intensity and, therefore, of doubtful nature. A second square planar, CuN_2S_2 model, in which the nitrogens were at opposite corners of the square, yielded results very similar to the CuN_2S_2 model just described.

Table 3-4. Observed Frequencies, Calculated Frequencies, and Band Assignments for the CuN_2S_2 Square Planar Model[a]

Observed Frequencies (cm^{-1})[b]	Calculated Frequencies (cm^{-1})	Band Assignments
491 w		
473 w		
452 w		
424 s	442	49% ν(Cu-N) + 49% $\nu(Cu-S_1)$
404 vs	404	92% ν(Cu-N)
369 s	342	50% ν(Cu-N) + 50% $\nu(Cu-S_1)$
302 w		
275 (sh), w		
261 m	244	88% $\nu(Cu-S_2)$
218 w		
208 (sh), vw		
194 (sh), w		
183 w		
158 vw	152	63% $\delta(S_1-Cu-N)$ + 29% $\delta(S_2-Cu-N)$
146 vw		
137 vw	132	69% $\delta(S_2-Cu-N)$ + 29% $\delta(S_1-Cu-N)$ + 10% $\delta(S_2-Cu-S_1)$
115 vw		

[a] v = very, s = strong, m = medium, w = weak, sh = shoulder
Contributions to band assignments less than 10% are not listed.
Calculated frequencies less than 100 cm^{-1} are not listed.

[b] The observed spectrum is shown in Fig. 3-4; features marked vw may likely be within the noise level of the spectrum.

IV. Flattened and Regular Tetrahedral Models, CuN_3S

The results for the tetragonally-distorted tetrahedral CuN_3S model are listed in Table 3-5. This model predicts two overlapping bands at about 404 cm^{-1}, which could account for the high intensity of that peak. However, all attempts to match the 369 cm^{-1} peak failed, and no band close to 261 cm^{-1} could be calculated. The set of refined force constants for the distorted tetrahedral model (Table 3-2) are satisfactory, except for H(N-Cu-S) which is essentially zero. All attempts to keep this force constant positive, while matching the 369 cm^{-1} peak, failed. However, this model does predict Raman bands at 194 and 146 cm^{-1} at which frequencies weak features are observed.

Calculations using a CuN_3S regular tetrahedron yielded results quite similar to those obtained for the distorted tetrahedral model. Thus, the lack of calculated 369 and 261 cm^{-1} bands, plus an unrealistic force field are strong evidence that a tetrahedral CuN_3S model is an undesirable description of the active site in azurin.

V. Flattened and Regular Tetrahedral Models, CuN_2S_2

The calculated frequencies for the tetragonally distorted tetrahedral CuN_2S_2 model are listed in Table 3-6. These frequencies match the four most intense Raman bands quite well. Although the calculated lower frequencies do not coincide as well, they are closer to observed values than those obtained for any of the previous models. The lower frequencies may be expected to match less well, because the calculation fits the four stretching frequencies by refining mainly stretching force constants, while leaving the bending force constants

Table 3-5. Observed Frequencies, Calculated Frequencies, and Band Assignments for the CuN_3S Distorted Tetrahedral Model[a]

Observed Frequencies (cm^{-1})[b]	Calculated Frequencies (cm^{-1})	Band Assignments
491 w		
473 w		
452 w		
424 s	430	56% ν(Cu-S) + 40% ν(Cu-N)
404 vs	409	93% ν(Cu-N)
	407	87% ν(Cu-N) + 10% ν(Cu-S)
369 s	352	70% ν(Cu-N) + 30% ν(Cu-S)
302 w		
275 (sh), w		
261 m		
218 w		
208 (sh), vw		
194 (sh), w	195	98% δ(N-Cu-N)
183 w	177	99% δ(N-Cu-N)
158 vw		
146 vw	146	74% δ(N-Cu-N) + 25% (S-Cu-N)
137 vw		
115 m		

[a] v = very, s = strong, m = medium, w = weak, sh = shoulder
Contributions to band assignments which are less than 10% are not listed. Calculated frequencies less than 100 cm^{-1} are not listed.

[b] The observed spectrum is shown in Fig. 3-4; features marked vw may likely be within the noise level of the spectrum.

Table 3-6. Observed Frequencies, Calculated Frequencies, and Band Assignments for the CuN_2S_2 Distorted Tetrahedral Model[a]

Observed Frequencies (cm^{-1})[b]	Calculated Frequencies (cm^{-1})	Band Assignments
491 w		
473 w		
452 w		
424 s	424	97% ν(Cu-N)
404 vs	404	81% ν(Cu-N) + 17% $\nu(Cu-S_1)$
369 s	370	15% ν(Cu-N) + 62% $\nu(Cu-S_1)$ + 11% $\nu(Cu-S_2)$
302 w		
275 (sh), w		
261 m	260	19% $\nu(Cu-S_1)$ + 58% $\nu(Cu-S_2)$ + 11% $\delta(N-Cu-S_1)$
218 w		
208 (sh), vw	210	80% $\delta(N-Cu-S_1)$ + 19% $\delta(N-Cu-S_2)$
194 (sh), w	202	41% $\delta(N-Cu-S_1)$ + 30% $\nu(Cu-S_2)$ + 27% $\delta(N-Cu-S_2)$
183 w		
158 vw	160	80% $\delta(N-Cu-S_2)$ + 18% $\delta(N-Cu-S_1)$
146 vw		
137 vw	130	37% $\delta(N-Cu-S_2)$ + 35% δ(N-Cu-N) + 22% $\delta(N-Cu-S_1)$
115 m	102	69% $\delta(S_1-Cu-S_2)$ + 27% δ(N-Cu-N)

[a] v = very, s = strong, m = medium, w = weak, sh = shoulder Contributions to band assignments which are less than 10% are not listed. S_1 = sulfur at 2.10 Å and S_2 = sulfur at 2.75 Å.

[b] The observed spectrum is shown in Fig. 3-4; features marked vw may likely be within the noise level of the spectrum.

virtually unchanged. Therefore, if the initial values of the bending force constants were slightly incorrect, the calculations of the lower frequencies would also be inaccurate. The Raman spectrum does show a wide band at 218 cm^{-1}, which could be the 210 and 202 cm^{-1} calculated peaks. The calculated frequencies at 160 and 130 cm^{-1} could correspond to the observed peaks at 158 and 137 cm^{-1}.

The set of refined force constants for the CuN_2S_2 distorted tetrahedral model is realistic, with values generally observed in other Cu(II)-S and Cu(II)-N complexes. Of particular significance is the ratio of the two Cu-S stretching force constants (0.533), which is extremely close to what would be predicted from the ratio of the frequencies assigned to Cu-S stretching modes[43,44]. The CuN_2S_2 regular tetrahedral model predicts frequencies very similar to the CuN_2S_2 distorted tetrahedron model.

Conclusion

Various geometries have been used in calculations of the vibrational energies of the active site in azurin. Although the trigonal bipyramid and CuN_3S distorted tetrahderal models accurately predict some of the observed resonance Raman Cu-ligand stretching frequencies, they require unrealistic force fields to do so. In addition, these models do not accurately predict the possible lower frequency Cu-ligand bending modes which are observed. The square planar models accurately predict the very intense 404 cm^{-1} Raman band, but force constant refinements could not fit the observed intense resonance enhanced peaks at 424 cm^{-1} and 369 cm^{-1}. Although no model examined accurately

predicts the frequencies for all of the very low energy bending modes (some of which are of a dubious nature due to their low intensities), the CuN_2S_2 tetragonally distorted tetrahedral model comes the closest, while also accurately predicting the higher frequency Cu-ligand stretching frequencies. The refined force constants for this model are similar to those found in Cu(II)-N and Cu(II)-S complexes. The regular tetrahedron models gave vibrational frequencies very similar to the distorted tetrahedron models, however, considering the results from other spectroscopic techniques it is concluded that a CuN_2S_2 distorted tetrahedron is indeed the model which best describes the active site in azurin.

CHAPTER 4

HEMERYTHRIN

Introduction

Hemerythrin is an oxygen carrying protein found in four different invertebrate phyla: sipunculids, polychaetes, priapulids, and brachiopods.[45] Hemerythrin has a molecular weight of 108,000 Daltons and occurs as an octamer of identical subunits, each containing two iron atoms[46,47]. The protein can undergo many reactions and transformations of which the major ones are: (1) reversible combination with O_2, (2) chemical oxidation ($Fe^{2+} \rightarrow Fe^{3+}$) of oxyhemerythrin to methemerythrin upon addition of an oxidizing agent, such as $K_3Fe(CN)_6$, (3) addition of various ligands (N_3^-, SCN^-, Cl^-) to methemerythrin to form met derivatives[48] and (4) dissociation of the octamer into monomers by the addition of reagents that react with SH groups, such as cysteine.[49]

Of the several forms of hemerythrin that exist, the active sites of three general types have been studied most: deoxyhemerythrin, methemerythrin, and oxyhemerythrin. Of these, deoxyhemerythrin has afforded the least complete picture of its active site structure. Deoxyhemerythrin is colorless and therefore very little information about its active site is revealed by electronic spectroscopy. However, Mössbauer spectroscopy has shown that both iron atoms are in the high spin ferrous state, and that they are chemically equivalent.[50,51] Magnetic susceptibility confirms the high spin ferrous state, and also shows that little or no magnetic coupling exists between the iron

atoms.[51,52] X-ray crystallography on metaquohemerythrin[53,54] and metazidomyohemerythrin[55] have shown that in both cases one iron is bonded to three histidines, while the other iron is bonded to two histidines and a tyrosine. It is reasonable to assume that these same ligands occupy similar positions in deoxyhemerythrin.

Methemerythrin forms complexes with several small anionic ligands, such as water, thiocyanate, chloride, fluoride, and azide. The Mössbauer and magnetic susceptibility data of these complexes show that the iron atoms are high spin iron (III), are in similar environments within each complex, and are antiferromagnetically coupled.[50,51,56-58] This coupling suggests the presence of a bridging ligand between the iron atoms, the most likely being either oxygen or the exogenous ligand. Both the Mössbauer and magnetic susceptibility data are quite similar to that found for oxo-bridged iron(III) dimers.[45,56,59] In addition, the similarity in positions of near UV bands for several methemerythrin derivatives with those of known iron(III) μ-oxo-bridged compounds suggests such a bridge in the protein,[46,48,50,60] as do resonance Raman experiments on metazidohemerythrin.[46]

The spectroscopic and magnetic data for oxyhemerythin are similar to those for methemerythrin, indicating similar active sites for the two proteins. Again, Mössbauer[50,51] and magnetic susceptibility[57,58] measurements reveal an active site comprised of two strongly antiferromagnetically coupled high spin ferric atoms. However, Mössbauer data also reveal that both irons are involved in oxygen binding and that their environments are different.[50,51] Raman spectroscopy

has been used to determine that the bound dioxygen ligand exhibits a peroxide-like electronic state (O_2^{2-}).[60a]

Two models for the active site of methemerythrin have been proposed as a result of independent X-ray crystallographic studies on metazidomyohemerythrin (I)[55] and metaquohemerythrin (II)[54], as shown below. Although the two models are similar there are some major differences. Structure I shows a μ-oxo bridge, whereas structure II shows two μ-carboxy bridges contributed by glutamic acid and aspartic

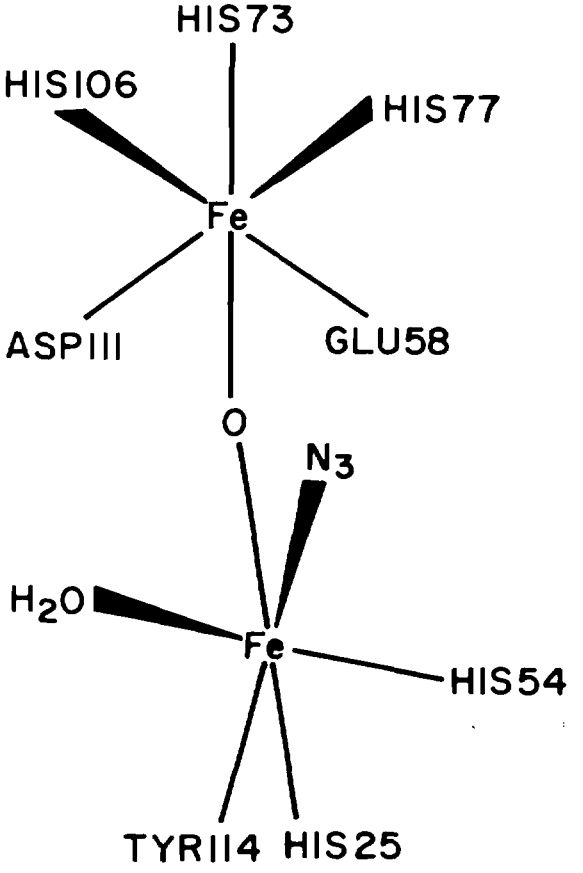

I

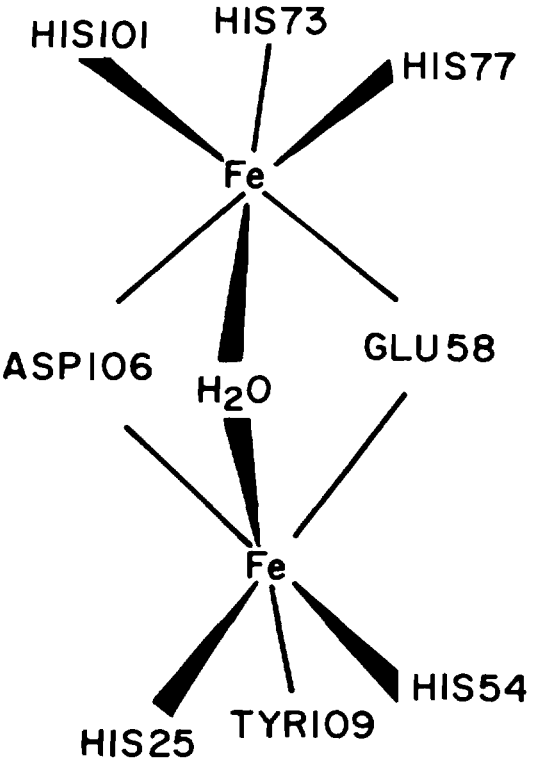

II

acid sidechains from the protein backbone. In addition, structure II is a face-sharing bioctahedron, which places restraints on Fe-O-Fe bridging angles (70°), and therefore dictates a Fe-Fe distance somewhat less than 3 Å (assuming standard Fe-O bond lengths of about 2 Å). Structure I puts no rigid restraints on the Fe-Fe distance, although for a typical μ-oxo bridged iron(III) dimer (an Fe-O-Fe angle of about 145° is common) this distance would be about 3.5 Å. The metal-metal distances determined in both independent crystallographic studies support their respective models (3.44 Å for I and ∿ 3.05 Å for II).[61] Thus, the two models suggest different active sites for the two methemerythrins, although spectroscopic comparisons of hemerythrins from four different species of sipunculids revealed no major differences in the active site.[62]

Two questions need to be answered to clarify the active site structure of hemerythrin; which (if either) of the proposed crystallographic models is correct, and how is the exogenous ligand (N_3^-, O_2, ...) bound to the iron center? Data to help answer these questions can be obtained by examination of the isotopic shifts observed in the Raman spectrum, when substitution with an isotopic exogenous ligand ($^{15}N_3^-$, $^{18}O_2$, ^{16}O-^{18}O) is employed.

The magnitude and number of isotopic splittings observed in the Raman spectrum are very sensitive to ligand geometry. For instance, it has been determined by a mixed isotope experiment on metazido- and oxy- hemerythrin that the exogenous ligand occupies a nonsymmetrical position with respect to the two Fe atoms (see Chapter 5 for details).[63,64] By matching observed isotopic shifts with those calculated for various

geometric orientations of the exogenous ligand, it is possible to "home in" on the correct geometric environment of the ligand in the active site.

Method

Several general models can be constructed to illustrate the exogenous ligand environment in the active site of oxyhemerythrin (Figure 4-1). Analogous structures can be constructed for metazidohemerythrin. As mentioned earlier, Kurtz, et al. have experimentally determined that the ligand is bonded in a nonsymmetrical fashion with respect to the Fe atoms.[63,64] This eliminates structures I, II, and V as viable candidates for active site models. Of the three remaining possibilities, structure III can represent the previously proposed face-sharing bioctahedron model (depending on the Fe-O-Fe angle employed), while structure IV represents the μ-oxo bridged model proposed for metazidomyohemerythrin.

Figure 4-2 shows the parameters used for the μ-monooxygen bridged model in the isotopic shift calculations of oxyhemerythrin. The calculations were made using the Wilson GF matrix method, which is described in Chapter 2. Variations in the bonding geometry were accomplished by changing the angles ϕ, β, and γ. These angles were varied iteratively by a computer program, which is detailed in Appendix A. Figure 4-3 shows the parameters used for the μ-oxo bridged model. ϕ, β, and γ were varied as in the μ-monooxygen bridged model. The combination of angular parameters that yield calculated isotopic shifts which provide the best match to the observed Raman data should then describe the active site geometry in oxyhemerythrin.

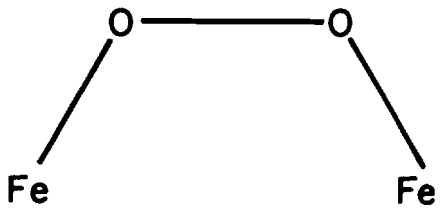

μ-peroxo bridged
(planar bridge)

I

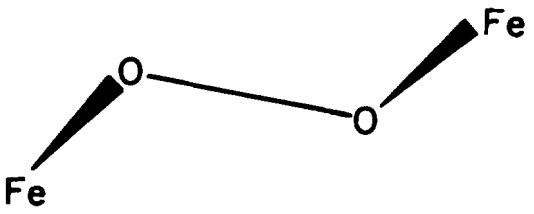

μ-peroxo bridged
(nonplanar)

II

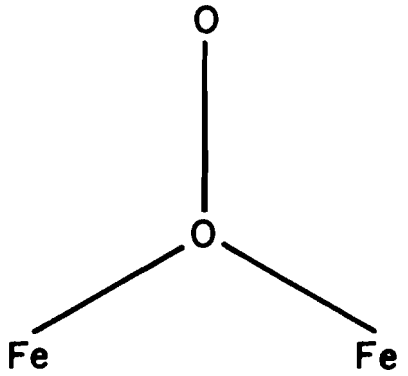

μ-monooxygen bridged

III

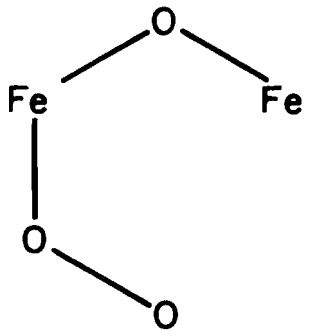

μ-oxo bridged

IV

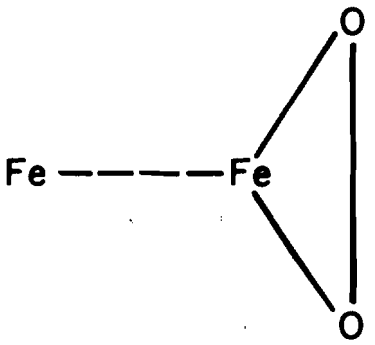

V side-bonded dioxygen

Figure 4-1. Models for the active site structure of oxyhemerythrin.

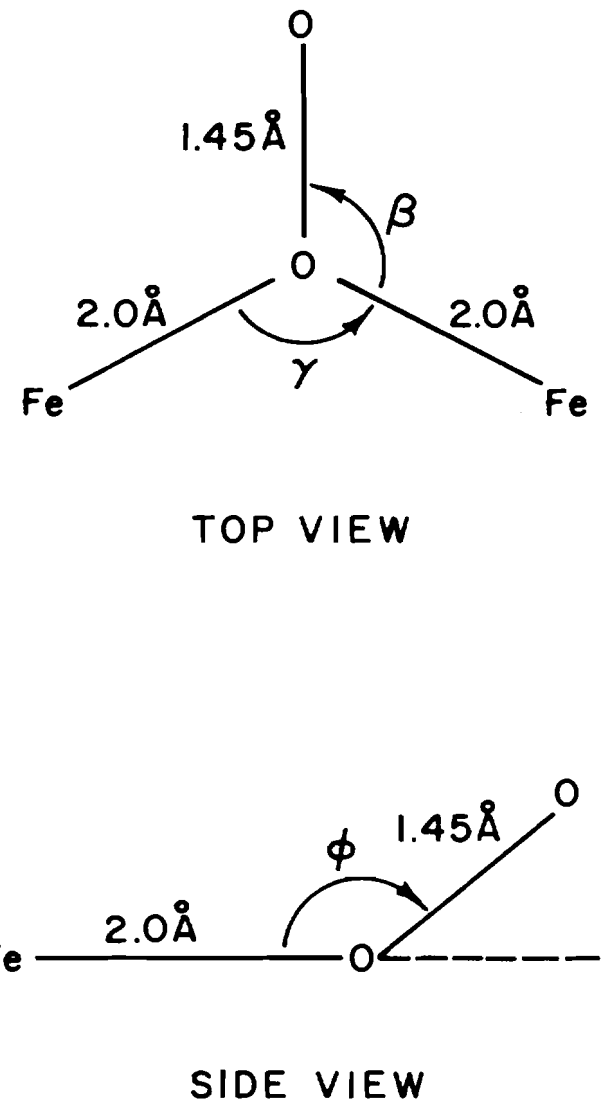

Figure 4-2. μ-Monooxygen bridged model. The structure represents a confacial bioctahedron when $\gamma = 70.5°$.

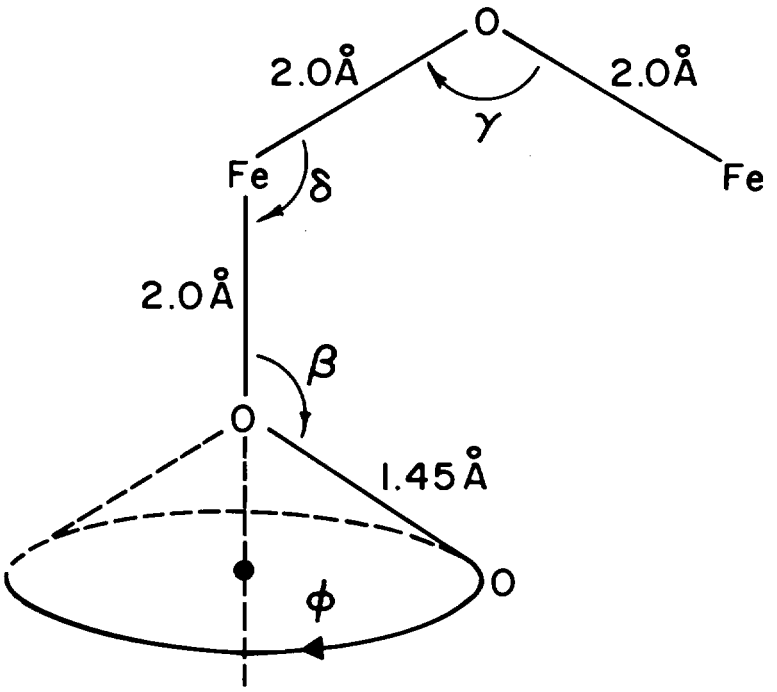

Figure 4-3. μ-Oxo bridged model.

Results and Discussion

Table 4-1 lists the observed isotopic shifts in oxyhemerythrin and Appendix B lists the complete sets of frequency calculations for the μ-monooxygen bridged and μ-oxo bridged models for oxyhemerythrin. Table 4-2 lists a summary of the model parameters which yield calculated vibrational frequencies closest to the observed experimental values for the μ-monooxygen bridged model.

The data summary clearly shows that there are many possible orientations which correctly predict the observed isotopic shifts. However, most of the favorable orientations obtained from ν(Fe-O) calculations do not match those obtained from the ν(O-O) calculations. This could be the fault of an inaccurate, or invalid force field. However, it will be seen in Chapter 5 that the general valence force field works very well for oxyhemocyanin so that there is no obvious reason why it should not also work satisfactorily for oxyhemerythrin. There are four geometries which result in calculated ν(Fe-O) and ν(O-O) frequencies which match the observed experimental values, and these are listed in Table 4-3. A ϕ value of 75° would place the O-O bond in an unfavorable location, because it would be close to an Fe-O bond, and also would place the terminal oxygen atom extremely close to either the aspartic acid or glutamic acid residue, which are probable iron ligands. However, a ϕ of 110° would be a more favorable geometry for the O_2 molecule, and this geometry is shown in Figure 4-4 for γ values of 110° and 120°. γ values of 110° and 120° would yield Fe-Fe distances of 3.28 Å and 3.46 Å, respectively. These distances are strikingly close

Table 4-1. Raman Frequencies (cm^{-1}) and Observed Isotopic Shifts (cm^{-1}) of Oxyhemerythrin.[a]

Mode	$^{16}O_2$	$^{18}O_2$	Isotopic Shift ($^{16}O_2$-$^{18}O_2$)	^{16}O -^{18}O	^{18}O -^{16}O	Isotopic Shift (^{16}O-^{18}O)-(^{18}O-^{16}O)
ν(O-O)	844	798	46	825	820	5
ν(Fe-O)	504	482	22	501	484	17

[a] Values taken from references 60a, 63 and 64.

Table 4-2. Geometric Parameters for the μ-Monooxygen Bridged Model which Best Predict the Observed Isotopic Splittings in Oxyhemerythrin.

Parameters for ν(Fe-O)			Parameters for ν(O-O)		
γ(deg)	β(deg)	φ(deg)	γ(deg)	β(deg)	φ(deg)
70.5	60	0-30	70.5	60	110-120
	70	0-20		70	80-90,120-140
	80	20-50		80	70-80,130,140
	120	100-110		90	60,120-130
	130	90-100		100	50-60,110-120
				110	40-60,100-110
90	70	110-120		120	40-90
	110	70			
	120	70-80	90	70	70-80,100-110
				80	60-70,110-120
110	60	100,150-160		90	60-70,110-120
	70	110-120		100	60-70,110-120
		170-180		110	70-80,100-110
	110	60-80			
	120	50,80	100	60	60-90
	140	0-10		70	60-70,100-110
				80	60,110-120
120	60	100		90	60,120
	70	110-120		100	60-70,120-130
	110	0-20,60-70		110	80,110-130
	120	20-30		120	90-120
	130	40,100			
			110	60	50-90
130	60	100-110		70	40-50,100-110
	70	130-180		80	50,110-120
	110	0-50		90	50-60,120-130
	120	0-30		100	60-70,130-140
	130	10-30		110	80,130-140
	140	0-40		120	90-140
140	60	90-100	120	60	0-40,70-90
	110	0-40		70	0-30,100-110
	120	70-80		80	30-50,120
	130	110-120		90	50-60,130-140
				100	60-70,140-150
				110	70,140-180
				120	100-180

Table 4-2 (continued)

Parameters for $\nu(0\text{-}0)$

γ(deg)	β(deg)	ϕ(deg)
130	60	0-10
	70	0-30,90-110
	80	0-40
	90	40-50,140-160
	100	60-70,170-180
	110	80-90
	120	100-120
140	60	60-80
	70	90-110
	80	120-150
	90	10-40
	100	50-60
	110	70-90
	120	100-130
	130	160-180

Table 4-3. Parameters which are Favorable for Both ν(O-O) and ν(Fe-O) Calculations, using the μ-Monooxygen Bridged Model.

γ(deg)	β(deg)	ϕ(deg)
110	70	110
	110	75
120	70	110
	110	70

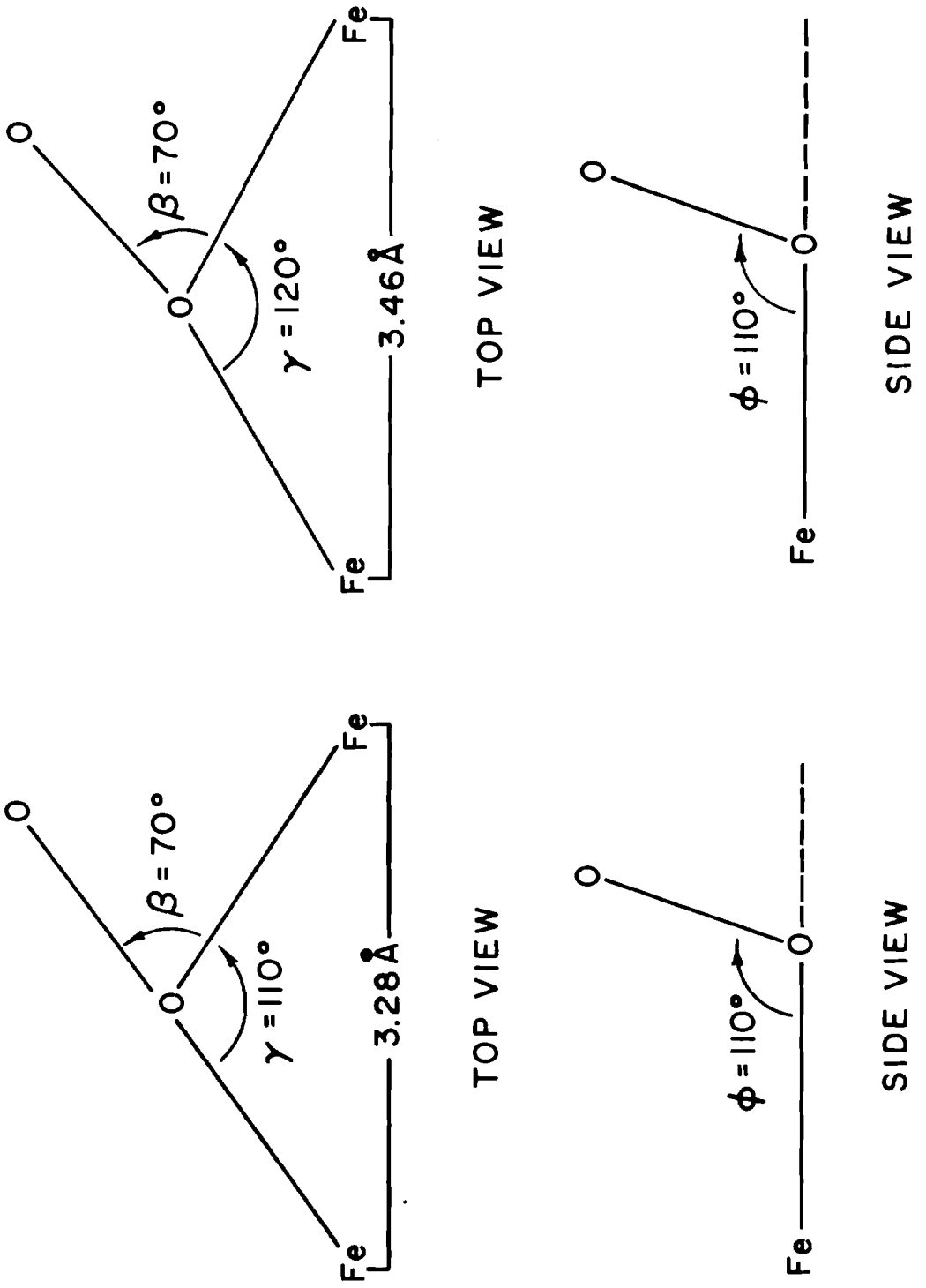

Figure 4-4. Favorable geometries for the active site of oxyhemerythrin using the μ-monooxygen bridged model. ϕ=110°, β=70°, γ=110°, 120°. In the side view, the two iron atoms are eclipsed.

to those obtained from X-ray crystallographic studies of metazidomyohemerythrin by Hendrickson and coworkers.[55] These models would eliminate a true confacial bioctahedron from consideration, since its Fe-Fe distance and Fe-O-Fe angle would be < 3 Å and 70.5°, respectively. However, these models do not eliminate a similar structure which would incorporate bridging oxygen atoms from aspartic acid or glutamic acid side chains, since slightly shorter Fe-O_2 bond distances would allow a larger Fe-O-Fe angle and a shorter Fe-Fe distance (Fe-Fe distances of 3.11 Å and 2.95 Å are obtained for Fe-O distances of 1.9 Å and 1.8 Å respectively, when $\gamma = 110°$). Table 4-4 summarizes the best geometries for the μ-oxo bridged model. The degree of isotopic splitting for ν(O-O) changes little with variations in ϕ, γ, α (Figures 4-3, 4-5). In addition, ν(Fe-O) is not sensitive to changes in these angles, except when $\gamma \leq 90°$. The insensitivity of these angles to geometric variations could be due to the fact that as γ becomes large (>90°) the O_2 moiety is further removed from the Fe-O-Fe framework, thus making variations of ϕ and γ less important. In the μ-monooxygen bridged model, the O_2 moiety is always situated close to (between) the two iron atoms, and ϕ and γ are very sensitive to geometric changes. The μ-oxo bridged model gives definite geometries only when $\gamma \leq 90°$. This angle is extremely small for a μ-oxo bridge, and no model complexes are known which have an Fe-oxo-Fe angle less than 130°. However, an angle of about 90° would be consistent with an O-R bridging group (R is some group bonded to the oxygen atom, such as an amino acid sidechain), thus the "oxo" bridge in the model may be more accurately described as a bridging group from an amino acid sidechain, probably asp 111 or glu 58.

An oxo bridge cannot be ruled out entirely, because the μ-oxo bridged model does give favorable β values, even though ϕ is insensitive to changes. In all the favorable geometries for the μ-oxo bridged model, β≈68° or β≈115°. These values for β are the same as those predicted for the μ-monooxygen bridged model, and also the same as those predicted for oxyhemocyanin (Chapter 5). Thus, the angle which the O_2 moiety makes with the Fe...Fe axis (coplanar) seems to be a very important parameter in these models.

It is difficult to say which geometry is "best" for the μ-oxo bridged model when $\gamma \neq 90°$, because of the insensitivity of ϕ. The best parameters are $\phi = 70°\text{-}130°$, $\beta = 70°$ (Fig. 4-6A), and $\phi = 80°\text{-}110°$, $\beta = 110°$ (Fig. 4-6B), for γ close to 90°.

Conclusion

The most probable geometries shown in Figure 4-3 and Figure 4-6 for the μ-monooxygen and μ-oxo bridged models, respectively, are very similar. This is to be expected, because the μ-oxo model with $\gamma = 90°$ becomes essentially a μ-monooxygen model with an additional oxygen bridge. The addition of a third oxygen bridge should not alter the favored geometry significantly due to the insensitivity of α rotation (Figure 4-5).

It is interesting to note that of all the possible parameters studied for the μ-oxo model, the best results were obtained when $\gamma = 90°$. This would indicate that it is very important that the oxygen, which is bonded to the iron, be located equidistant from both Fe atoms,

Table 4-4. Geometric Parameters for the μ-Oxo Bridged Model which Best Predict the Observed Isotopic Splitting in Oxyhemerythrin.

γ(deg)	β(deg)	ϕ(deg)[a]	γ(deg)	β(deg)	ϕ(deg)[a]
70.5	130	60-120	70.5	68	*
				115	
90	68	70-130			
	110	80-110	90	68	*
				110	*
100	68	*			
	120	*	100	68	*
				110	*
110	68	*			
	120	*	110	68	*
				115	*
120	68	*			
	120	*	120	68	*
				115	*
130	68	*			
	120	*	130	68	*
				115	*
140	68	*			
	120	*	140	68	*
				115	*

[a] * indicates that the isotopic splitting was insensitive to changes in the angle ϕ.

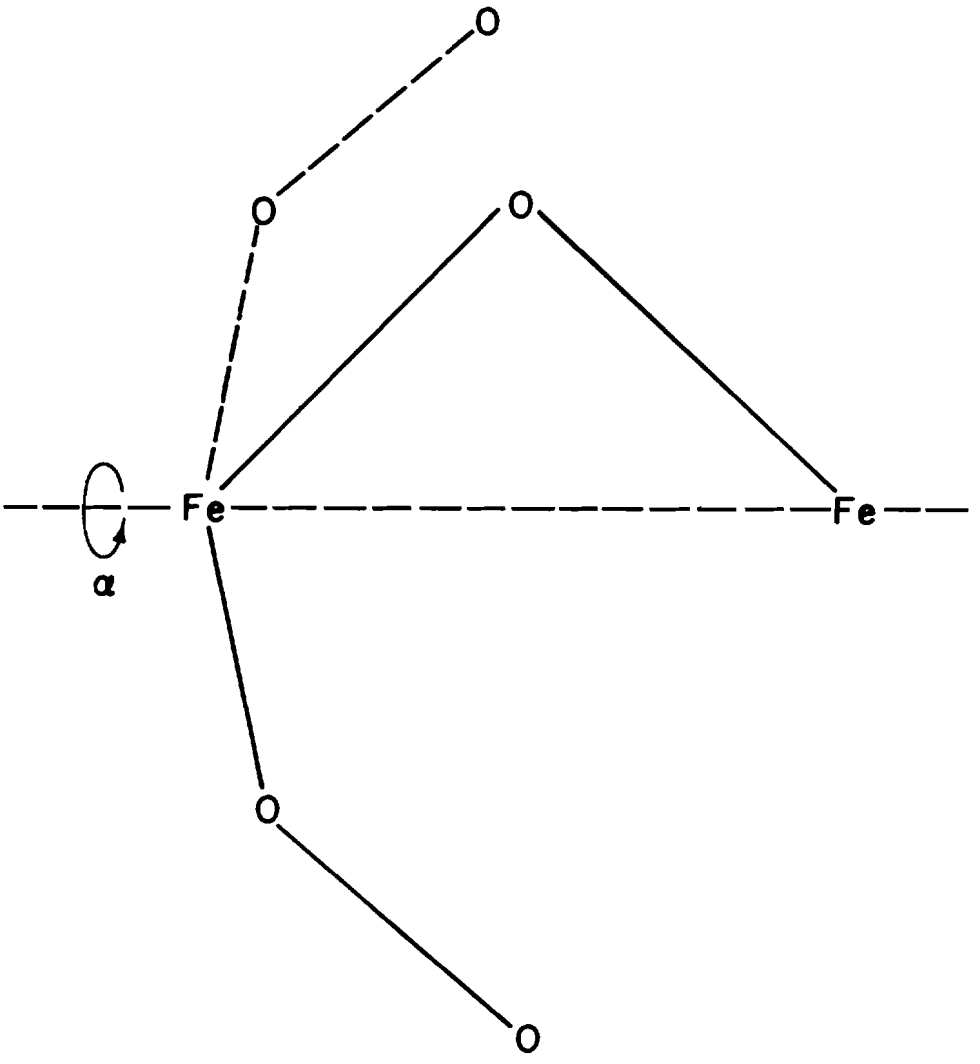

Figure 4-5. Rotation of O_2 α-degrees with respect to the Fe-O-Fe plane.

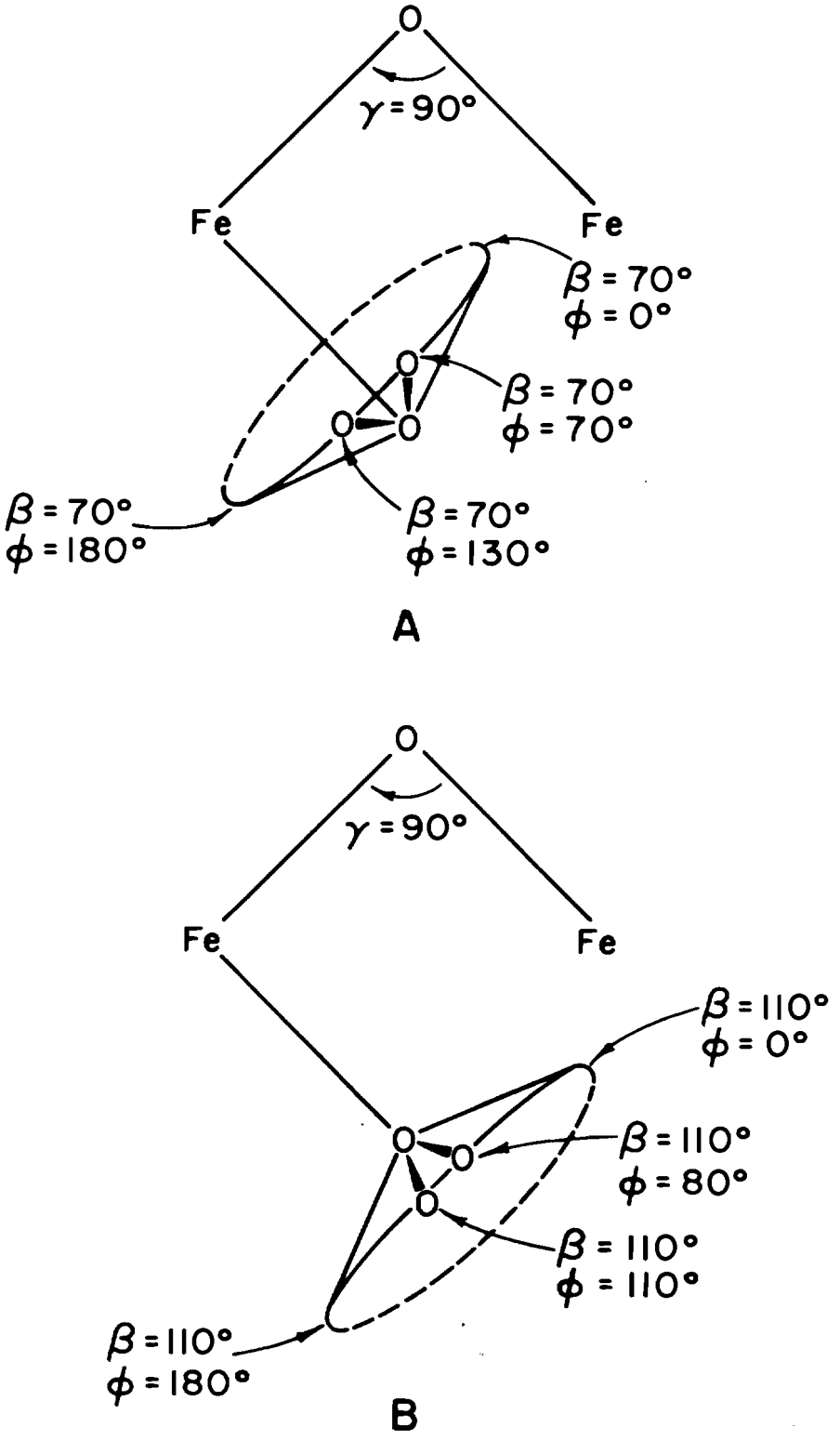

Figure 4-6. Most favorable geometries for the μ-oxo bridged model for oxyhemerythrin. The O_2 positions shown are the outer limits for a range of favorable geometries (see Table 4-4 for the favorable ranges).

as it is when $\gamma = 90°$. If this oxygen atom is equidistant from both Fe atoms, it is likely that it is bound to both irons, thus the μ-oxo bridged model itself suggests that the μ-monooxygen bridged model is the more realistic. This does not rule out the existence of an oxo bridge. Using the μ-monooxygen model with $\gamma = 115°$, an oxo bridge can be added that yields an Fe-oxo-Fe angle of 140° (Fe-oxo distance is 1.8 Å), which is within the range of Fe-oxo-Fe angles observed in oxo-bridged iron dimer complexes.[65,66] The addition of an oxo bridge to the favored geometry for the μ-monooxygen model did not significantly alter the calculated frequencies. Thus, the combined results obtained for the μ-oxo, and μ-monooxygen bridged models predict the structure shown in Figure 4-7 to be a likely candidate for the active site in oxyhemerythrin. This structure would require an Fe-Fe distance of 3.28 Å, $\gamma = 110°$ to 3.46 Å, $\gamma = 120°$, which is in the range of those observed from the crystallographic studies mentioned earlier for a μ-oxo bridged model.[55] However, as previously mentioned, slightly shorter Fe-O distances would significantly reduce the Fe-Fe distance and result in a model extremely close to that proposed by Stenkamp and coworkers.[54] Therefore, the present study cannot definitively state which, if either, crystallographic model most accurately describes the active site of oxyhemerythrin. However, the calculations do strongly suggest that the O_2 molecule is bound to both iron atoms through one oxygen atom.

One might expect the dioxygen molecule to bind at approximately tetrahedral angles to the iron atoms ($\phi = \beta = 109°$). The ϕ value of $\sim 110°$ is nearly tetrahedral, but a $\beta \sim 70°$ places the O_2 slightly

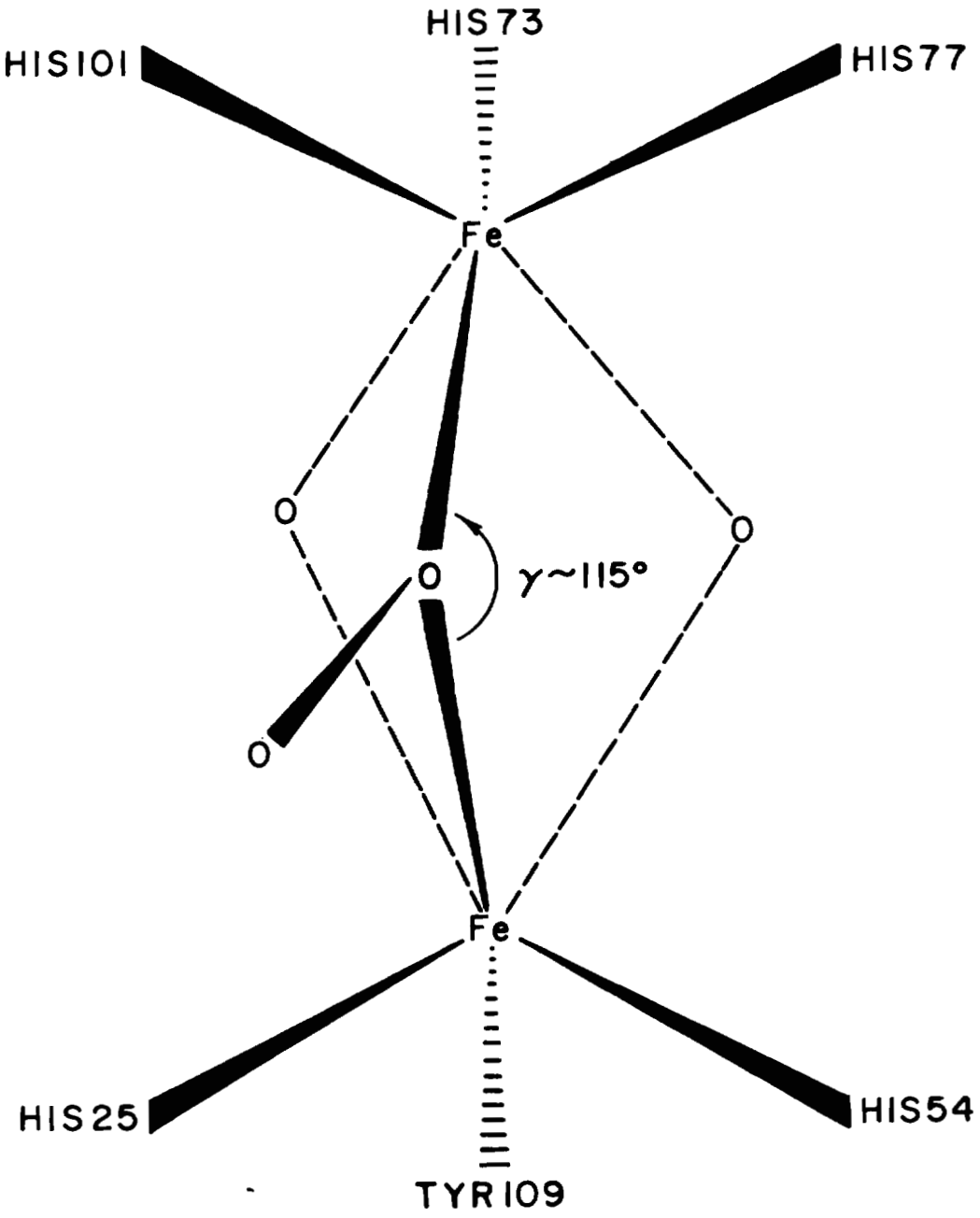

Figure 4-7. Model for the active site of oxyhemerythrin. The angle Fe-O-O (β) = 70° and the angle O_2 makes with the Fe-O-Fe plane (ϕ) $\sim$ 110°. The dotted lines indicate that asp 106, glu 58, or an oxo bridge may be bound to either or both iron atoms.

closer to a histidine ligand (in the true bioctahedron the iron ligands are eclipsed). One possible explanation is hydrogen bonding between the bound peroxide and protein, which would require the terminal oxygen atom to move closer to the protein backbone. This would explain the Mössbauer data, which indicates equivalent iron environments in deoxy- and met- hemerythrin, but nonequivalent irons in oxyhemerythrin.[50,51] Support for protonation of the bound peroxide comes from observations that replacement of H_2O by D_2O in oxyhemerythrin causes shifts in peroxide-related vibrational frequencies in the resonance Raman spectrum.[46] Another explanation may be that the model used for the calculations was inadequate. Possibly the addition of the histidine and tyrosine ligands, plus the incorporation of repulsion force constants between nonbonded atoms (Urey-Bradley force field) would yield slightly different favorable geometries. It should also be mentioned that different Fe-O bond lengths would alter the Fe-Fe distance, and possibly alter the geometry which best predicts the experimentally observed isotopic splitting. In addition, it is possible that a different force field would have yielded different results for the μ-oxo bridged model. However, it is felt that it is more important to be consistent with all models, and that if slightly different bond lengths or force fields were used consistently the results would be essentially the same.

CHAPTER 5

HEMOCYANIN

Introduction

Hemocyanin is an oxygen carrying copper protein found in arthropods (crabs, crawfish, lobsters) and molluscs (snails, squids, octopus).[67] The functional subunit of the protein binds one dioxygen molecule per two copper atoms,[68-70] and electron microscopic studies have revealed that the protein exists in highly aggregated forms.[71-73] Native hemocyanin is extremely large with a molecular weight of approximately 3×10^6 - 20×10^6 Daltons;[74] the average subunit weight is about 25,000 - 75,000.

Oxyhemocyanin has a blue color and optical absorption bands at about 280, 346, and 580 nm.[74] The 280 nm band is a protein band, and the two lower energy absorptions are copper-related. These copper bands are optically active and the CD spectra are remarkably similar to the Cu(II) complex of Ac-Gly-Gly-His,[75,76] which indicates the presence of a nitrogen ligand(s), probably an imidazole nitrogen(s) from a histidine residue(s). EPR results[77,78] support this, and the results of photooxidation show that the copper bands are destroyed at the same rate as the histidines.[79,80]

Resonance Raman spectroscopy has been used to determine the electronic state of the dioxygen moiety of oxyhemocyanin as peroxide-like, due to the low O_2 stretching frequency (749 cm^{-1}).[81] A peroxide-type dioxygen ligand suggests a cupric state for the copper atoms.

However, oxyhemocyanin is diamagnetic, which would necessitate that the cupric atoms be antiferromagnetically coupled.[77,82-84] Indeed, EPR studies of methemocyanin in the presence of N_3^- showed that the binuclear Cu pair were uncoupled in two discrete steps, (1) from strongly antiferromagnetic coupling to magnetic dipole-dipole coupling, accompanied by a separation of the copper atoms, to (2) completely uncoupled cupric ions.[85] Magnetic susceptibility measurements on oxyhemocyanin have revealed that the coupling is extremely strong and have set a lower limit for the coupling constant, J, at 550 cm^{-1}.[86]

The mode of uncoupling of the cupric ions, mentioned above in the N_3^- EPR experiment, would suggest the presence of an endogenous bridge between the metal atoms. Additional evidence for an endogenous bridge has come from the studies of Himmelwright, et al., on half-met-L and met-apo-L hemocyanin derivatives (L is a series of anionic ligands, eg. CN^-, N_3^-, SCN^-, halides).[87] The half-met protein contains a (Cu(II)..Cu(I)) center, and the met-apo form has a (Cu(II)..( )) active site. The experiments on these two forms revealed that ligands bind far more tightly to the half-met form, thereby supporting an exogenous bridge. It was also found that an additional coordination position is available at the Cu(II) site for only certain half-met-L-derivatives, namely when L = CN^-, N_3^-, and SCN^-. These ligands are expected to keep the copper atoms more than 5 Å apart, possibly breaking the endogenous bridge. Further support comes from the observation that no second coordination position is found for the met-apo-L derivatives. Finally, EPR studies on the met-apo, half-met, met, and dimer active sites of hemocyanin have indicated that there are both exogenous, and endogenous

bridges in the oxyhemocyanin active site and that this site contains a pair of tetragonal, magnetically-coupled Cu(II) atoms, with the lack of an EPR signal due to coupling through the protein (endogeneous) bridge.[88,89]

As with hemerythrin, not much is known about the mode of binding of the dioxygen molecule in oxyhemocyanin. As mentioned above, Freedman, et al., verified the dioxygen's peroxide-like electronic structure, using resonance Raman spectroscopy.[81] Excitation profiles from these experiments were used to assign CD bands at 490 and 570 nm to $O_2^{2-} \rightarrow$ Cu(II) charge transfer, which lead to a molecular orbital scheme that predicted a nonplanar Cu-O_2-Cu active site of C_2 symmetry for oxyhemocyanin (Figure 5-1). Several additional model structures can be constructed which account for the magnetic parameters of oxyhemocyanin, as shown in Figure 5-2. In an elegant experiment, Kurtz and coworkers inserted an unsymmetrically labeled dioxygen molecule into deoxyhemerythrin to determine that the oxygen atoms were located in inequivalent positions at the iron center, thus eliminating several possible active site geometries.[63] This experiment has now been applied to oxyhemocyanin, however, with drastically different results.[90] In addition, theoretical calculations of mixed isotopic splitting, similar to those in the previous chapter, have been carried out in an attempt to further define the active site geometry for oxyhemocyanin.

Method

Much information can be gained about the oxygen environment in oxyhemocyanin when an unsymmetrically labeled (mixed isotope)

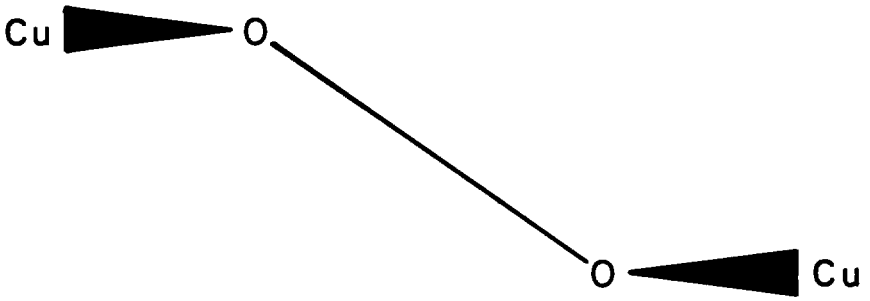

Figure 5-1. Nonplanar μ-dioxygen bridge model for the active site of oxyhemocyanin.

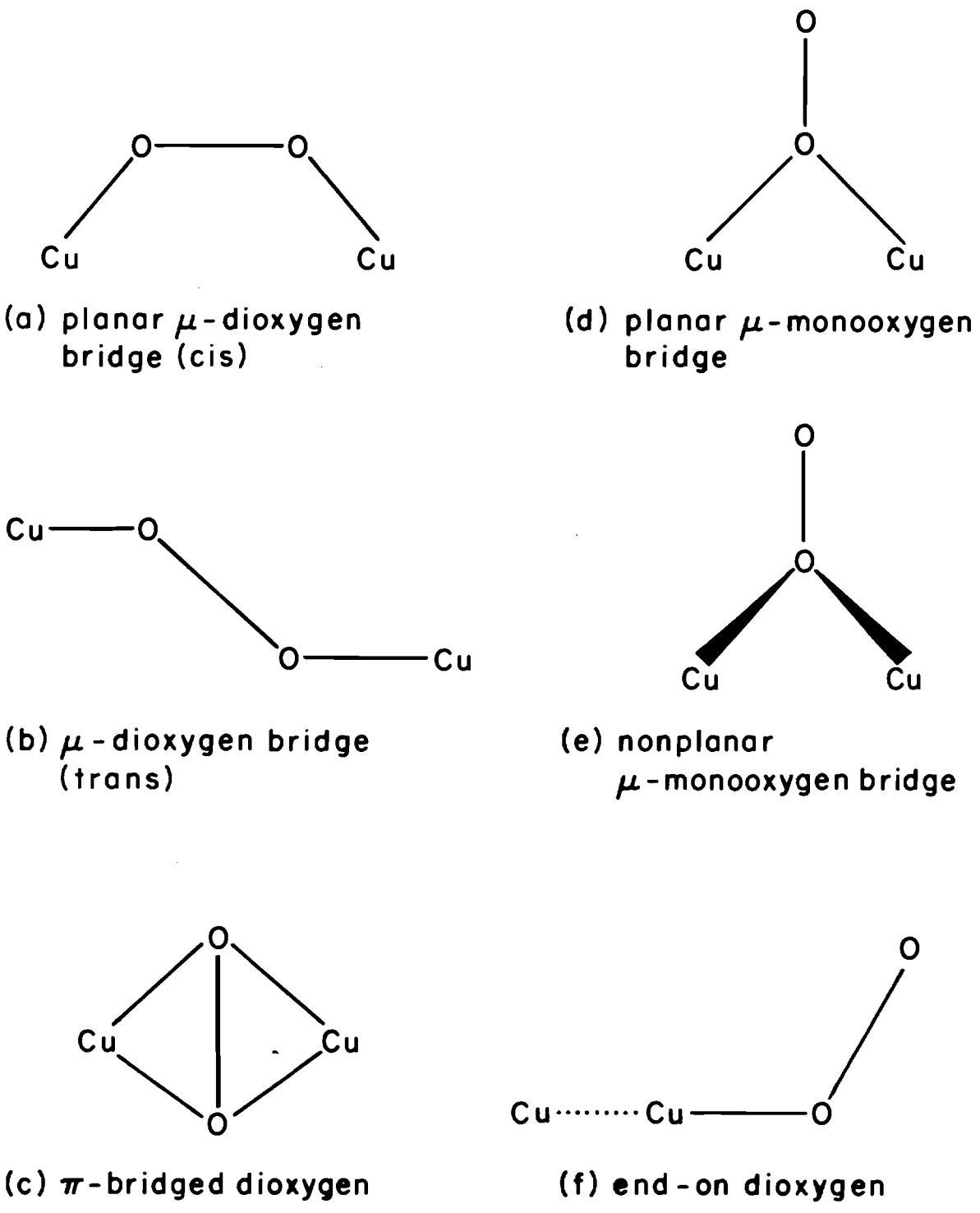

Figure 5-2. Possible models for the active site of oxyhemocyanin.

molecule is inserted into deoxyhemocyanin. Figure 5-3 shows the Raman spectrum of such an isotopic mixture of oxygen gas. The highest and lowest energy peaks correspond to the stretching modes of $^{16}O_2$ and $^{18}O_2$ respectively, and the large central peak is the O_2 stretching band for the mixed isotope ^{16}O-^{18}O. Since the gas mixture is 55.11 atom % ^{18}O, one would expect the peaks corresponding to $^{16}O_2$, ^{16}O-^{18}O, and $^{18}O_2$ to exhibit intensity ratios of 0.66:1.63:1.00, respectively. The measured intensity ratios[91] of 0.71:1.63:1.00 are in excellent agreement with the expected values. The full band widths at half-maximum intensity of the three peaks were 8.3, 7.6 and 7.3 cm^{-1} (± 0.5 cm^{-1}), respectively.

If the oxygen atoms in oxyhemocyanin are in equivalent positions with respect to the Cu atoms (Figure 5-1, Figure 5-2(a)-(c)), the peroxide stretching region of the Raman spectrum should exhibit three absorption bands corresponding to the $^{16}O_2^{2-}$, $(^{16}O$-$^{18}O)^{2-}$, and $^{18}O_2^{2-}$ stretches, and the intensity ratios should be identical to those of the free O_2 gas mixture. If, however, the oxygens are in nonequivalent positions (Figure 2(d)-(f)) the ^{16}O-^{18}O peak should be split into two bands of equal intensity, one corresponding to a Cu-^{16}O-^{18}O structure where ^{16}O is bonded to a Cu atom, and one to a Cu-^{18}O-^{16}O structure. As mentioned earlier, Kurtz and coworkers found a split mixed isotope O-O stretching peak in the Raman spectrum of oxyhemerythrin, indicating a nonequivalent environment for the oxygen atoms in the iron protein.

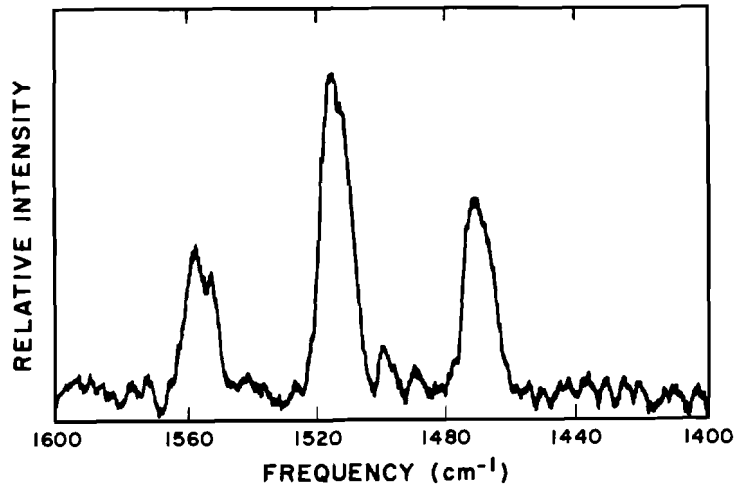

Figure 5-3. Raman spectrum of 55.11 atom % ^{18}O gas mixture. Excitation wavelength is 5145 Å, scan rate is 1.0 $cm^{-1}sec^{-1}$, spectral slitwidth is 8.0 cm^{-1}, and the scattered light was collected at 90 deg. to the incident radiation. The spectrum is an averaged sum of 12 individual scans.

Results and Discussion

I. Resonance Raman Spectrum of Oxyhemocyanin with Unsymmetrically Labeled Oxygen.

Figure 5-4 shows the 0-0 stretching region in the resonance Raman spectrum of Busycon canaliculatum hemocyanin, which has been oxygenated with a 55.11 atom % ^{18}O gas mixture. The spectrum shows peaks at 749, 728, and 708 cm^{-1}, with relative intensities, based on peak heights, of 0.66:1.63:1.00. The relative intensities are in excellent agreement with those mentioned earlier for the free gas. The measured peak widths are 16.8, 14.5 and 12.5 cm^{-1}($\pm$ 1 cm^{-1}), respectively, for the spectrum obtained with 10.0 cm^{-1} slits and 15.0, 11.7, and 9.9 cm^{-1} ($\pm$ 1 cm^{-1}), respectively, for a spectrum recorded with 6.0 cm^{-1} slits. The greater width of the 749 cm^{-1} peak is due to its overlap with a 760 cm^{-1} vibrational band of the protein backbone, that was revealed in a previous resonance Raman experiment with $^{18}O_2$ B. canaliculatum oxyhemocyanin.[81] This $^{18}O_2$ oxyhemocyanin study also revealed a peak at 749 cm^{-1} in the native protein which shifted to 708 cm^{-1} upon $^{18}O_2$ incorporation. These peaks were assigned to the 0-0 stretching modes for bound $^{16}O_2$ and $^{18}O_2$, respectively.

The excellent agreement in peak intensity ratios from protein and gaseous samples strongly suggests that only one species contributes to the 728 cm^{-1} peak in oxyhemocyanin. However, a curve-fitting analysis of 10 cm^{-1} slit resolution Raman peaks shows that a splitting of 3 cm^{-1}, or less, would not have been detectable in the intensity ratios.

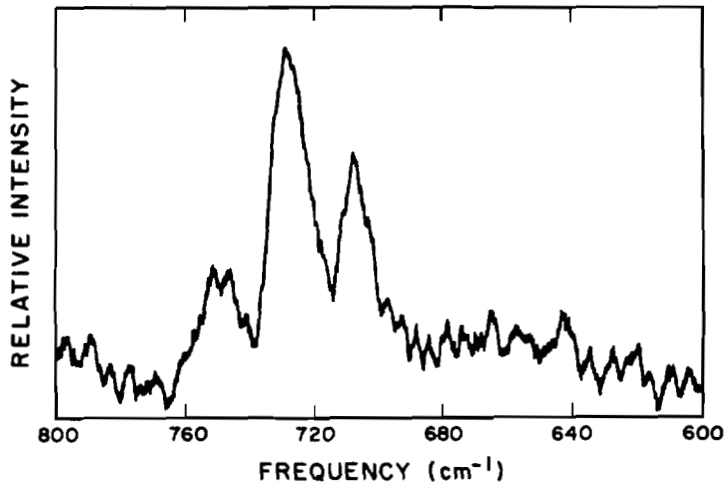

Figure 5-4. Resonance Raman spectrum of Busycon canaliculatum hemocyanin, which has been oxygenated with 55.11 atom % ^{18}O. Excitation wavelength is 5309 Å, scan rate is 0.5 $cm^{-1}sec^{-1}$, spectral slitwidth is 10 cm^{-1}, and the scattered light was collected at 180 deg. to the incident radiation. The spectrum is an averaged sum of 50 individual scans.

II. Favorable Geometries for the Active Site as Determined by Wilson GF Calculations.

It is possible the oxygens are not spectroscopically equivalent, and there is an isotopic split of 3 cm^{-1} or less in the 728 cm^{-1} peak. This can be tested by utilizing the Wilson GF matrix method for calculation of the O-O stretching frequencies in several test structures of the active site. This method is described in detail in Chapter 2 and Appendix A. Figure 5-5 shows the molecular models used; the angles β, ϕ, and γ were varied as in the preceding chapter. The peaks at 749 and 708 cm^{-1} were used to derive a set of peroxide force constants, and the resulting refined force field was used to calculate the O_2 stretching frequency (or frequencies) for the mixed isotope oxygen molecular ion 728 cm^{-1} peak. The force field used was the general valence model which neglects repulsive forces between nonbonded atoms (it has been found in this laboratory and elsewhere[92] that neglecting the repulsive, or interacting forces, between nonbonded atoms makes little difference in the calculated frequencies for these molecular models).

Table 5-1 summarizes the most favorable geometries, those which exhibit a mixed isotopic splitting $\leq$ 3 cm^{-1}. The entire set of data are listed in Appendix C in both tabular and graphical forms. Table 5-1 shows that for the μ-monooxygen model only β values between 70° and 110° give splitting $\leq$ 3 cm^{-1}. If the copper atoms in this model are placed 3.6 Å apart, as reported from EXAFS studies, the Cu-O-Cu angle is 128°, and a β angle of 116° (ϕ = 180°) would place each oxygen atom equidistant from each copper atom. Figures 5-2(d) and

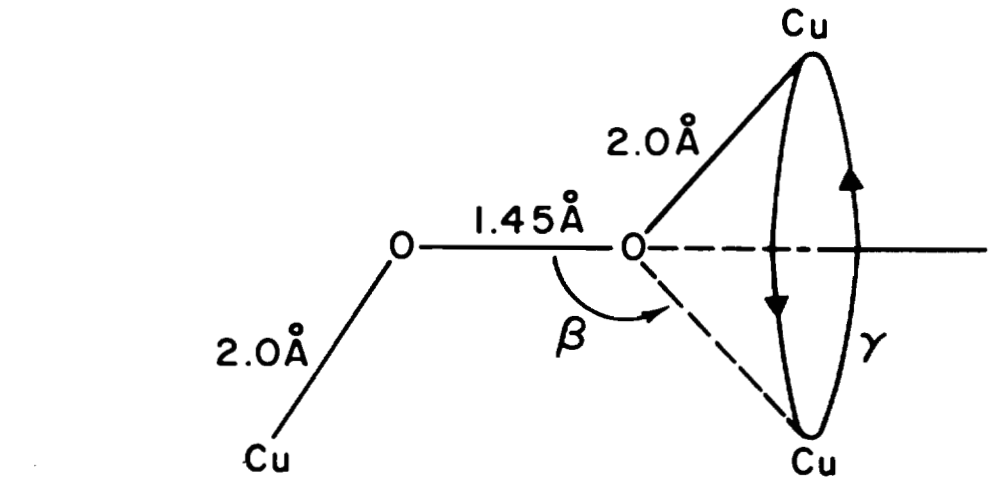

μ - dioxygen bridge

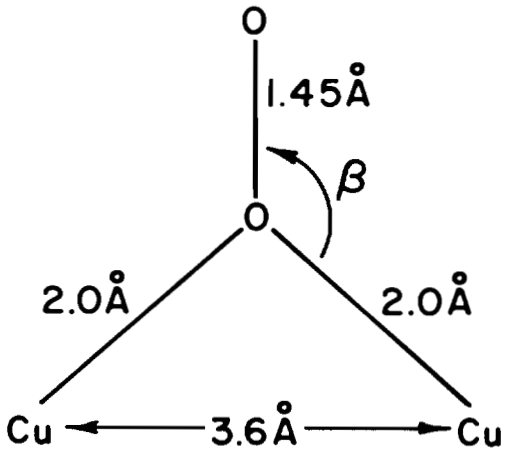

μ-monooxygen bridge
(β = 60°-140°)

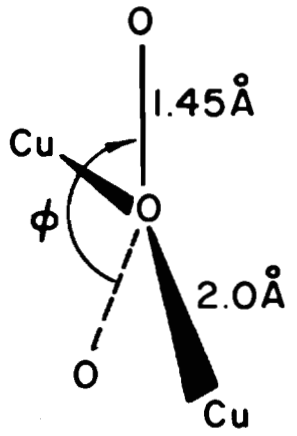

μ-monooxygen bridge
(side view showing α
rotation. (ϕ = 0°-180°)

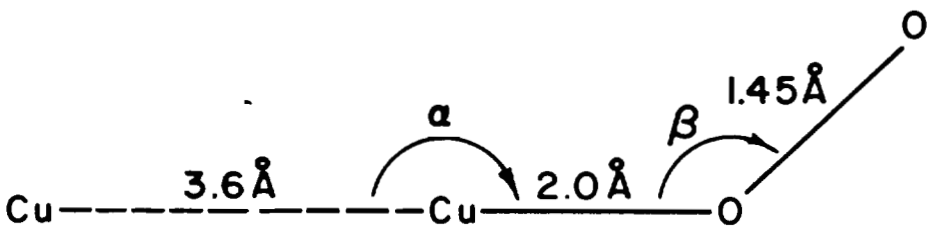

end-on dioxygen
(α = 45°-180°, β = 60°-140°)

Figure 5-5. Molecular models used in the isotopic splitting calculations.

Table 5-1. Angular Parameters which Result in Mixed Isotopic Splitting $\leq 3\ cm^{-1}$.

Model	β(deg)	ϕ(deg)
μ-monooxygen bridge	60	no splitting $\leq 3\ cm^{-1}$
	70	52-90
	80	52-110
	90	58-122
	100	70-128
	110	89-128
	120	no splitting $\leq 3\ cm^{-1}$
	130	no splitting $\leq 3\ cm^{-1}$
	140	no splitting $\leq 3\ cm^{-1}$
end-on dioxygen	60-125 β angles < 60° were not examined	
μ-dioxygen bridge	all values of β and γ gave zero splitting, with a $\nu_s(^{16}O\text{-}^{18}O)$ identical to that experimentally observed.	

5-2(e) show this arrangement. As shown in Figure 5-6, all favorable β values are less than 116°, which would result in the peroxide being shifted closer to one copper atom, as was found to be the case with the μ-monooxygen model for oxyhemerythrin (Chapter 4). ϕ values less than $\sim$ 90° would be unfavorable, since the resulting geometry would place the terminal oxygen extremely close to a copper atom. The most favorable parameters for the μ-monooxygen bridged model are β = 70°-110° and ϕ = 90°-128°; these are shown in Figure 5-6.

Calculations on the end-on binding model revealed that favorable geometries were obtained when β = 60°-125°. β angles of less than 90° are unlikely, due to repulsion factors and the fact that oxygen generally bonds at approximately tetrahedral angles. Variations of α made no difference in the calculations, probably because the two copper atoms were treated as though they were not bonded together, thus α becomes relatively meaningless. Figure 5-7 shows that the most likely geometry for the end-on dioxygen bound model is one where β angles vary between 90° and 125°, with values nearest 125° being the most likely.

The μ-dioxygen model showed no isotopic splitting, which is what one would expect for spectroscopically equivalent oxygen atoms. The calculations also predicted a $\nu(^{16}O-^{18}O)$ at 728 cm^{-1}, in <u>exact agreement</u> with experimental results, which justifies the validity of using a general valence force field in the solution of the secular equation. Considering the Cu-Cu distance of 3.6 Å, Cu-O and O-O distances of 2.0 Å and 1.45 Å respectively, and a Cu-O-O bond angle of 120°, the most likely geometry for this model is one in which the second

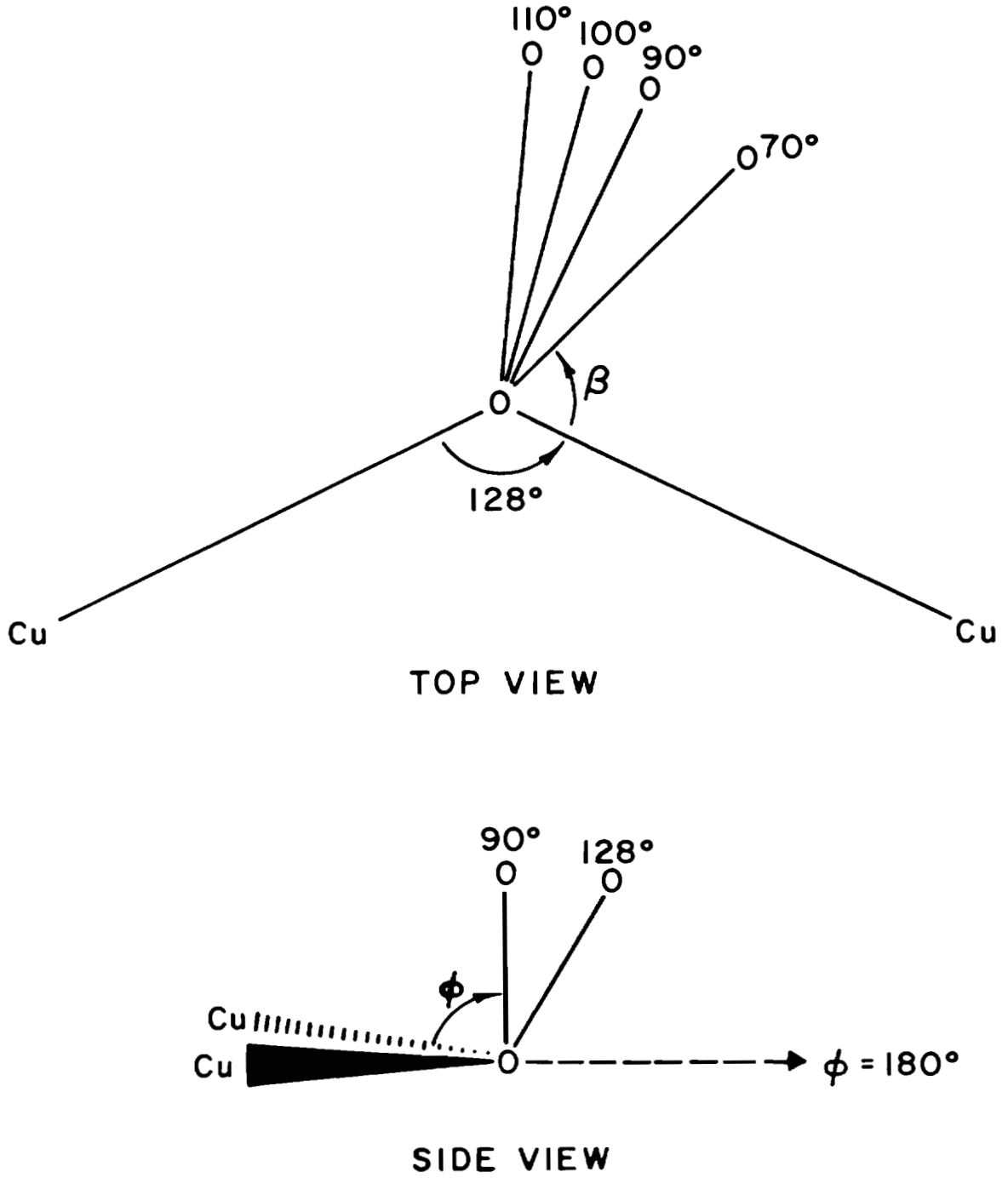

Figure 5-6. Most favorable geometries for the μ-monooxygen model.

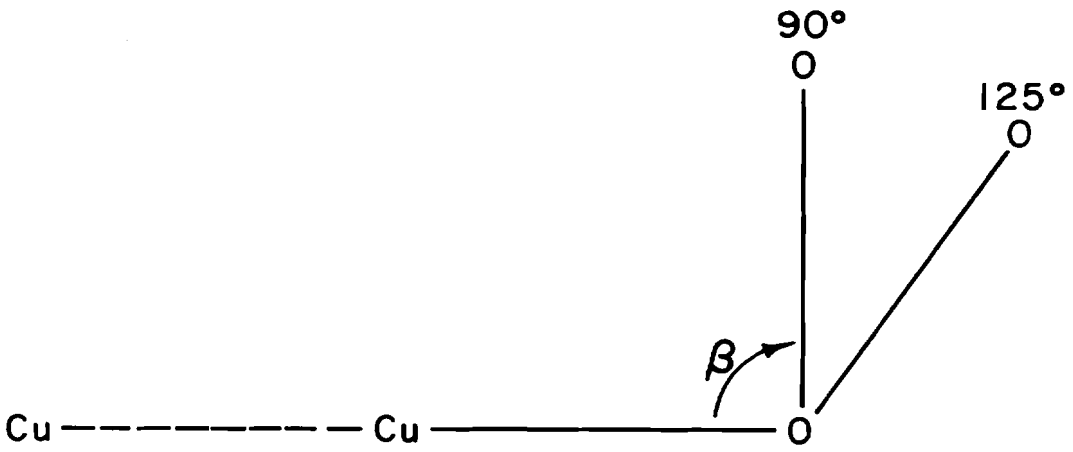

Figure 5-7. Most favorable geometry for the end-on dioxygen bound model. The favorable values of β range from 90°-125°.

Cu atom is 35° out of the Cu-O-O plane (each Cu is 17.5° above and below a line running through the O_2 bond) as shown in Figure 5-8.

Conclusion

Although one cannot conclude which of these possible models truly represents the active site of oxyhemocyanin it must be noted that the end-on model does not have the exogenous bridge required by the studies of Himmelwright and coworkers.[88,89] Both the μ-peroxo and μ-monooxygen models have exogenous bridges and O_2 geometries which will correctly predict the observed Raman data, however, the μ-monooxygen model has similar O_2 geometries which predict the observed isotopic splittings for both oxyhemerythrin and oxyhemocyanin ($\beta = 80°$, $\phi = 110°$) even though significantly different isotopic splittings are observed for the two proteins (ν(O-O) split 5 cm^{-1} for oxyhemerythrin). These geometries also predict metal-metal distances for both proteins which come extremely close to those observed in EXAFS and X-ray crystallographic studies. It is unfortunate that no ν(Cu-O) peaks have been observed for oxyhemocyanin, since they could be compared with calculated ν(Cu-O) frequencies, thus further reducing the number of favorable geometries, and possibly indicating one geometry which would be more favorable than all others.

Possibly the most important lesson to be learned from the calculations on oxyhemocyanin are illustrated in Figure C-1 of Appendix C. This graph shows the mixed isotopic splittings calculated for all the μ-monooxygen model geometries examined. There are an incredible number of geometries which yield a splitting ≤ 3 cm^{-1}, and most of these

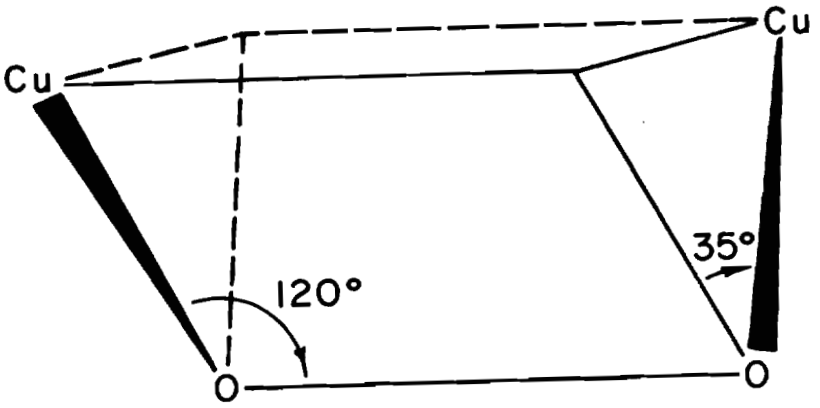

Figure 5-8. Favorable geometry for the μ-dioxygen bridged model.

exhibit a splitting very close to zero, even though the resulting geometries place the two oxygen atoms in symmetrically nonequivalent positions with respect to the coppers. This is unfortunate, because even with a higher resolution spectrum of oxyhemocyanin, one could not rule out the μ-monooxygen model, although many possible geometries could be eliminated.

CHAPTER 6

EXPERIMENTAL

I. Preparation and characterization of the Cu(II), (III) complexes of biuret and oxamide.

The Cu(II) complex of biuret, potassium bis(biuretato)cuprate-(II) dihydrate, $K_2[Cu(bis)_2]\cdot 2H_2O$, was synthesized by a previously reported method.[14] Some difficulty was encountered in obtaining pure crystalline material so the following method of crystallization was employed. Absolute ethanol was added dropwise to the red-violet reaction mixture of 0.005 mole $Cu(OAc)_2$, 0.01 mole biuret, 3 g KOH, and 20 ml abs. EtOH. A white material began to precipitate and the solution was filtered, abs. EtOH was added dropwise, yielding more white precipitate, which was again filtered out of solution. This procedure was repeated until no more white precipitate formed. Continued addition of EtOH resulted in precipitate of a violet-colored material, which was removed by the same method used for the white precipitate. Finally, the characteristic rose red crystalline material of $K_2[Cu(biu)_2]\cdot 2H_2O$ formed. This product was filtered, washed with abs. EtOH, and dried <u>in vacuo</u> over $CaSO_4$. The product exhibited a band at 505 nm which is characteristic of $K_2[Cu(biu)_2]\cdot 2H_2O$, and has an infrared spectrum identical to that obtained by Nakamoto and coworkers.[14] The white precipitate was determined to be unreacted biuret, and an infrared spectrum of the violet material proved it to be the hydroxy-bridged

Cu(II) biuretato dimer, $K_2[[Cu(biu)(OH)]_2]\cdot 4H_2O$, which was characterized by McLellan, et al.[93]

Potassium bis(oxamidato)cuprate(II), $K_2[Cu(ox)_2]$ was prepared in DMSO as previously described and the product has an infrared spectrum identical to that previously reported for the compound.[5]

Potassium bis(biuretato)cuprate(III), $K[Cu(biu)_2]$ was prepared chemically, using $K_2S_2O_8$ as an oxidizing agent, and electrochemically as previously reported.[17] The brown product has no EPR signal and an infrared spectrum identical to the one obtained by Bour, et al., for $K[Cu(biu)_2]$.

Potassium bis(oxamidato)cuprate(III), $K[Cu(ox)_2]$, was prepared electrochemically as previously described.[17] In addition this compound was obtained by chemical oxidation of $K_2[Cu(ox)_2]$, by adding an excess of $K_2S_2O_8$ to a slurry of $K_2[Cu(ox)_2]$ in DMSO. The mixture was stirred for four hours at room temperature, and then allowed to stand overnight. On standing, the mixture changed from a light red to a yellow-green color. The solid product was filtered, washed with hot distilled water 10 times, and dried in vacuo over $CaSO_4$. The resulting product showed no EPR signal and an infrared spectrum identical to that previously reported for $K[Cu(ox)_2]$.[17]

All chemicals used were reagent grade. Infrared spectra were obtained on a Perkin-Elmer model 621 grating infrared spectrophotometer. Samples were prepared as potassium bromide pellets and Nujol mulls on cesium iodide plates. The spectra shown are those of the KBr pellets. Raman spectra were obtained on a modified Jarrell-Ash model 25-300 spectrophotometer equipped with an RKB, Inc. digital grating drive and an

ITT FW 130 photomultiplier, all interfaced to a Computer Automation 24k minicomputer and peripherals. The operation of the instrument has been detailed elsewhere.[94] A Coherent Radiation CR-04 argon ion laser and a Spectra Physics Model 164 krypton ion laser were used for excitation of Raman spectra. Laser light was passed through narrow band pass interference filters to eliminate plasma lines. EPR spectra were obtained at room temperature on a Varian E-3 EPR Spectrometer.

II. Preparation of Busycon canaliculatum hemocyanin

The B. canaliculatum hemolymph was centrifuged at 12,000 g for 10 min. The sedimented material was then lightly pelleted by centrifuging at 640,000 g for 10 minutes. These pellets were gently dissolved in distilled water and concentrated (3 mM Cu) through a Millipore Pellicon filter into a sterilzed, air-tight vial for storage at 4°C.

Deoxygenation was carried out on a 0.2 ml. sample in a 5 ml chamber by alternating slow evacuation and equilibration with N_2 (Airco purified) saturated with water vapor. The ^{16}O-^{18}O hemocyanin was prepared by equilibrating the colorless deoxyhemocyanin with ^{16}O-^{18}O (Miles Laboratories 55.11 atom % ^{18}O) at approximately 200 Torr.

Raman spectra were obtained at room temperature using 5145 Å (free O_2 gas) and 5309 Å (hemocyanin) excitation. The spectrometer has been described above (part I).

III. Vibrational frequency calculations

The calculations were carried out on a Prime 350 computer. The Prime 350 is a multi-user, multi-language, multi-programmed system, which utilizes a virtual memory of 2 million bytes (real memory of 512 K bytes) and can accommodate program sizes up to 768 K bytes.

The computer programs are described in Chapter 2.

REFERENCES AND NOTES

1. E. B. Wilson, Jr., J. Chem. Phys., 7, 1047 (1939).
2. Ibid., 15, 736 (1947).
3. F. A. Cotton, Chemical Applications of Group Theory, 2nd Ed., pp. 309-316, Wiley-Interscience, New York, 1971.
4. P. Gans, Vibrating Molecules, pp. 134-150, Chapman and Hall, Ltd., London, 1971.
5. L. H. Jones, Inorganic Vibrational Spectroscopy, Vol. 1, pp. 19-24, Marcel Dekker, Inc., New York, 1971.
6. J. H. Schachtschneider, Technical Report No. 57-65, Shell Development Co., Emeryville, CA., 1966.
7. H. Fuhrer, V. B. Kartha, K. G. Kidd, P. J. Krueger, and H. H. Mantsch, Computer Programs for Infrared Spectroscopy, Bulletin No. 15, National Research Council of Canada, Ottawa, 1976.
8. E. B. Wilson, J. C. Decius, and P. C. Cross, Molecular Vibrations, pp. 169-173, McGraw-Hill, New York, 1955.
9. M. C. Urey and C. A. Bradley, Phys. Rev., 38, 1969 (1931).
10. J. Fujita, A. E. Martell, and K. Nakamoto, J. Chem. Phys., 36, 339 (1962).
11. R. A. Condrate and K. Nakamoto, ibid., 42, 2590 (1965).
12. J. R. Kincaid and K. Nakamoto, Spectrochim. Act., 32A, 277 (1976).
13. H. C. Freeman, J. E. W. L. Smith and J. C. Taylor, Acta Crystallogr. 14, 407 (1961).

14. B. B. Kedzia, P. X. Armendarez and K. Nakamoto, J. Inorg. Nucl. Chem., 30, 849 (1968).

15. P. X. Armendarez and K. Nakamoto, Inorg. Chem., 5, 796 (1966).

16. G. R. Byrkacz, R. D. Libby, and G. A. Hamilton, J. Am. Chem. Soc., 98, 628 (1976).

17. J. J. Bour, P. J. M. W. L. Birker and J. J. Steggerda, Inorg. Chem., 10, 1202 (1971).

18. J. Fujita, A. E. Martell and K. Nakamoto, J. Chem. Phys., 36, 324 (1962).

19. Ibid., 36, 331 (1962).

20. J. A. Ladd and W. J. Orville-Thomas, Spectrochim. Acta, 22, 919 (1966).

21. P. Gans, Vibrating Molecules, pp. 27-28, Chapman and Hall, Ltd., London, 1971.

22. P. Cossee and J. H. Schachtschneider, J. Chem. Phys., 44, 97 (1966).

23. P. J. M. W. L. Birker, Inorg. Chem., 16, 2478 (1977).

24. F. A. Cotton and G. Wilkinson, Advanced Inorganic Chemistry, 3rd ed., pp. 723-725, Interscience, New York, 1972.

25. S. Peng, G. C. Gordon and V. L. Goedken, Inorg. Chem., 17, 119 (1978).

26. S. C. Jackels, K. Farmery, E. K. Barefield, N. J. Rose and D. H. Busch, Inorg. Chem., 11, 2892 (1972).

27. D. A. Baldwin, R. M. Pfeiffer, D. W. Reichgott and N. J. Rose, J. Am. Chem. Soc., 95, 5152 (1973).

28. J. R. Dyer, Applications of Absorption Spectroscopy of Organic Compounds, pp. 32-52, Prentice-Hall, Englewood Cliffs, N. J., 1965.

29. L. J. Bellamy, The Infrared Spectra of Complex Molecules, Vol. 1, pp. 231-276, John Wiley, New York, 1975.

30. D. W. Margerum, K. L. Chellappa, F. B. Bosser and G. L. Burse, J. Am. Chem. Soc., 97, 6894 (1975).

30a. M. Goldberg and I. Pecht, Biochemistry, 15 4197 (1976).

31. J. A. Fee, Struct. Bonding, 25, 1 (1975).

32. E. T. Adman, R. E. Stenkamp, L. C. Sieker, and L. H. Jensen, J. Mol. Biol., 123, 35 (1978).

33. T. D. Tullius, P. Frank, and K. O. Hodgson, Proc. Nat. Acad. Sci. (U.S.A.), 75, 4069 (1978).

34. V. Miskowski, S.-P. W. Tang, T. G. Spiro, E. Shapiro, and T. H. Moss, Biochemistry, 14, 1244 (1975).

35. E. I. Solomon, J. W. Hare, and H. B. Gray, Proc. Nat. Acad. Sci. (U.S.A.)., 73, 1389 (1976).

36. E. I. Solomon, J. Rawlings, D. R. McMillin, P. J. Stephens, and H. B. Gray, J. Am. Chem. Soc., 98, 8046 (1976).

37. D. R. McMillin, R. C. Rosenberg, and H. B. Gray, Proc. Nat. Acad. Sci. (U.S.A.), 71, 4760 (1974).

38. P. M. Colman, H. C. Freeman, J. M. Guss, M. Murata, V. A. Norris, J. A. M. Ramshaw, and M. P. Venkatappa, Nature, 272, 319 (1978).

39. The program which calculated the F matrix and adjusted the force constants was supplied by the National Research Council of Canada (Bulletin No. 15, 1976) and modified for our purposes.

40. K. Nakamoto, J. Fujita, R. A. Condrate, and Y. Morimoto, J. Chem. Phys., 39, 423 (1963).

41. G. Durgaprasad, D. N. Sathyanarayana, and C. C. Patel, Can. J. Chem., 47, 631 (1969).

42. A. Ray, D. N. Sathyanarayana, G. D. Prasad, and C. C. Patel, Spectrochim. Act., 29A, 1579 (1973).

43. P. Gans, Vibrating Molecules, pp 28, Chapman and Hall, Ltd., London, 1971.

44. Force constants are generally proportional to the square of the frequencies. In this case, the ratio of the force constants for the two Cu-S stretching modes should be $(261)^2 \div (369)^2 = 0.50$.

45. M. Y. Okamura and I. M. Klotz, in Inorganic Biochemistry, p. 321, G. L. Eichhorn ed., Elsevier, New York, 1973.

46. D. M. Kurtz, Jr., D. F. Shriver and I. M. Klotz, Coord. Chem. Rev., 24, 147 (1977).

47. J. S. Loehr and T. M. Loehr, in Advances in Inorganic Biochemistry, Vol. 1, pp. 235, G. L. Eichhorn and L. G. Marzilli, eds., Elsevier North Holland, Inc., New York, 1979.

48. S. Keresztes-Nagy and I. M. Klotz, Biochemistry, 4, 919 (1965).

49. Ibid., 2, 923 (1963).

50. K. Garbett, D. W. Darnall, I. M. Klotz, and R. J. P. Williams, Arch. Biochem. Biophys., 135, 419 (1969).

51. J. L. York and A. J. Bearden, Biochemistry, 8. 4549 (1970).

52. M. Y. Okamura, I. M. Klotz, C. E. Johnson, M. R. C. Winter, and R. J. P. Williams, Biochemistry, 8, 1951 (1969).

53. R. E. Stenkamp, L. C. Sieker, and L. H. Jensen, Acta Cryst., A34, 1014 (1978).

54. Ibid., Proc. Nat. Acad. Sci. U.S.A., 73, 349 (1976).

55. W. A. Hendrickson, G. L. Klippenstein, and K. B. Ward, Ibid., 72, 2160 (1975).

56. K. S. Murray, Coord. Chem. Rev., 12, 1 (1974).

57. J. H. Dawson, H. B. Gray, H. E. Hoenig, G. R. Rossmann, J. M. Schredder, and R. H. Wang, Biochemistry, 11, 461 (1972).

58. T. H. Moss, C. Moleski, and J. L. York, Biochemistry, 10, 840 (1971).

59. I. M. Klotz, G. L. Klippenstein, and W. A. Hendrickson, Science, 192, 335 (1976).

60. H. B. Gray and H. J. Schugar in Inorganic Biochemistry, pp. 102, G. L. Eichhorn, ed., Elsevier, New York, 1973.

60a. J. B. R. Dunn, D. F. Shriver, and I. M. Klotz, Proc. Nat. Acad. Sci. (U.S.A.), 70, 2582 (1973).

61. R. E. Stenkamp and L. H. Jensen, in Advances in Inorganic Biochemistry, Vol. 1, pp. 219, G. L. Eichhorn and L. G. Marzilli, eds., Elsevier, North Holland, Inc., New York, 1979.

62. J. B. R. Dunn, J. S. Loehr, A. W. Addison, R. E. Bruce, and T. M. Loehr, Biochemistry, 16, 1743 (1977).

63. D. M. Kurtz, Jr., D. F. Shriver and I. M. Klotz, J. Am. Chem. Soc., 98, 5033 (1976).

64. D. M. Kurtz, Ph.D. Dissertation, p. 69, Northwestern University, 1977.

65. F. E. Mabbs, V. N. McLachlan, D. McFadden, and A. T. McPhail, J.C.S. Dalton, 2016 (1973).

66. P. Coggon, A. T. McPhail, F. E. Mabbs, and V. N. McLachlan, J. Chem. Soc. (A), 1014 (1971).

67. R. Lontie and R. Witters in Inorganic Biochemistry, pp. 344-343, G. L. Eichhorn, ed., Elsevier, New York, 1975.

68. A. C. Redfield, T. Coolidge and H. Montgomery, J. Biol. Chem., 76, 197 (1978).

69. R. Guillement and G. Gosselin, Compt. Rend. Soc. Biol., 11, 733 (1932).

70. W. A. Rawlinson, Aust. J. Exp. Biol. Med. Sci., 18, 131 (1940).

71. W. G. Schutter, E. F. J. Van Bruggen, J. Bonaventura, C. Bonaventura and B. Sullivan in Structure and Function of Haemocyanin, pp. 15-17 J. V. Bannister, ed., Springer-Verlag, New York, 1977.

72. E. F. J. van Bruggen, in Physiology and Biochemistry of Haemocyanins, pp. 37, F. Ghiretti, ed., Academic Press, London, 1968.

73. E. F. J. van Bruggen, V. Schuiten, E. H. Wiebenga and M. Gruber, J. Mol. Biol., 7, 2491 (1963).

74. Ochiai, Ei-ichiro, Bioinorganic Chemistry, pp. 218-220, Allyn and Bacon, Boston, 1977.

75. K. E. van Holde, Biochemistry, 6, 93 (1967).

76. G. F. Bryce and F. R. N. Gurd, J. Biol. Chem., 241, 1439 (1966).

77. J. F. Bogs, J. R. Pilbrow, G. J. Troup, C. Moore, and T. D. Smith, J. Chem. Soc., 965 (1969).

78. H. van der Deen and H. Hoving, Biochemistry, 16, 3519 (1977).

79. E. J. Wood and W. H. Bannister, Biochim. Biophys. Acta, 154, 10 (1968).

80. Y. Engelborghs, R. Witters and R. Lontie, Arch. Int. Physiol. Biochim., 76, 372 (1968).

81. T. B. Freedman, J. S. Loehr and T. M. Loehr, J. Am. Chem. Soc., 98, 2809 (1976).

82. T. Nakamura and H. S. Mason, Biochem. Biophys. Res. Commun., 3, 297 (1960).

83. W. E. Blumberg, in J. Peisach, P. Aisen, and W. E. Blumberg, The Biochemistry of Copper, p. 472, Academic Press, New York, 1966.

84. R. Lontie and R. Witters, ibid., p. 455.

85. P. E. McMahill and H. S. Mason, Biochem. Biophys. Res. Commun., 84, 749 (1978).

86. D. M. Dooley, R. A. Scott, J. Ellinghaus, E. I. Solomon and H. B. Gray, Proc. Nat. Acad. Sci. U.S.A., 75, 3019 (1978).

87. R. S. Himmelwright, N. C. Eickman and E. I. Solomon, J. Am. Chem. Soc., 101, 1576 (1979).

88. N. C. Eickman, R. S. Himmelwright and E. I. Solomon, Proc. Nat. Acad. Sci. U.S.A., 76, 2094 (1979).

89. R. S. Himmelwright, N. C. Eickman and E. I. Solomon, Biochem. Biophys. Res. Commun., 86, 628 (1979).

90. T. J. Thamann, J. S. Loehr and T. M. Loehr, J. Am. Chem. Soc., 99, 4187 (1977), see Appendix D, page 118.

91. The oxygen gas intensity ratios were calculated from peak height and peak area measurements on four independent, signal-averaged Raman spectra obtained with 568.2 , 514.5 (two spectra), and 488.0 nm excitation wavelengths. The reported ratios, normalized to the intense $^{18}O_2$ peak, are the mean values of the four data sets: 0.71 (Γ 0.09):1.63 (Γ 0.07).

92. H. van der Deen and H. Hoving, Biophys. Chem., 9, 169 (1979).

93. A. W. McLellan and G. A. Nelson, J. Chem. Soc., (A), 137 (1967).

94. T. M. Loehr, W. E. Keyes, and P. A. Pincus, Anal. Biochem., 96, 456 (1979).

APPENDIX A

The computer program used for the calculations in Chapters 4 and 5 automatically varied the angles ϕ, β, and γ by the use of a "command file." The sequence of operation is as follows.

1. Initial values of ϕ, β, and γ are put into an "input file." Also included in input files are bond distances, a trial force field, and the observed Raman frequencies for <u>two</u> of the isotopes ($^{16}O_2$ and $^{18}O_2$ were used).
2. The calculations are made, using the Wilson GF matrix method, and a refined force field is obtained which correctly predicts the observed frequencies for the isotopes used in step 1.
3. The refined force field from step 2 is used to calculate the vibrational frequencies for all the isotopes ($^{16}O_2$, ^{16}O-^{18}O, ^{18}O-^{16}O, $^{18}O_2$).
4. The calculated frequencies for <u>all</u> the isotopes used are stored in an "output file."
5. The command file now edits the input file of step 1 and replaces ϕ with a new value, but leaves β and γ constant.
6. The entire cycle is now repeated (steps 1-5), until the last value of ϕ has been used in the calculations.
7. ϕ is returned to its original value and β is changed (γ remains constant).
8. Steps 1-7 are now repeated until all β values are used.
9. β is returned to its original value and γ is changed.

10. Steps 1-9 are repeated until all γ values have been used.

11. The computer gets tired and quits.

This completes the sequence of calculations, which have yielded calculated isotopic shifts for all preprogrammed values of ϕ, β, and γ. For the μ-oxo bridged model there is an additional angle, δ, which must be varied; δ was put in the sequence after γ.

APPENDIX B

Table I. Calculated Isotopic Shifts for the μ-monooxygen Bridged Model of Oxyhemerythrin, when $\gamma = 70.5°$.[a]

					ν(0-0)				
					β				
φ	60	70	80	90	100	110	120	130	140
0	25	21	17	13	11	9	8	8	-
10	25	21	17	13	10	9	8	8	-
20	25	21	16	13	10	9	7	8	-
30	24	21	15	12	9	7	7	7	-
40	23	17	13	10	8	6	6	7	-
50	21	15	10	8	6	5	5	7	-
60	17	11	8	5	4	4	5	7	-
70	14	8	5	4	3	3	4	7	-
80	9	6	4	2	2	3	4	8	-
90	7	4	3	1	2	3	5	10	-
100	4	3	2	1	2	5	9	12	-
110	5	4	2	3	4	6	11	15	-
120	5	4	3	4	6	9	15	19	-
130	5	5	5	6	8	12	17	20	-
140	6	6	6	8	10	14	18	22	-
150	7	7	8	10	12	16	20	22	-
160	8	7	9	11	13	18	20	23	-
170	8	8	9	11	13	18	20	23	-
180	8	8	10	10	13	18	20	22	-
					ν(Fe-O)				
0	18	16	18	20	21	23	24	24	-
10	17	17	18	20	21	23	24	23	-
20	17	16	18	19	21	23	24	23	-
30	16	16	17	20	22	23	24	23	-
40	14	14	17	20	22	23	24	23	-
50	11	14	17	21	22	24	23	23	-
60	7	14	19	21	23	24	23	22	-
70	11	16	19	22	24	24	23	22	-
80	15	19	19	23	24	24	22	20	-
90	19	21	-22	24	24	23	21	18	-
100	21	22	24	24	24	22	18	16	-
110	22	24	24	24	22	20	16	14	-
120	24	24	24	23	21	19	13	19	-
130	24	24	24	23	21	19	17	21	-
140	24	24	23	23	21	19	21	22	-
150	24	24	23	23	21	21	22	22	-
160	25	24	23	23	21	21	21	22	-
170	25	24	23	22	21	21	21	22	-
180	24	24	23	23	22	21	21	21	-

[a] Indicates an unrealistic force field.

Table II. Calculated Isotopic Shifts for the μ-monooxygen Bridged Model of Oxyhemerythrin, when $\gamma = 90°$.

ν(O-O)

ϕ \ β	60	70	80	90	100	110	120	130	140
0	17	16	16	16	16	15	15	15	15
10	16	16	16	15	16	16	15	15	15
20	15	15	15	15	15	15	15	15	15
30	15	14	14	14	14	14	14	14	15
40	13	12	12	12	12	12	12	13	13
50	12	10	10	9	9	10	11	12	13
60	10	8	7	6	6	8	10	11	13
70	8	6	4	4	4	6	8	10	12
80	7	4	2	2	2	4	7	9	12
90	7	3	2	1	1	3	6	9	12
100	6	4	2	2	2	4	6	9	12
110	7	5	4	2	4	5	7	9	12
120	9	8	6	6	6	7	8	11	12
130	10	10	9	8	8	9	10	11	13
140	12	12	11	11	11	11	12	12	13
150	13	14	13	13	13	12	13	13	14
160	14	14	14	15	14	14	14	15	15
170	15	15	15	16	15	15	15	15	15
180	14	14	14	15	15	15	15	15	15

ν(Fe-O)

0	23	22	22	23	22	23	23	23	23
10	23	22	23	23	23	23	23	23	23
20	23	23	23	23	23	23	23	23	23
30	22	22	23	23	23	23	23	23	23
40	23	23	23	23	23	23	23	23	23
50	23	23	23	23	23	23	23	23	23
60	23	23	23	23	23	23	23	23	23
70	22	23	23	23	23	23	23	23	23
80	22	23	23	23	23	23	23	23	23
90	22	23	23	23	23	23	23	23	23
100	23	23	23	23	23	23	23	23	23
110	23	23	23	23	23	23	23	23	23
120	23	23	23	23	23	23	23	23	23
130	23	23	23	23	23	23	23	23	23
140	23	23	23	23	23	23	23	23	23
150	23	23	23	23	23	23	23	23	23
160	23	23	23	23	23	23	23	23	23
170	23	24	23	23	23	23	23	23	23
180	23	23	23	23	23	23	23	23	24

Table III. Calculated Isotopic Shifts for the μ-monooxygen Bridged Model of Oxyhemerythrin, when $\gamma = 100°$.

ν(O-O)

ϕ \ β	60	70	80	90	100	110	120	130	140
0	12	13	14	15	17	19	19	18	17
10	12	13	14	15	17	18	19	18	16
20	11	11	13	15	16	17	17	18	16
30	10	10	12	13	15	16	17	17	16
40	9	9	10	11	13	15	16	17	16
50	8	7	7	8	10	13	14	15	15
60	6	6	5	5	7	10	14	15	15
70	5	4	2	3	4	7	12	14	15
80	5	3	2	1	2	5	8	12	15
90	6	3	1	1	1	3	6	9	12
100	8	5	2	1	2	3	5	8	10
110	10	7	4	3	3	4	6	7	9
120	13	10	7	5	4	5	6	8	9
130	15	13	10	8	6	6	7	8	9
140	17	15	12	10	8	8	8	8	9
150	18	17	15	12	10	10	9	9	9
160	19	18	16	14	12	11	9	9	10
170	19	18	17	15	13	11	10	10	10
180	18	18	16	14	13	12	10	10	9

ν(Fe-O)

0	23	22	22	21	22	22	22	22	21
10	23	23	23	22	21	23	22	22	21
20	23	23	22	22	22	22	23	22	21
30	23	23	22	21	21	22	23	22	21
40	23	23	23	21	21	21	23	22	21
50	23	23	23	21	21	21	23	22	22
60	23	23	23	21	20	19	22	22	21
70	23	23	23	22	20	17	17	22	21
80	22	23	23	22	21	19	18	18	19
90	21	22	23	23	23	21	21	20	19
100	19	21	22	23	24	23	23	22	20
110	19	17	21	22	23	24	23	23	22
120	22	16	19	21	23	23	24	23	23
130	21	19	19	21	23	23	24	24	23
140	21	21	20	21	23	23	24	24	24
150	21	21	21	21	23	23	24	24	24
160	22	21	21	21	23	23	23	24	24
170	22	21	21	22	23	23	23	24	23
180	22	21	22	22	23	23	23	24	24

Table IV. Calculated Isotopic Shifts for the μ-monooxygen Bridged Model of Oxyhemerythrin, when γ = 110°.

ν(O-O)

	β								
φ	60	70	80	90	100	110	120	130	140
0	9	10	11	14	17	20	21	21	18
10	8	9	11	14	17	20	22	21	19
20	8	9	10	13	16	19	21	21	18
30	7	7	8	11	14	18	20	21	18
40	7	6	7	9	12	16	20	20	18
50	6	4	5	7	10	14	18	19	18
60	5	3	3	4	7	11	15	19	18
70	5	3	2	2	4	7	12	17	17
80	4	2	1	1	2	5	9	13	16
90	5	2	1	1	1	3	6	10	13
100	8	4	2	1	1	3	5	8	11
110	11	6	4	1	2	2	5	7	9
120	15	10	6	4	3	3	4	7	9
130	21	13	9	6	4	5	5	6	8
140	23	17	12	8	6	5	6	6	8
150	24	19	14	10	8	7	7	7	8
160	25	20	15	12	9	7	7	7	8
170	24	21	15	13	9	8	7	8	8
180	23	20	16	12	10	8	8	7	8

ν(Fe-O)

0	24	23	22	21	20	20	21	21	18
10	24	23	21	21	20	20	21	21	18
20	24	23	22	20	19	20	21	21	18
30	24	23	22	21	19	19	21	21	19
40	24	24	23	21	19	18	20	21	19
50	23	24	22	21	19	16	18	20	19
60	23	24	23	21	19	16	14	19	19
70	23	23	24	22	21	17	14	11	18
80	22	23	23	24	22	19	17	14	13
90	20	22	23	24	24	21	19	17	16
100	17	20	22	23	24	23	21	20	18
110	14	18	21	23	24	24	23	21	20
120	10	16	19	22	23	24	24	23	21
130	10	14	18	21	23	25	24	24	22
140	15	14	18	21	23	24	25	24	22
150	17	16	18	21	23	23	25	24	23
160	18	16	19	21	23	23	25	25	23
170	18	16	19	21	23	23	25	25	23
180	18	18	20	21	23	23	24	24	23

Table V. Calculated Isotopic Shifts for the μ-monooxygen Bridged Model of Oxyhemerythrin, when $\gamma = 120°$.[a]

					ν(O-O)				
					β				
φ	60	70	80	90	100	110	120	130	140
0	5	6	8	11	15	19	23	27	-
10	6	6	8	11	15	19	23	26	-
20	5	5	7	11	14	18	23	26	-
30	5	5	6	9	12	16	22	27	-
40	4	3	5	8	11	13	21	26	-
50	4	3	4	5	8	10	19	26	-
60	4	2	2	4	6	7	15	24	-
70	4	1	1	2	4	5	13	19	-
80	5	2	1	1	2	3	9	15	-
90	6	3	1	1	1	3	7	11	-
100	8	4	2	1	1	2	5	9	-
110	11	6	3	1	2	2	5	7	-
120	15	9	5	3	2	3	4	7	-
130	19	13	8	4	3	4	4	-	-
140	23	15	10	6	5	5	4	-	-
150	27	17	12	8	5	5	4	-	-
160	28	19	13	9	7	6	5	-	-
170	29	19	13	9	7	6	6	-	-
180	27	20	14	10	7	6	5	-	-
					ν(Fe-O)				
0	24	23	22	21	18	17	18	19	-
10	25	23	22	20	18	17	18	19	-
20	25	23	23	20	18	16	17	19	-
30	25	24	23	20	18	16	17	19	-
40	25	24	23	21	19	15	14	17	-
50	23	24	24	21	19	15	12	14	-
60	23	25	24	22	19	16	12	7	-
70	22	23	24	24	22	17	13	6	-
80	21	23	25	24	22	19	16	11	-
90	19	22	23	25	24	22	19	14	-
100	16	20	23	24	24	24	21	17	-
110	14	18	22	23	25	24	22	19	-
120	10	16	21	23	25	25	23	20	-
130	8	14	19	22	24	25	24	-	-
140	7	14	18	22	23	25	24	-	-
150	8	13	18	21	23	25	25	-	-
160	10	14	18	21	23	25	25	-	-
170	11	15	19	21	23	25	25	-	-
180	13	16	19	21	23	25	25	-	-

[a] Indicates an unrealistic force field.

Table VI. Calculated Isotopic Shifts for the μ-monooxygen Bridged Model of Oxyhemerythrin, when $\gamma = 130°$.[a]

					ν(0-0)				
					β				
φ	60	70	80	90	100	110	120	130	140
0	5	4	6	8	11	16	19	23	31
10	4	5	6	8	12	15	20	23	30
20	4	4	5	7	11	15	19	24	31
30	4	4	5	7	10	14	21	23	31
40	4	3	4	5	8	12	18	23	31
50	4	3	3	5	7	11	16	22	31
60	4	3	3	5	6	9	14	20	31
70	4	3	2	3	4	7	11	17	31
80	4	3	2	2	3	5	9	15	30
90	7	4	2	1	3	4	7	12	-
100	8	5	2	2	2	3	6	10	-
110	8	6	3	2	2	3	5	8	-
120	13	8	5	3	2	2	4	7	-
130	15	10	6	3	2	2	4	7	-
140	18	11	7	5	4	3	4	6	-
150	19	12	8	5	4	3	4	6	-
160	21	13	9	6	4	4	4	6	-
170	20	13	9	6	4	4	4	6	-
180	20	13	10	6	5	4	4	6	-
					ν(Fe-0)				
0	25	24	23	21	20	17	16	15	17
10	25	25	24	22	19	17	16	17	17
20	25	25	23	22	19	17	17	17	18
30	24	24	23	22	20	17	16	16	18
40	25	25	24	22	20	17	15	15	17
50	24	25	24	23	20	17	14	12	14
60	23	25	25	24	22	19	15	10	9
70	22	24	25	24	22	19	15	10	3
80	22	23	25	24	24	21	17	12	0
90	20	23	24	25	24	22	19	15	-
100	18	22	23	25	24	24	21	17	-
110	16	20	23	25	25	24	22	19	-
120	14	19	22	23	25	24	23	20	-
130	12	18	21	23	25	25	24	22	-
140	10	16	20	23	25	25	24	22	-
150	11	16	20	23	24	25	25	23	-
160	11	17	19	23	23	25	25	23	-
170	13	17	19	23	23	24	25	23	-
180	13	17	20	22	24	25	25	24	-

[a] Indicates an unrealistic force field.

Table VII. Calculated Isotopic Shifts for the μ-monooxygen Bridged Model of Oxyhemerythrin, when $\gamma = 140°$. [a]

					ν(0-0)				
					β				
φ	60	70	80	90	100	110	120	130	140
0	3	4	4	6	9	13	18	22	30
10	2	4	4	6	9	13	18	22	30
20	3	3	4	5	9	13	17	22	30
30	4	3	3	5	7	12	17	22	30
40	4	3	3	5	7	11	16	21	30
50	4	2	3	3	5	10	14	20	30
60	4	3	2	3	5	8	12	19	30
70	5	2	2	3	3	6	11	17	29
80	5	3	2	2	3	5	9	15	29
90	7	4	2	2	2	4	7	13	27
100	8	5	2	2	2	3	6	11	-
110	10	5	3	2	2	3	5	9	-
120	12	7	4	2	2	2	5	8	-
130	14	8	5	3	2	2	4	7	-
140	15	9	5	3	2	2	4	7	-
150	16	9	6	4	2	2	4	6	-
160	17	11	7	4	3	3	4	6	-
170	17	11	7	4	3	2	4	5	-
180	16	11	7	5	4	3	4	4	-
					ν(Fe-0)				
0	25	24	23	22	20	17	15	13	13
10	25	25	24	22	20	17	15	14	16
20	24	24	24	23	20	17	15	13	15
30	24	25	24	23	20	17	14	13	15
40	23	24	24	23	21	18	14	12	12
50	23	25	25	23	22	18	15	11	10
60	22	24	25	24	22	19	15	11	6
70	21	23	25	24	23	20	17	11	4
80	20	23	24	25	24	22	17	12	1
90	18	22	24	25	24	22	19	13	0
100	17	21	23	25	24	23	20	15	-
110	15	20	23	24	25	24	22	18	-
120	14	19	23	24	25	24	22	18	-
130	13	18	22	23	25	25	23	20	-
140	12	18	21	23	25	25	23	21	-
150	13	17	21	23	25	25	25	22	-
160	13	17	21	23	25	25	25	22	-
170	13	17	21	23	25	25	24	23	-
180	25	17	20	23	25	24	24	23	-

[a] Indicates an unrealistic force field.

Table VIII. Calculated Isotopic Shifts for the μ-oxo Bridged Model for Oxyhemerythrin, when $\gamma = 70.5°$, and $\delta = 90°$.

					ν(0-0)				
					β				
ϕ	60	70	89	90	100	110	120	130	140
0	8	5	2	1	2	4	6	9	12
10	8	5	3	1	2	3	6	9	12
20	8	5	3	2	2	3	6	8	12
30	8	4	2	2	2	4	6	8	12
40	8	4	2	1	2	3	6	9	12
50	8	5	2	1	2	4	6	8	12
60	8	4	2	1	2	3	5	9	12
70	8	4	2	1	2	3	6	8	12
80	8	4	2	1	2	3	6	9	12
90	8	4	1	1	1	3	6	9	12
100	8	4	1	1	1	3	6	9	12
110	8	4	1	1	2	4	6	8	12
120	9	5	1	2	2	4	6	8	12
130	8	4	3	1	2	3	6	8	12
140	8	4	2	2	2	3	6	8	12
150	9	5	3	2	2	4	6	9	12
160	8	5	2	1	2	3	6	8	12
170	8	4	2	2	2	3	6	8	12
180	8	4	2	2	2	3	6	8	12
					ν(Fe-0)				
0	15	18	21	23	23	21	19	16	13
10	15	18	21	23	23	21	19	16	14
20	14	19	21	23	23	21	19	16	14
30	15	19	21	23	23	21	19	16	14
40	14	19	21	23	23	22	20	16	14
50	14	19	21	23	23	21	19	16	14
60	14	19	21	23	23	21	20	17	16
70	14	18	21	23	23	21	20	18	16
80	14	19	21	23	23	21	20	17	16
90	14	18	21	23	23	21	20	17	16
100	14	18	21	22	22	22	20	17	16
110	14	18	21	22	23	21	19	17	15
120	13	18	21	22	22	21	19	17	15
130	13	18	21	22	22	21	19	15	13
140	14	18	21	22	22	20	19	15	13
150	14	18	21	22	22	21	19	16	13
160	14	18	21	22	21	20	18	15	13
170	14	18	21	22	22	21	18	15	13
180	14	18	21	22	22	21	18	15	13

Table IX. Calculated Isotopic Shifts for the μ-oxo Bridged Model for Oxyhemerythrin, when $\gamma = 90°$, and $\delta = 90°$.

					ν(0-0)				
					β				
φ	60	70	80	90	100	110	120	130	140
0	8	5	4	3	4	7	10	13	16
10	8	5	4	3	4	6	10	13	16
20	8	4	4	3	4	6	10	13	15
30	8	4	3	2	3	6	9	12	16
40	8	4	2	2	3	5	9	12	16
50	8	4	2	2	2	5	8	12	15
60	8	4	2	1	2	4	8	12	14
70	8	4	2	1	2	4	8	12	14
80	8	4	2	0	1	4	8	12	14
90	8	4	2	0	1	4	8	12	15
100	8	4	2	1	2	4	8	12	15
110	8	4	2	1	2	4	8	12	15
120	8	4	2	2	2	4	8	12	14
130	8	4	2	2	2	4	8	12	14
140	8	4	2	2	2	4	8	12	15
150	8	5	4	2	4	6	9	12	14
160	8	6	4	3	4	6	10	12	15
170	8	6	4	4	4	6	10	12	15
180	8	6	4	4	4	6	10	12	14
					ν(Fe-O)				
0	13	15	14	19	21	18	14	9	5
10	12	15	19	19	21	18	14	9	4
20	12	15	18	19	21	18	14	9	4
30	12	15	18	19	21	19	15	8	4
40	11	16	19	19	21	19	15	9	3
50	12	15	19	19	21	19	15	8	3
60	12	15	17	19	21	19	15	8	4
70	12	16	17	19	20	19	15	9	3
80	12	16	18	20	19	17	15	8	3
90	13	17	19	19	18	16	12	8	4
100	13	17	19	19	18	17	13	8	4
110	13	17	19	19	18	16	12	8	4
120	13	17	19	18	17	14	12	8	4
130	14	17	19	18	16	13	10	8	5
140	14	18	19	18	15	12	9	8	4
150	14	18	19	18	15	12	8	8	5
160	14	19	19	18	16	10	7	8	5
170	13	18	19	18	14	10	7	7	5
180	13	19	19	18	14	10	9	7	5

Table X. Calculated Isotopic Shifts for the μ-oxo Bridged Model for Oxyhemerythrin, when $\gamma = 100°$, and $\delta = 90°$.

ν(0-0)

	β								
φ	60	70	80	90	100	110	120	130	140
0	8	4	2	1	2	4	6	10	14
10	8	4	2	1	2	4	6	10	14
20	8	3	1	1	2	4	7	10	14
30	7	4	2	1	2	3	7	11	14
40	7	4	2	1	1	4	7	11	14
50	8	4	1	1	]	4	7	11	15
60	7	3	1	0	1	3	6	11	14
70	8	3	2	1	1	3	6	10	14
80	8	4	2	1	1	3	7	10	14
90	8	4	2	1	1	3	7	10	14
100	8	4	2	1	1	3	7	10	14
110	8	4	1	1	1	3	7	10	14
120	7	3	1	0	1	3	7	10	14
130	8	4	2	1	2	4	6	10	14
140	8	4	2	1	1	4	7	11	14
150	8	4	2	0	1	3	7	11	14
160	8	4	2	1	2	3	6	11	14
170	8	4	2	1	2	4	6	10	14
180	8	4	2	1	2	4	7	10	14

ν(Fe-0)

0	14	18	21	22	21	19	16	14	12
10	14	18	21	22	21	19	16	14	12
20	14	18	21	22	21	19	16	14	12
30	14	19	21	22	21	19	16	14	12
40	14	19	21	22	22	19	16	13	12
50	14	19	21	23	22	20	17	14	12
60	14	18	21	23	21	19	17	14	12
70	14	18	21	23	21	21	17	14	13
80	14	19	22	23	22	20	17	14	13
90	15	19	22	23	22	20	17	14	13
100	14	19	21	23	23	21	17	15	14
110	14	19	21	23	22	21	17	15	13
120	14	19	21	23	22	20	18	14	13
130	14	18	21	23	22	20	18	14	13
140	14	18	21	23	22	20	17	14	13
150	14	19	21	23	22	20	17	14	12
160	14	19	21	23	22	20	17	15	12
170	14	19	21	23	22	21	17	15	12
180	14	19	21	23	22	21	17	15	12

Table XI. Calculated Isotopic Shifts for the μ-oxo Bridged Model for Oxyhemerythrin, when $\gamma = 110°$, and $\delta = 90°$.

ν(0-0)

	β								
ϕ	60	70	80	90	100	110	120	130	140
0	7	4	2	1	2	4	7	11	15
10	8	4	2	1	2	4	7	11	15
20	8	3	1	1	2	3	7	11	15
30	8	4	2	0	2	3	7	11	15
40	8	4	2	1	1	4	7	10	14
50	8	4	1	1	2	3	7	11	14
60	7	3	2	0	1	3	6	11	15
70	8	3	2	1	1	3	6	11	15
80	8	4	2	1	1	4	6	11	15
90	8	4	2	1	1	4	7	11	15
100	8	4	2	1	1	4	7	11	15
110	8	3	1	1	1	4	6	11	15
120	8	4	1	0	1	3	6	11	15
130	7	4	2	1	2	3	7	11	14
140	8	4	2	1	1	4	6	11	14
150	8	4	1	0	1	4	7	10	14
160	8	4	2	1	2	3	7	10	14
170	7	4	2	1	2	3	7	11	14
180	8	4	2	1	2	3	7	11	14

ν(Fe-O)

0	15	19	21	22	22	20	18	14	12
10	15	19	21	22	22	20	18	14	12
20	15	19	21	22	22	20	18	14	13
30	15	19	21	22	22	20	18	15	13
40	14	19	21	23	22	20	18	15	13
50	14	19	21	23	22	20	18	15	12
60	15	19	21	23	23	20	18	15	13
70	14	18	21	23	22	20	18	15	13
80	14	19	22	23	22	21	17	15	13
90	15	19	22	23	22	21	17	14	13
100	15	19	22	23	22	20	18	14	12
110	14	19	22	23	22	20	17	14	13
130	14	19	22	23	22	21	18	15	13
140	14	19	22	23	22	21	17	15	13
150	14	19	22	23	22	21	18	15	13
160	15	19	22	23	22	20	18	14	12
170	15	19	21	23	22	20	18	15	13
180	15	19	21	23	22	20	18	15	13

Table XII. Calculated Isotopic Shifts for the μ-oxo Bridged Model for Oxyhemerythrin, when $\gamma = 120°$, and $\delta = 90°$.

ν(O-O)

	β								
φ	60	70	80	90	100	110	120	130	140
0	7	4	2	1	2	4	7	11	15
10	7	4	2	1	2	4	7	11	15
20	8	3	1	1	2	3	7	11	15
30	8	4	4	1	2	3	7	11	15
40	8	4	2	1	1	4	7	10	15
50	8	4	1	1	2	3	7	11	15
60	7	3	1	0	1	3	6	11	15
70	8	3	2	1	1	3	6	11	15
80	8	4	2	1	1	4	6	11	15
90	8	4	2	1	1	4	7	11	15
100	8	4	2	1	1	4	7	11	15
110	8	3	2	1	1	4	6	11	15
120	8	4	1	0	1	3	6	11	14
130	7	4	2	1	2	3	7	11	14
140	8	4	2	1	1	4	6	10	14
150	8	4	1	0	1	4	7	10	14
160	8	4	2	1	2	3	7	11	15
170	7	4	2	1	2	3	7	11	14
180	8	4	2	1	2	3	7	11	14

ν(Fe-O)

0	15	19	21	22	22	20	18	14	13
10	15	19	21	22	22	20	18	14	13
20	15	19	21	22	22	20	18	15	13
30	15	19	21	22	22	20	18	15	13
40	15	19	21	23	22	20	18	15	13
50	14	19	21	23	22	20	18	15	13
60	15	19	21	23	23	20	18	15	12
70	14	19	21	23	22	20	18	15	12
80	14	19	21	23	22	21	17	15	12
90	14	19	22	23	22	20	17	14	13
100	15	19	22	23	22	20	18	14	13
110	14	19	22	23	22	20	18	15	13
120	14	19	22	23	22	20	17	14	13
130	14	19	22	23	22	20	18	15	13
140	14	19	22	23	22	21	17	15	13
150	14	19	22	23	22	20	18	14	13
160	15	19	22	23	22	20	18	15	13
170	15	19	21	23	22	20	18	15	13
180	15	19	21	23	22	20	18	15	13

Table XIII. Calculated Isotopic Shifts for the μ-oxo Bridged Model for Oxyhemerythrin, when $\gamma = 130°$, and $\delta = 90°$.

ν(0-0)

	β								
φ	60	70	80	90	100	110	120	130	140
0	7	4	2	1	2	4	7	11	15
10	7	4	2	1	2	4	7	11	15
20	8	3	1	1	2	4	7	11	15
30	8	4	2	1	2	3	7	11	15
40	8	4	2	1	1	4	7	10	15
50	8	4	1	1	2	3	7	11	15
60	7	3	1	0	1	3	6	11	15
70	8	3	2	1	1	3	6	11	15
80	8	4	2	1	1	4	6	11	15
90	8	4	2	1	1	4	7	11	15
100	8	4	2	1	1	4	7	11	15
110	8	3	1	1	1	4	6	11	15
120	8	4	1	0	1	3	6	11	14
130	7	4	2	1	2	3	6	11	14
140	8	4	2	1	1	4	7	10	14
150	8	4	1	0	1	4	7	10	14
160	8	4	2	0	2	3	7	11	15
170	7	4	2	0	2	3	7	11	14
180	8	4	2	0	2	3	7	11	14

ν(Fe-O)

0	15	19	22	22	22	20	18	14	14
10	15	19	21	22	22	20	18	14	13
20	15	19	21	22	22	20	18	15	13
30	15	19	21	22	22	20	18	15	13
40	15	19	21	23	22	20	18	15	13
50	14	19	21	23	22	20	18	15	13
60	15	19	21	23	23	20	18	15	12
70	14	19	21	23	22	20	18	15	12
80	14	18	21	23	22	21	17	15	12
90	14	19	22	23	22	20	17	14	13
100	15	19	22	23	22	20	18	14	13
110	14	19	22	23	22	20	18	15	13
120	14	19	22	23	22	20	17	14	13
130	14	19	22	23	22	21	17	15	13
140	14	19	22	23	22	21	18	15	13
150	14	19	22	23	22	20	18	14	13
160	15	19	22	23	22	20	17	15	13
170	15	19	21	23	22	20	18	15	13
180	15	19	21	23	22	20	18	15	13

Table XIV. Calculated Isotopic Shifts for the μ-oxo Bridged Model for Oxyhemerythrin, when $\gamma = 140°$, and $\delta = 90°$.

ν(0-0)

	β							
ϕ	60	70	80	90	100	110	120	130	140
0	7	4	2	1	2	4	7	11	15
10	8	4	2	1	2	4	7	11	15
20	8	3	1	1	2	4	7	11	15
30	8	4	2	1	2	3	7	11	15
40	8	4	1	1	1	3	7	10	15
50	8	4	1	1	2	4	7	11	15
60	7	3	1	0	1	3	6	11	15
70	8	3	2	1	1	3	6	11	15
80	8	4	2	1	1	3	7	11	15
90	8	4	2	1	1	3	7	11	15
100	8	4	2	1	1	3	7	11	15
110	8	3	1	1	1	3	6	11	15
120	8	4	1	0	1	3	6	11	14
130	7	4	2	1	2	4	6	11	14
140	8	4	2	1	1	4	7	10	14
150	8	4	1	0	1	4	7	10	14
160	8	4	2	1	2	3	7	11	14
170	7	4	2	1	2	3	7	11	14
180	8	4	2	1	2	3	7	11	14

ν(Fe-O)

0	15	19	22	22	22	20	18	14	14
10	15	19	22	22	22	21	18	14	13
20	15	19	21	22	22	21	18	15	13
30	15	19	21	22	22	21	18	15	13
40	15	19	21	23	22	21	18	15	13
50	14	19	21	23	22	21	18	15	13
60	15	19	21	23	23	21	18	15	12
70	14	19	21	23	22	21	18	15	12
80	14	18	21	23	22	20	17	15	12
90	14	19	22	23	22	20	17	14	13
100	15	19	22	23	22	20	18	14	13
110	14	19	22	23	22	20	18	15	13
120	14	19	22	23	22	21	17	14	13
130	14	19	22	23	22	21	17	15	13
140	14	19	22	23	22	21	18	15	13
150	14	19	22	23	22	20	18	14	13
160	14	19	21	23	22	20	18	15	13
170	15	19	21	23	22	20	18	15	13
180	15	19	21	23	22	20	18	15	13

Table XV. Calculated Isotopic Shifts for the μ-oxo Bridged Model for Oxyhemerythrin, when $\gamma = 120°$, $\delta = 90°$, and $\alpha = 45°$.

ν(0-0)

	β								
φ	60	70	80	90	100	110	120	130	140
0	7	4	2	1	2	4	7	11	15
10	7	4	2	1	2	4	7	11	15
20	8	3	1	1	2	3	7	11	15
30	8	4	2	1	2	3	7	11	15
40	8	4	2	1	1	4	7	10	15
50	8	4	1	1	2	3	7	11	14
60	7	3	1	0	1	3	6	11	15
70	8	3	2	1	1	3	6	11	15
80	8	4	2	1	1	4	6	11	15
90	8	4	2	1	1	4	7	11	15
100	8	4	2	1	1	4	7	11	15
110	8	3	1	1	1	4	6	11	15
120	8	4	1	0	1	3	6	11	15
130	7	4	2	1	2	3	7	11	14
140	8	4	2	1	1	4	6	10	14
150	8	4	1	0	1	4	7	10	14
160	8	4	2	1	2	3	7	11	14
170	7	4	2	1	2	3	7	11	14
180	8	4	2	1	2	3	7	11	14

ν(Fe-0)

0	15	19	21	22	22	20	18	14	12
10	15	19	21	21	22	20	18	14	13
20	15	19	21	21	22	20	18	15	13
30	15	19	21	21	22	20	18	15	13
40	15	19	21	23	22	20	18	15	13
50	14	19	21	23	22	20	18	15	13
60	15	19	21	23	23	20	18	15	13
70	14	19	21	23	22	20	18	15	13
80	14	19	22	23	22	21	17	15	13
90	14	19	22	23	22	21	17	15	13
100	15	19	22	23	22	20	18	14	12
110	14	19	22	23	22	20	18	15	13
120	14	19	22	23	22	20	17	14	13
130	14	19	22	23	22	21	18	15	13
140	14	19	22	23	22	21	17	15	13
150	14	19	22	23	22	20	18	14	13
160	15	19	22	23	22	20	18	15	13
170	15	19	21	23	22	20	18	15	13
180	15	19	21	23	22	20	18	15	13

APPENDIX C

Table I. Calculated Isotopic Shifts for the μ-monooxygen Bridged Model of Oxyhemocyanin.

	β								
ϕ	60	70	80	90	100	110	120	130	140
0	4.6	4.8	5.5	6.5	7.6	8.6	9.3	9.3	9.7
10	4.5	4.8	5.4	6.4	7.5	8.5	9.2	9.6	9.7
20	4.4	4.5	5.2	6.1	7.1	8.2	9.0	9.3	9.5
30	4.2	4.1	4.6	5.5	6.6	7.7	8.5	9.0	9.3
40	3.9	3.7	3.9	4.7	5.9	7.0	8.0	8.6	9.0
50	3.7	3.1	3.2	3.8	4.9	6.2	7.3	8.1	8.7
60	3.7	2.7	2.5	2.9	4.0	5.3	6.5	7.6	8.2
70	3.7	2.4	1.9	2.1	3.1	4.4	5.8	6.9	7.8
80	4.0	2.5	1.7	1.6	2.3	3.6	5.0	6.3	7.4
90	4.7	2.8	1.7	1.4	1.7	2.9	4.4	5.8	6.9
100	5.1	3.5	2.1	1.5	1.6	2.5	4.0	5.3	6.5
110	6.4	4.4	2.8	1.9	1.8	2.5	3.7	5.0	6.2
120	7.4	5.4	3.8	2.7	2.3	2.6	3.6	4.8	6.0
130	8.3	6.4	4.8	3.6	3.0	3.0	3.7	4.7	5.8
140	9.1	7.3	5.8	4.5	3.7	3.4	3.9	4.7	5.8
150	9.8	8.1	6.7	5.4	4.3	3.8	4.0	4.7	5.7
160	10.3	8.7	7.3	6.0	4.9	4.3	4.3	4.8	5.7
170	10.6	9.1	7.7	6.4	5.3	4.5	4.5	5.0	5.7
180	10.8	9.2	7.8	6.5	5.4	4.6	4.4	4.9	5.7

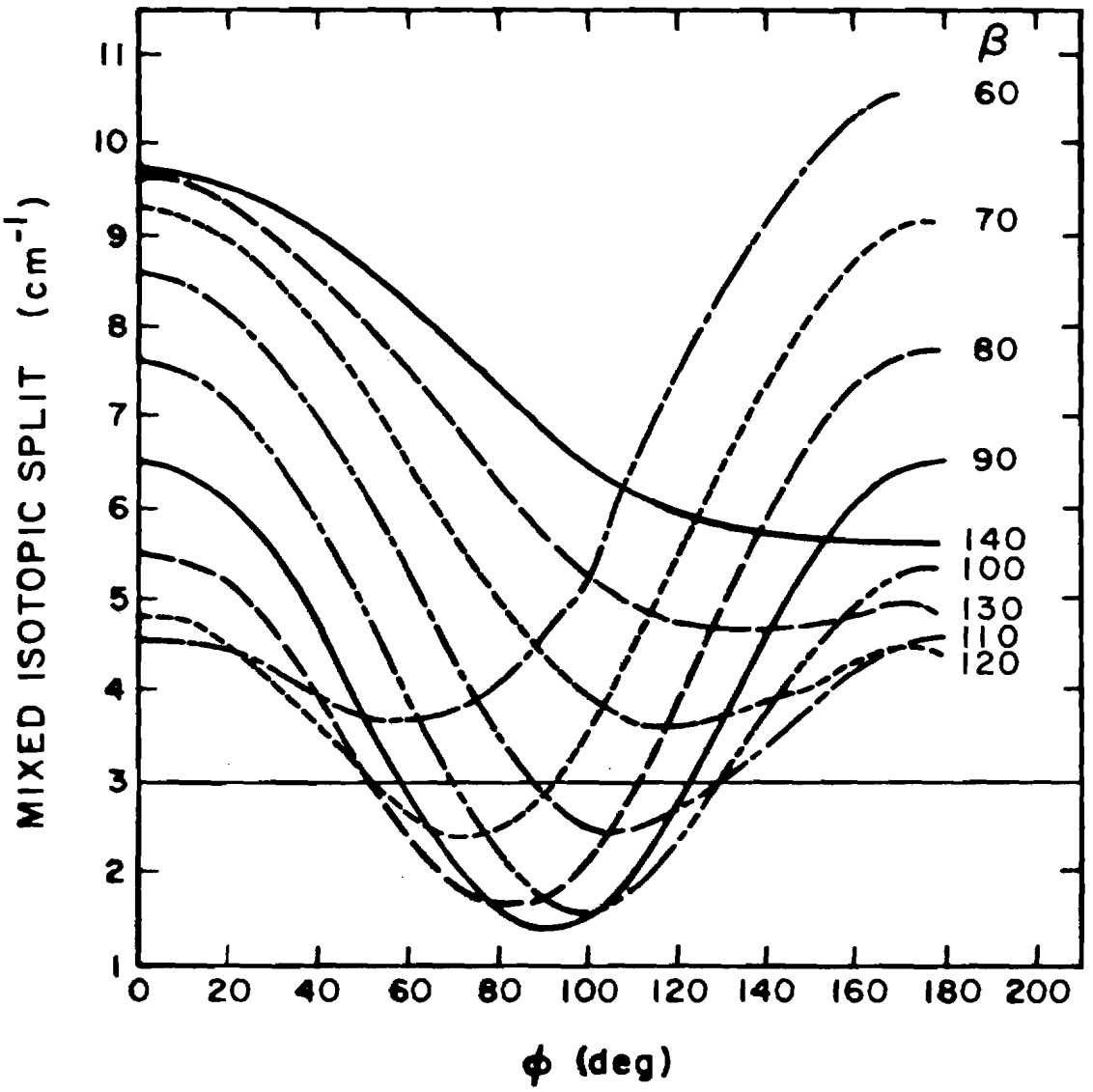

Figure C-1. Calculated isotopic shifts for the μ-monooxygen bridged model of oxyhemocyanin.

Table II. Calculated Isotopic Shifts for the end-on Binding Model of Oxyhemocyanin.

	α			
β	45	90	135	180
60	2.7	2.8	2.8	2.8
70	1.7	1.7	1.7	1.7
80	1.0	0.9	1.0	0.9
90	0.7	0.7	0.7	0.7
100	0.9	0.9	0.9	0.9
110	1.5	1.5	1.5	15.
120	2.6	2.6	2.6	2.6
130	3.8	3.8	3.8	3.9
140	5.0	4.9	5.0	5.0

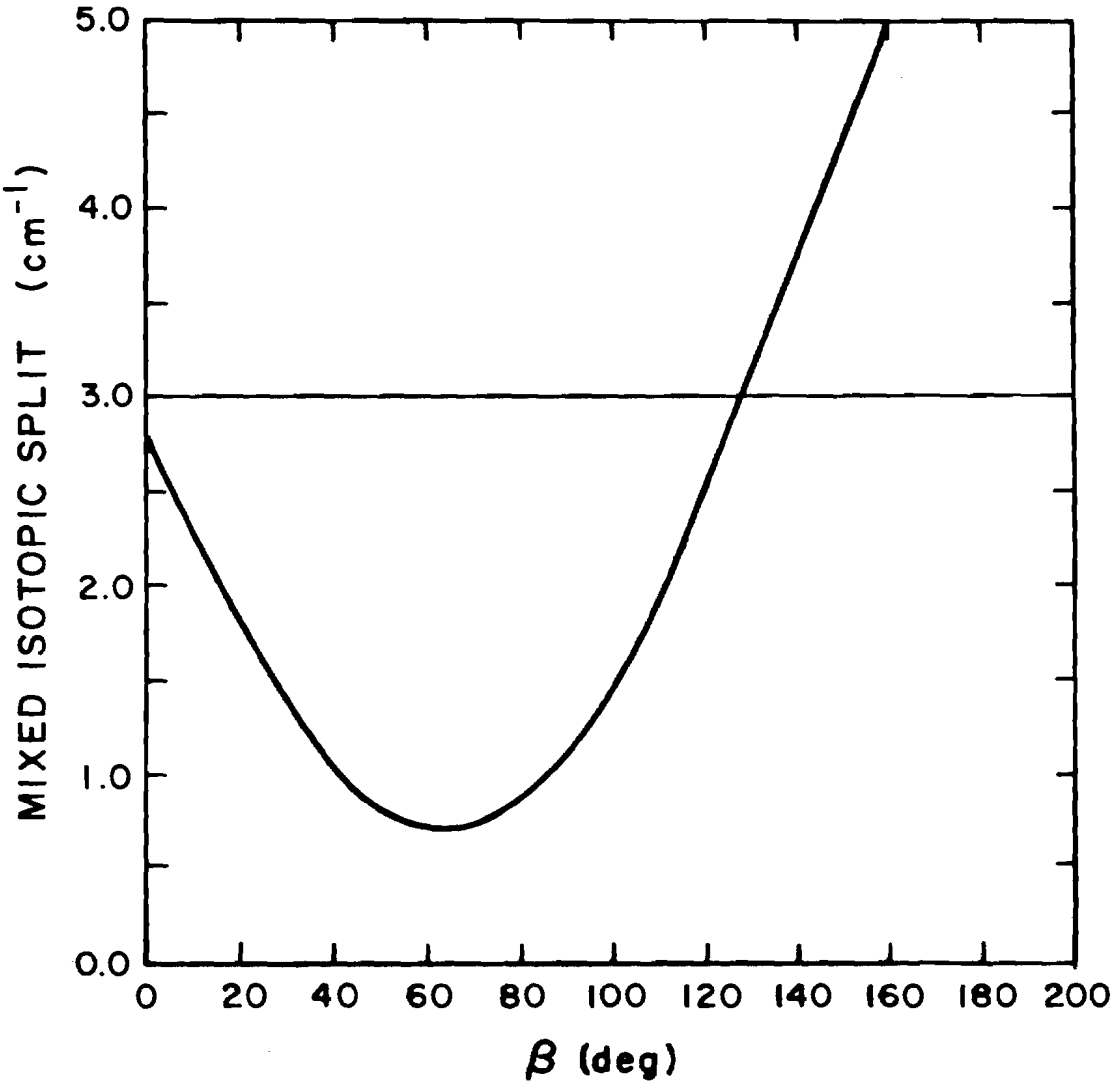

Figure C-2. Calculated isotopic shifts for the end-on binding model of oxyhemocyanin.

[Reprinted from the Journal of the American Chemical Society, 99, 4187 (1977).]

Resonance Raman Study of Oxyhemocyanin with Unsymmetrically Labeled Oxygen

Sir:

We wish to report the results of a resonance Raman spectroscopic investigation of the reaction between hemocyanin, a copper-containing respiratory protein, and a mixed isotope molecular oxygen. Recently, we determined that the O–O stretching vibration of the protein-bound O_2 occurs at 744 cm^{-1} in *Cancer magister* hemocyanin and at 749 cm^{-1} in *Busycon canaliculatum* hemocyanin and shifts to 704 and 708 cm^{-1}, respectively, when >90 atom % $^{18}O_2$ is employed in place of atmospheric oxygen.[1] These frequencies indicate that oxygen is bound as a peroxide ion in oxyhemocyanin and that oxygen binding is an oxidative addition process in which O_2 is reduced and the two Cu(I) centers of colorless deoxyhemocyanin are converted to the blue Cu(II) state. Magnetic susceptibility measurements on oxyhemocyanin place the lower limit of exchange coupling at 625 cm^{-1} for the antiferromagnetically coupled cupric dimers.[2]

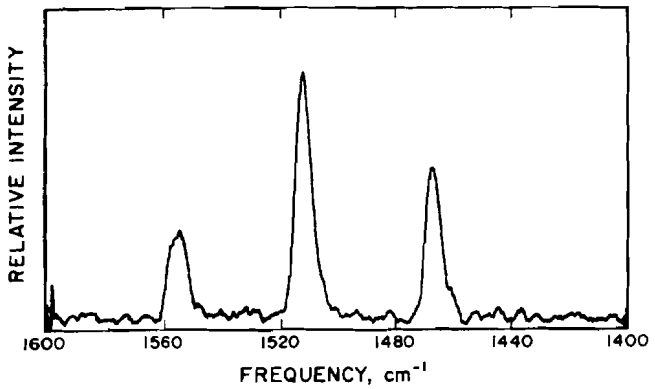

Figure 1. Gas phase Raman spectrum of molecular oxygen (55 atom % ^{18}O). The spectrum is a signal average of 12 repetitive scans subjected to a 25-point computer smoothing using the Savitzky-Golay technique (A. Savitzy and M. J. E. Golay, *Anal. Chem.*, **36**, 1627 (1964)). Excitation, spike-filtered 514.5-nm laser radiation, 0.2 W, 90° scattering geometry, single pass; slit width, 8 cm^{-1}; scan rate, 1.0 cm^{-1}/s; digitizing increment, 0.2 cm^{-1}.

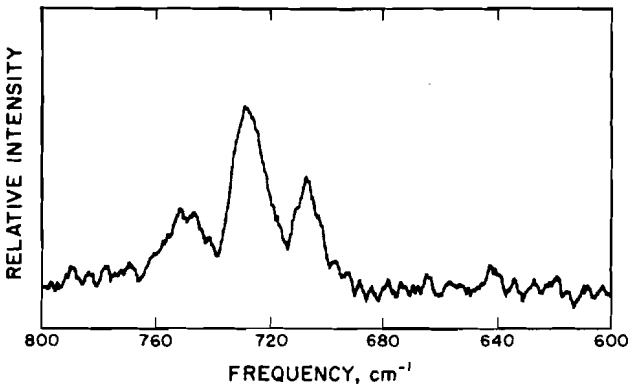

Figure 2. Resonance Raman spectrum of *B. canaliculatum* hemocyanin oxygenated with 55 atom % ^{18}O gas. The spectrum is a signal average of 50 repetitive scans subjected to 25 point smoothing. Excitation, spike-filtered 530.9-nm laser radiation, 30 mW at the sample, ~180° scattering geometry; slit width, 10 cm^{-1}; scan rate, 0.5 cm^{-1}/s; digitizing increment, 0.2 cm^{-1}.

The nonheme iron respiratory protein, hemerythrin, exhibits several similarities to hemocyanin. In the oxygenated protein the O-O stretching frequency is observed at 844 cm^{-1}, indicating that oxygen binding to hemerythrin also involves an oxidative addition process that yields O_2^{2-} bound to two Fe(III).[3] Furthermore, the two Fe(III) atoms in oxyhemerythrin are also antiferromagnetically coupled.[4] In an elegant experiment, Kurtz et al.[5] used oxyhemerythrin containing unsymmetrically labeled O_2 to demonstrate that the two oxygen atoms in the bound peroxide moiety are not equivalent. We have now obtained resonance Raman data for oxyhemocyanin which differ significantly from those in the hemerythrin study and indicate that, in contrast to hemerythrin, the oxygen atoms bound to hemocyanin appear to be equivalent.

A representative gas-phase Raman spectrum of mixed-isotope oxygen (Miles Laboratories, 55.11 atom % ^{18}O) in the O_2 stretching region is shown in Figure 1. The peaks corresponding to ^{16}O-^{16}O, ^{16}O-^{18}O, and ^{18}O-^{18}O vibrations exhibit intensity ratios[6] of 0.71:1.63:1.00, in excellent agreement with the ratios expected from the analytical composition (0.66:1.63:1.00). The full band widths at half-maximum intensity (FWHM) of the three peaks are 8.3, 7.6, and 7.3 cm^{-1} (±0.5 cm^{-1}), respectively.

Busycon canaliculatum hemocyanin was prepared as previously described.[1] Hemocyanin samples for this study were lightly pelleted (20 min at 325 000g), deoxygenated, and equilibrated with the oxygen-isotope mixture. The resonance Raman spectrum in the 600–800-cm^{-1} region (Figure 2) shows three peaks at 749, 728, and 708 cm^{-1}. The relative intensities of these three peaks, based on peak heights, are 0.66:1.63:1.00, respectively, and lie well within the standard deviations, *s*, of the intensity ratios observed in the free gaseous mixture. The measured peak widths (FWHM) are 16.8, 14.5, and 12.5 cm^{-1} (±1 cm^{-1}), respectively, for the spectrum obtained with 10.0-cm^{-1} slits and 15.0, 11.7, and 9.9 cm^{-1} (±1 cm^{-1}), respectively, for a spectrum recorded with 6.0-cm^{-1} slits. The greater width of the 749-cm^{-1} peak is due to its overlap with an ~760-cm^{-1} vibrational mode of the protein itself that was clearly revealed in the $^{18}O_2$ hemocyanin samples in our previous studies.[1,7]

The excellent agreement in peak intensity ratios from protein and gaseous samples strongly suggests that only one species contributes to the 728-cm^{-1} peak in oxyhemocyanin. However, a curve-fitting analysis of 10-cm^{-1} slit resolution Raman peaks shows that a splitting of 3 cm^{-1} or less would not have been detectable in the intensity ratios. Although the peak widths are more difficult to quantitate, they show only slight evidence for broadening of the central peak. Since even the maximum probable splitting for oxyhemocyanin is considerably less than the 5-cm^{-1} splitting observed for oxyhemerythrin,[5] it is likely that the bound oxygens are spectroscopically equivalent in oxyhemocyanin. The structure which best explains the collective spectral properties and molecular orbital description of the active site of hemocyanin is the previously proposed nonplanar, μ-dioxygen bridged geometry (I).[1]

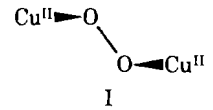

I

In the oxyhemerythrin study, the width of the bound ^{16}O-^{18}O peak at 822 cm^{-1} is nearly twice that of the two flanking peaks (844 and 798 cm^{-1}) and its height is diminished accordingly.[5] These data could only be consistent with nonequivalent oxygens in the Fe_2O_2 site, as suggested by structures II and III. Thus, the resonance Raman spectroscopic data indicate that oxygen is coordinated differently in these two respiratory proteins.[8]

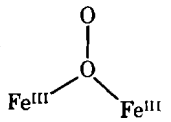

II

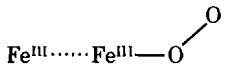

III

Such differences in oxygen coordination are quite reasonable in view of the following information on metal-metal distances in these proteins. (1) The x-ray crystallographic data on *Themiste dyscritum* hemerythrin indicate an Fe···Fe separation of less than 3 Å (L. H. Jensen, personal communication). (2) The Cu···Cu distance calculated from EPR spectra of NO hemocyanin is ~6 Å.[9] (3) The Cu···Cu separation of I falls in the range 3.5 to 5.0 Å based upon a model with Cu-O = 2.0 Å, O-O = 1.5 Å, and variable Cu-O-O and dihedral angles.[1]

Acknowledgment. We are grateful to the National Institutes of Health for support of this research (GM 18865) and to the National Science Foundation for funds used toward the purchase of a precision grating drive[10] (DMR 73-02610). We are deeply indebted to Dr. Phil Pincus and Mr. Terry Reasor, both of the Oregon Graduate Center, for their assistance in the computerization of the Raman spectrophotometer.

References and Notes

(1) T. B. Freedman, J. S. Loehr, and T. M. Loehr, *J. Am. Chem. Soc.*, **98**, 2809 (1976).
(2) E. I. Solomon, D. M. Dooley, R.-H. Wang, H. B. Gray, M. Cerdonio, F. Mogno, and G. L. Romani, *J. Am. Chem. Soc.*, **98**, 1029 (1976).

(3) J. B. R. Dunn, D. F. Shriver, and I. M. Klotz, *Proc. Natl. Acad. Sci. U.S.A.*, **70**, 2582 (1973).
(4) J. W. Dawson, H. B. Gray, H. E. Hoenig, G. R. Rossman, J. M. Schredder, and R.-H. Wang, *Biochemistry*, 11, 461 (1972).
(5) D. M. Kurtz, Jr., D. F. Shriver, and I. M. Klotz, *J. Am. Chem. Soc.*, **98**, 5033 (1976).
(6) The oxygen gas intensity ratios were calculated from peak height and peak area measurements on four independent, signal-averaged Raman spectra obtained with 568.2-, 514.5- (two spectra), and 488.0-nm excitation wavelengths. The reported ratios, normalized to the intensity of the ~1467-cm^{-1} $^{18}O_2$ peak, are the mean values of the four data sets: 0.71 (*s* 0.09):1.63 (*s* 0.07).
(7) J. S. Loehr, T. B. Freedman, and T. M. Loehr, *Biochem. Biophys. Res. Commun.*, **56**, 510 (1974).
(8) Similar results have been obtained by D. M. Kurtz, Jr., D. F. Shriver, and I. M. Klotz (personal communication) on oxyhemocyanin from *Limulus polyphemus*. With the 9-cm^{-1} FWHM observed in their spectra, they estimated that a splitting of 3 cm^{-1} or less could not have been detected.
(9) A. J. M. Schoot-Uiterkamp, H. van der Deen, H. J. C. Berendsen, and J. F. Boas, *Biochim. Biophys. Acta*, **372**, 407 (1974).
(10) The computerized Raman instrumentation consists of a Jarrell-Ash 25-300 spectrometer newly equipped with an RKB, Inc. "Polydrive". Data are collected in core of a Computer Automation 24K computer, and stored on magnetic disks using a Computer Automation dual floppy-disk subsystem. We are using a Tektronix 4010 graphics terminal and 4610 Hard Copy Unit.
(11) Department of Chemistry, Portland State University, Portland, Ore. 97207.

Thomas J. Thamann, Joann S. Loehr,[11] and Thomas M. Loehr*
Department of Chemistry and Biochemical Sciences
Oregon Graduate Center, Beaverton Oregon 97005
Received March 21, 1977

BIOGRAPHICAL NOTE

The author was born in Beech Grove, Indiana on January 25, 1948, the first of five children of Joseph and Alma Thamann. He attended primary and secondary schools in Indianapolis, and in June, 1971 received the B.S. degree in chemistry from Indiana University. During the next four years, the author was employed as an analytical chemist for the Health and Hospital Corporation, while simultaneously working part-time toward a graduate degree in chemistry. In May, 1974 he received the M.S. degree from Purdue University. The author was enrolled at the Oregon Graduate Center, Beaverton, Oregon in October, 1975 to pursue studies leading to the Ph.D. degree in chemistry. Having completed those studies, he now leaves to begin a postdoctoral research appointment at the Massachusetts Institute of Technology, Cambridge, MA.